

Technical Report Documentation Page

1. Report No. FHWA/TX-07/0-5197-2		2. Government Accession No.		3. Recipient's Catalog No.	
4. Title and Subtitle An Investigation of the Tensile Strength of Prestressed AASHTO Type IV Girders at Release				5. Report Date March 2007	
				6. Performing Organization Code	
7. Author(s) Robin Tuchscherer, David Mraz, and Oguzhan Bayrak				8. Performing Organization Report No. 0-5197-2	
9. Performing Organization Name and Address Center for Transportation Research The University of Texas at Austin 3208 Red River, Suite 200 Austin, TX 78705-2650				10. Work Unit No. (TRAIS)	
				11. Contract or Grant No. 0-5197	
12. Sponsoring Agency Name and Address Texas Department of Transportation Research and Technology Implementation Office P.O. Box 5080 Austin, TX 78763-5080				13. Type of Report and Period Covered Research Report 9/1/04 - 2/28/07	
				14. Sponsoring Agency Code	
15. Supplementary Notes Project performed in cooperation with the Texas Department of Transportation and the Federal Highway Administration.					
16. Abstract The intention of the research presented in this report was to determine the source of flexural cracking of AASHTO Type IV girders. Cracking was observed in the end regions of the beams at the time of prestress transfer. Seven full-scale AASHTO Type IV beam specimens were fabricated and tested. Strains were measured in the end regions of each beam; resulting in 14 separate tests. Beams with an extreme fiber tensile stress greater than $4.5\sqrt{f'_c}$ exhibited cracking at the time of release. In addition to the full-scale beam tests, an extensive amount of material data was collected through testing and literature review. Split cylinder and modulus of rupture tests did not accurately represent the tensile strength of concrete in a Type IV beam specimen. Limiting the extreme fiber tensile to $4\sqrt{f'_c}$ will prevent cracking at release.					
17. Key Words Allowable release stress, tensile stress limit, prestress transfer, top fiber tensile cracking, early age material properties				18. Distribution Statement No restrictions. This document is available to the public through the National Technical Information Service, Springfield, Virginia 22161; www.ntis.gov.	
19. Security Classif. (of report) Unclassified	20. Security Classif. (of this page) Unclassified		21. No. of pages 167		22. Price



An Investigation of the Tensile Strength of AASHTO Type IV Girders at Release

Robin Tuchscherer
David Mraz
Oguzhan Bayrak

CTR Technical Report:	0-5197-2
Report Date:	March 2007
Project:	0-5197
Project Title:	An Investigation of the Tensile Strength of AASHTO Type IV Girders at Release
Sponsoring Agency:	Texas Department of Transportation
Performing Agency:	Center for Transportation Research at The University of Texas at Austin

Project performed in cooperation with the Texas Department of Transportation and the Federal Highway Administration.

Center for Transportation Research
The University of Texas at Austin
3208 Red River
Austin, TX 78705

www.utexas.edu/research/ctr

Copyright (c) 2007
Center for Transportation Research
The University of Texas at Austin

All rights reserved
Printed in the United States of America

Disclaimers

Author's Disclaimer: The contents of this report reflect the views of the authors, who are responsible for the facts and the accuracy of the data presented herein. The contents do not necessarily reflect the official view or policies of the Federal Highway Administration or the Texas Department of Transportation (TxDOT). This report does not constitute a standard, specification, or regulation.

Patent Disclaimer: There was no invention or discovery conceived or first actually reduced to practice in the course of or under this contract, including any art, method, process, machine manufacture, design or composition of matter, or any new useful improvement thereof, or any variety of plant, which is or may be patentable under the patent laws of the United States of America or any foreign country.

Notice: The United States Government and the State of Texas do not endorse products or manufacturers. If trade or manufacturers' names appear herein, it is solely because they are considered essential to the object of this report.

Engineering Disclaimer

NOT INTENDED FOR CONSTRUCTION, BIDDING, OR PERMIT PURPOSES.

O. Bayrak

Research Supervisor

Acknowledgments

The funds provided by the Texas Department of Transportation (TxDOT) that made the completion of this project possible are greatly appreciated. The support of the project director Jeff Cotham (Bridge Division) and other members of TxDOT including Randy Cox (Bridge Division), Keith Ramsey (Bridge Division), Joe Roche (Construction Division), Jason Tucker (Construction Division), and Andy Naranjo (Construction Division) are also very much appreciated.

Products

This report contains Product P3, analysis method to predict cracking in the beam ends and primary causes for Short Type IV beam end cracking, located in Chapter 4.

Table of Contents

PREAMBLE	xv
CHAPTER 1 Introduction	1
1.1 Cracking Problem	1
1.2 Scope of Research.....	2
1.2.1 Early Age Material Properties	3
1.2.2 Mechanics of Prestress Transfer	3
1.3 Overview of Research: Report Organization.....	4
CHAPTER 2 Literature Review.....	5
2.1 Introduction.....	5
2.2 Elastic Stress Distribution.....	5
2.3 Background on Prestressed Concrete.....	7
2.4 Previous Research of the Tensile Strength Limit	9
2.5 Historical Development of Concrete Tensile Strength Limits.....	19
2.5.1 Conventionally Reinforced Concrete.....	19
2.5.2 Prestressed Concrete	20
2.6 Previous Research on the Modulus of Elasticity	22
2.7 Previous Research on the Use of Match Curing Technology.....	28
2.8 Summary	29
CHAPTER 3 Experimental Program	31
3.1 Introduction.....	31
3.2 Background.....	31
3.2.1 Transfer Length of Prestressing Force.....	33
3.2.2 Allowable Stress Method: Classical Beam Theory	34
3.2.3 Prestress Losses due to Elastic Shortening	37
3.2.4 Early-Age Mechanical Properties of Concrete	37
3.3 Match Curing Technology	42
3.4 Prestressing Facility	44
3.5 Strand Properties.....	46
3.6 Steel Reinforcement Properties.....	48
3.7 Instrumentation	48
3.7.1 General.....	48
3.7.2 Steel Reinforcement Gauges vs. Concrete Gauges.....	50
3.7.3 Instrumentation of Prestressing Strand	52
3.7.4 Instrumentation of Steel Reinforcement	53
3.7.5 Temperature Instrumentation.....	54
3.8 Fabrication of Test Specimens.....	55
3.8.1 Prestressing of Strands.....	55
3.8.2 Casting of Concrete.....	56

3.8.3	Releasing of Strands	59
3.9	Design of Beam Specimens	61
CHAPTER 4 Discussion of Results		67
4.1	Introduction.....	67
4.2	Preliminary Concrete Material Testing.....	67
4.2.1	Compressive Strength	68
4.2.2	Tensile Strength	69
4.2.3	Tensile – Compressive Strength Relationship	70
4.3	Material Data Associated with the Fabrication of Type IV Beam Specimens	72
4.3.1	Compressive Strength	72
4.3.2	Tensile Strength	73
4.3.3	Modulus of Elasticity.....	74
4.4	Sectional Analysis.....	76
4.4.1	Linear-Elastic Analysis Considering Actual Material Data.....	76
4.5	Transfer Length.....	79
4.6	Crack Control: New Design vs. Old Design	80
4.7	Preventing Cracking at Release	81
4.7.1	Predicting Concrete Cracking Capacity.....	81
4.7.2	Mechanics of Stress Transfer.....	85
4.7.3	Cracking in End Regions of Short Type IV Beams	90
4.8	Curing Temperature Profile	92
CHAPTER 5 Conclusions and Recommendations		99
5.1	Summary of Short Type IV Beam Cracking Problem	99
5.2	Short Type IV Beam Cracking Problem: Source.....	99
5.3	Short Type IV Beam Cracking Problem: Solutions.....	101
APPENDIX A		103
APPENDIX B		107
APPENDIX C		109
APPENDIX D		113
APPENDIX E		131
APPENDIX F		139
APPENDIX G		145
REFERENCES.....		149

List of Tables

Table 3-1: Allowable concrete tensile stress limits at prestress transfer.....	38
Table 3-2: Summary of Mixture Designs.....	40
Table 3-3: Elastic Analysis of Prestressing Bed	48
Table 3-4: 6-5-Sack Type III Cement Mix Design	58
Table 3-5: Summary of Test Specimens	67
Table 4-1: Summary of Mix Designs.....	70
Table 4-2: Concrete Compressive Strengths at the time of Release	75
Table 4-3: Concrete Tensile Strengths at the time of Release	75
Table 4-4: Modulus of Elasticity at top and bottom of “tall” cylinders.....	77
Table 4-5: Calculations for Determining Top Fiber Tensile Stress	80
Table 4-6: Predicted Maximum Tensile Stresses.....	81
Table 4-7: Result of Reducing Strand Eccentricity.....	93
Table 4-8: Result of Reducing Magnitude of Prestress Force	94
Table C-1: Determination of Prestressing Force per Strand.....	110
Table C-2: Determination of Prestressing Force per Strand.....	111
Table C-3: Determination of Prestressing Force per Strand.....	112
Table D-1: Compressive Strength of Concrete	114
Table D-2: Compressive Strength of Concrete	115
Table D-3: Compressive Strength of Concrete	116
Table D-4: Compressive Strength of Concrete	117
Table D-5: Compressive Strength of Concrete	118
Table D-6: Compressive Strength of Concrete	119
Table D-7: Compressive Strength of Concrete	120
Table D-8: Compressive Strength of Concrete	121
Table D-9: Tensile Strength of Concrete	122
Table D-10: Tensile Strength of Concrete	123
Table D-11: Tensile Strength of Concrete	124
Table D-12: Tensile Strength of Concrete	125
Table D-13: Tensile Strength of Concrete	126
Table D-14: Tensile Strength of Concrete	127
Table D-15: Tensile Strength of Concrete	128
Table D-16: Modulus of Elasticity of Concrete.....	129
Table E-1: Top and Bottom Fiber Stress Calculations, Beam 1	132
Table E-2: Top and Bottom Fiber Stress Calculations, Beam 2	133
Table E-3: Top and Bottom Fiber Stress Calculations, Beam 3	134
Table E-4: Top and Bottom Fiber Stress Calculations, Beam 4	135
Table E-5: Top and Bottom Fiber Stress Calculations, Beam 5	136
Table E-6: Top and Bottom Fiber Stress Calculations, Beam 6	137
Table E-7: Top and Bottom Fiber Stress Calculations, Beam 7	138

List of Figures

Figure 1-1: Typical flexural crack occurring at the time of release.....	3
Figure 1-2: 20-foot long AASHTO Type IV with flexural cracking (observed February 2, 2005)	3
Figure 2-1: Bernoulli's hypothesis: plane sections remain plane.	7
Figure 2-2: AASHTO Type IV beam loaded eccentrically, linear elastic stress distribution.....	8
Figure 2-3: Typical D-region (a) elastic stress trajectories; (b) elastic stresses (Schlaich et al. 1987)	9
Figure 2-4: Behavior of a conventionally reinforced concrete beam. (Collins and Mitchell 1997)	10
Figure 2-5: Behavior of a pretensioned concrete beam. (Collins and Mitchell 1997).....	10
Figure 2-6: Tensile strength of concrete.	12
Figure 2-7: Difference in tensile strain gradient for standard 6" beam and pretensioned Type IV girder.	13
Figure 2-8: Beam flexural tensile strength vs. compressive strength (Shah and Ahmad 1985)..	14
Figure 2-9: Beam flexural tensile strength vs. compressive strength (Kaplan 1959).	15
Figure 2-10: Splitting and beam flexural tensile stress vs. compressive stress (Walker and Bloem 1960)	16
Figure 2-11: Beam flexural tensile stress vs. compressive stress (Carasquillo et al. 1981)	17
Figure 2-12: Beam flexural tensile strength vs. compressive strength (Mirza et al. 1979).	18
Figure 2-13: Beam flexural tensile strength vs. compressive strength (Khan et al. 1996)	19
Figure 2-14: Beam flexural tensile strength vs. compressive strength (Mokhtarzadeh and French 2000)	20
Figure 2-15: Beam flexural tensile strength vs. compressive strength (Hueste et al. 2004).....	20
Figure 2-16: Summary of flexural tensile strength vs. compressive strength relationship (1330 data points).....	21
Figure 2-17: Modulus of elasticity of concrete as affected by density (Pauw 1960).....	25
Figure 2-18: Modulus of elasticity vs. compressive stress (Mirza et al. 1979)	26
Figure 2-19: Modulus of elasticity vs. compressive stress (Carasquillo et al. 1981).	27
Figure 2-20: Modulus of elasticity vs. compressive stress, 6x12-inch moist-cured cylinders (Mokhtarzadeh and French 2000).....	28
Figure 2-21: Modulus of elasticity vs. compressive stress, 4x8-inch heat-cured cylinders (Mokhtarzadeh and French 2000).....	28
Figure 3-1: Cracking in the end of a Type IV beam, without block-out.	34
Figure 3-2: Cracking in the end of a Type IV beam, with block-out.....	34
Figure 3-3: Prestressing Strand Transfer Length	36
Figure 3-4: Linear-elastic stress distribution of pretensioned member.....	36
Figure 3-5: Type IV cross sectional properties and top fiber stress.....	37
Figure 3-6: ASTM C39 Standard test method for determining the compressive strength of concrete.	41
Figure 3-7: ASTM C496 Standard test method for determining the splitting tensile strength of concrete.	42
Figure 3-8: ASTM C78 Standard test method for determining the flexural strength of concrete.	43
Figure 3-9: 6x54-inch cylinder. Modulus of Elasticity measured at top and bottom in accordance with ASTM C469.....	44

Figure 3-10: Concrete maturity is accelerated by temperature.....	44
Figure 3-11: Electronic match-curing controller and insulated cylinder molds.	45
Figure 3-12: Electrically Controlled Match Curing System	46
Figure 3-13: Prestressing Facility	47
Figure 3-14: AASHTO Type IV beam during fabrication.....	47
Figure 3-15: Free-body diagram of steel bulkheads subjected to prestressing forces.	48
Figure 3-16: Strain gauge affixed to strand wire.	49
Figure 3-17: Calibration curve for estimating applied force in strand.....	50
Figure 3-18: Thermocouple locations used to match-cure control cylinders.....	51
Figure 3-19: Location of embedded steel strain gauges, Beam 1	52
Figure 3-20: Location of concrete surface gauges, Beam 1	53
Figure 3-21: Experimentally measured strain profiles from steel and concrete strain gauges. ...	54
Figure 3-22: Prestressing strand gauge locations.....	55
Figure 3-23: Reinforcing bar strain gauge locations (Beams 2 through 7).....	56
Figure 3-24: End of specimen illustrating gauge locations.....	56
Figure 3-25: Thermocouple locations, 5'-0" from end of beam	57
Figure 3-26: Single strand stressing operation.....	57
Figure 3-27: Type III cement being added to a ready mix truck.	59
Figure 3-28: Form vibrators used to consolidate concrete.....	60
Figure 3-29: Rod vibrators used to consolidate concrete.....	60
Figure 3-30: Beam specimens were cured by covering with wet burlap and plastic.....	61
Figure 3-31: Torch-cutting prestressing strands.	61
Figure 3-32: Beam specimen immediately prior to being lifted	62
Figure 3-33: Reinforcement layout for typical beam specimen.....	63
Figure 3-34: TxDOT "new" design vs. "old" design: Top flange of Type IV beam.....	64
Figure 3-35: Beam specimens 1 through 3.	65
Figure 3-36: Beam specimens 4 through 6.	66
Figure 3-37: Beam specimen 7.	67
Figure 4-1: Compressive strength vs. time from different manufacturers.....	71
Figure 4-2: Tensile strength vs. time for four different manufacturers.	72
Figure 4-3: Tensile strength factor vs. time for four different manufacturers.	73
Figure 4-4: Tensile strength of concrete when compressive strength = 4000-psi.	74
Figure 4-5: Modulus of elasticity of "tall" cylinders	76
Figure 4-6: Modulus of elasticity in comparison with historical* data.	77
Figure 4-7: Properties used in determining concrete stresses at release.	79
Figure 4-8: Loss of prestress force along strand.	81
Figure 4-9: TxDOT's "new" design vs. "old" design (Top flange).....	82
Figure 4-10: "New" vs. "Old" designs for specimens that cracked.....	83
Figure 4-11: Applied tensile stress at release.....	84
Figure 4-12: Summary of flexural tensile strength in comparison with historical* data. *(Kaplan 1959), (Carasquillo et al. 1981), (Shah and Ahmad 1985), (Khan et al. 1996), (Mokhtarzadeh and French 2000).....	85
Figure 4-13: Difference in tensile strain gradient for 6x6-inch beam and Type IV girder.....	86
Figure 4-14: Measured concrete strength and corresponding predicted maximum tensile stress.	87
Figure 4-15: Planar location of experimentally measured strain profiles.....	88

Figure 4-16: Stress profile located 3-feet from end of beam.	89
Figure 4-17: Stress profile located 4-feet from end of beam.	90
Figure 4-18: Stress profile located 5-feet from end of beam.	91
Figure 4-19: Moment curvature relationship for different strand arrangements and prestress forces.	93
Figure 4-20: Time vs. temperature at various section locations (Beam 6).	95
Figure 4-21: Time vs. temperature along length of beam (Beam 4).	96
Figure 4-22: Time vs. temperature data for match-cured cylinders.	97
Figure 4-23: Compressive and tensile strength gains for different curing temperatures.	98
Figure A-1: TxDOT Standard Detail for Prestressed I-Beams. Page 1.	104
Figure A-2: TxDOT Standard Detail for Prestressed I-Beams. Page 2	105
Figure B-1: Strand Test, Spool #1	108
Figure B-2: Strand Test, Spool #2	108
Figure F-1: Predicted Stress Profiles 5-feet from End of AASHTO Type IV Beams.	140
Figure F-2: Predicted Stress Profile 4-feet from End of AASHTO Type IV Beams.	141
Figure F-3: Predicted Stress Profile 3-feet from End of AASHTO Type IV Beams.	142
Figure F-4: Predicted Stress Profile 2-feet from End of AASHTO Type IV Beams	143
Figure F-5: Predicted Stress Profile 1-feet from End of AASHTO Type IV Beams	144
Figure G-1: Time vs. Temperature Data Collected from Beam 5	146
Figure G-2: Time vs. Temperature Data Collected from Beam 6	146
Figure G-3: Time vs. Temperature Data Collected from Beam 7	147

PREAMBLE

Two distinct topics are covered in TxDOT Project 0-5197. These topics are addressed in two separate reports. The following report (Report 0-5197-2) evaluates the allowable tensile stress limit required at prestress transfer. In Report 0-5197-1, the effects of increasing the allowable compressive stress at prestress transfer are investigated.

CHAPTER 1

Introduction

1.1 CRACKING PROBLEM

Inspectors and Engineers representing Texas Department of Transportation (TxDOT) have seen a recent increase in the amount and severity of flexural cracks forming in the top flange of Type IV bridge girders (Figure 1.1). Typically, cracking was observed after the removal of formwork as the girder was being lifted from the casting bed. The crack lengths varied; however, 2-foot long cracks that are 0.01 to 0.025-inches were very typical. Girders that exhibited cracking were relatively short in length (20 to 60-ft) with highly eccentric strand configurations resulting in high levels of tensile stress in the top flange (Figure 1.2).



Figure 1.1 Typical flexural crack occurring at the time of release.

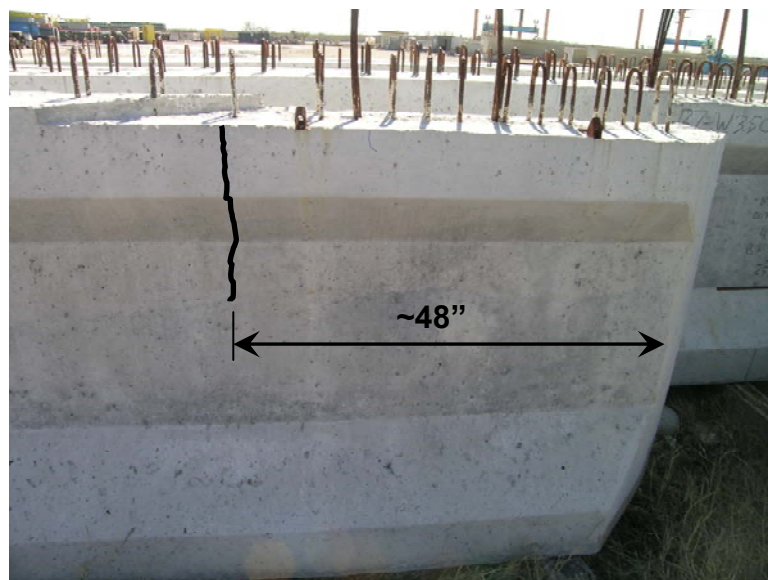


Figure 1.2 20-foot long AASHTO Type IV with flexural cracking (observed February 2, 2005).

According to AASHTO LRFD Bridge Design Specifications (AASHTO 2004) the extreme fiber tensile stress allowed at the time of release is as follows:

For members without bonded reinforcement: $200 \text{ psi or } 3\sqrt{f'_{ci}}$

For members with bonded reinforcement provided to resist the tensile force in concrete; computed on the basis of an uncracked section: $7.5\sqrt{f'_{ci}}$

Therefore, according to AASHTO LRFD, if cracking is to be prevented then the top fiber tensile stress should be limited to $3\sqrt{f'_{ci}}$. If cracking is permitted, then the top fiber tensile stress should be limited to $7.5\sqrt{f'_{ci}}$ and reinforcement provided to control cracking. Generally, the average tensile strength of concrete, as determined by the flexural capacity of a 6x6-inch beam (modulus of rupture), is equal to $7.5\sqrt{f'_{ci}}$. At release, calculated tensile stresses in the end regions of the Type IV beams that exhibited cracking were slightly less than the tensile strength of concrete ($6 \text{ to } 7.5\sqrt{f'_{ci}}$). Regardless of the provisions for the permissible tensile stress at release, TxDOT engineers rightfully want to know why the short Type IV beams are cracking when the tensile strength (as determined by modulus of rupture tests) is greater than the applied stress. Answering this question requires an in-depth review of the following:

- i) The contributing factors to the tensile strength of concrete.
- ii) The requirements of the design specifications.

As a result, the findings of the research project will give structural engineers a better understanding of the contributing factors to cracking, and enable them to more accurately stipulate allowable design stresses.

1.2 SCOPE OF RESEARCH

The intention of this research project is to identify the source of the cracking problem in short Type IV beams and suggest practical solutions to eliminate or reduce crack widths. In architectural applications cracking is generally only a problem from an aesthetic standpoint. This is not the case for highway applications. A much higher cracking capacity is required for bridge structures such as Type IV beams. That is because highway members have relatively higher serviceability requirements due to the cyclic nature of moving loads.

From the onset of the research project it was theorized that cracking at release is due to one of two things: lack of knowledge of the early-age material properties of concrete; or lack of knowledge of the structural mechanics of prestress transfer within the end regions of deep beams (classified as “disturbed” or “D-regions”). In the context of this report “early-age” refers to concrete that has cured for less than 24-hours. Investigating the assumptions and background of knowledge built into these contributing factors will provide better insight into the actual behavior of a specimen at release.

An overview of these two contributing factors is presented in the following sections.

1.2.1 Early Age Material Properties

In general, precast prestressed concrete is comprised of more expensive materials and fabricated to a higher level of quality than normal reinforced concrete. While being of higher quality, precast prestressed concrete is still an economical alternative to conventionally reinforced concrete. This is due to manufacturers' ability to automate and accelerate their fabrication process through the use of standard section geometries and Type III Portland cement. Type III Portland cement provides high strengths at early ages. It is chemically and physically similar to Type I cement except that its particles have been ground finer. In order to remain competitive, the tensioning of strands, casting of concrete, removal of forms, and releasing of strands must occur within a 24-hour time period. This means that, in less than 24-hours, concrete containing Type III cement must achieve the same strength that concrete containing Type I cement would achieve in 14 to 28-days.

Precast prestressed concrete beam manufacturers are required to verify the compressive strength of the concrete used in their beams at the time of release and at 28-days. Typically, they verify the strength of concrete at the time of release by testing standard 4-inch cylinders in compression. They are not required to directly test the tensile strength or the modulus of elasticity. That is because the tensile strength and modulus of elasticity have already been accounted for during the design process based on relationships with the compressive strength. However, these relationships have been derived for concrete mixes that are 28-days old, comprised of different materials, and have been cured under different curing conditions.

Part of the scope of this research project was to examine the empirical relationships used to relate concrete material properties to one another and make a determination of their validity and accuracy. This was achieved by gathering historical data that makes up the body of knowledge that is the basis for code provisions. Early-age material testing was conducted in the Phil M. Ferguson Structural Engineering Laboratory and compared with historical data. This information was also used in formatting the subsequent experimental work.

1.2.2 Mechanics of Prestress Transfer

What was also required was an investigation into the mechanics of stress transfer in the end regions of Type IV beams. When analyzing the structural behavior of a beam in flexure, assumptions about the deformed shape and mechanics of stress transfer are employed in order to simplify calculations. Currently, designers assume that plane sections remain plane and the stress profile of a section can be defined by the " $P/A \pm Mc/I$ " expression. However, in the end region of a 54-inch deep beam large forces are being transferred locally from the prestressing steel into the concrete. Referred to as a D-region, plane sections may not be remaining plane in this location. Therefore, another task of the research team was to instrument the end regions of seven full-scale beam specimens and compare experimentally measured strains with strains determined through the use of the classical beam theory.

Based on the findings of the literature review, early-age material testing, and full-scale beam tests, the research team obtained a better understanding of the early-age properties of concrete and mechanics of prestress transfer. As a result structural engineers should be able to calculate stresses in the end regions of pretensioned girders and specify design strengths with better accuracy.

1.3 OVERVIEW OF RESEARCH: REPORT ORGANIZATION

To begin with, a literature review was conducted in order to gain insight into current allowable tensile stress limits and fabrication techniques. A brief summary of the literature survey is included in Chapter 2. A review of the current code provisions and their origins are also included in Chapter 2.

A series of preliminary material tests were conducted at the Ferguson Laboratory. Concrete that was used in the fabrication of full-scale Type IV girders was collected from four different precast manufacturers and tested at the Ferguson Laboratory. A complete overview of the material testing program is included in Chapter 3. Data collected from these material tests provided good information of the early-age behavior of concrete made with Type III cement. In general, the concrete mixes collected from the four plants behaved consistently as would be determined by conventional empirical equations. Results of these tests are presented and discussed in Chapter 4.

Seven beam specimens were fabricated and instrumented with numerous strain gauges located variously along the height, length, and surface. For all specimens, strain data was used to compare typical strains derived from the " $P/A \pm Mc/I$ " expression with experimentally measured values. A complete overview of the experimental program is included in Chapter 3. The results collected from the full-scale beam specimens are presented and discussed in Chapter 4.

The research team determined that "plane sections remain plane" was a valid assumption for sections located where cracking had been observed; at least from the standpoint of a structural engineer wishing to determine the behavior of a Type IV girder. Predicting the amount of tensile stress at which a beam specimen cracks was another matter. Some beam specimens cracked with an extreme fiber tensile stress considerably lower than that which conventional wisdom suggests as being acceptable. This prompted closer scrutiny into the differences between control specimens and the in-situ concrete they are supposed to represent. A discussion of the contributing factors to cracking is included in Chapter 4.

Finally, the allowable stress limits specified in AASHTO are evaluated based on historic data and data collected as part of the current research project. Contributing factors to the cracking problem are identified and recommendations made to both eliminate and reduce crack widths. Recommendations to both prevent and control cracking are discussed in Chapter 4. Conclusions and recommendations are summarized in Chapter 5. As a result TxDOT design engineers should be able to estimate stresses in the end regions of pretensioned girders with greater assurance and accuracy.

CHAPTER 2

Literature Review

2.1 INTRODUCTION

The objective of this literature review is to gain insight into the origins of the current design provisions. When designing concrete members engineers use code equations that are based on theoretical and empirical background knowledge. Assumptions are made about material behavior and geometric properties, and then verified with experimental data. Included in this chapter is a comparative summary of the general body of knowledge that is used in formulating the current allowable tensile stress limits.

2.2 ELASTIC STRESS DISTRIBUTION

In order to simplify the design process, engineers utilize the assumption that the sections of a member remain plane as it bends in flexure (referred to as Bernoulli's hypothesis). Consider Figure 2-1, since the bending moment is the same at any cross section, the member will bend uniformly.

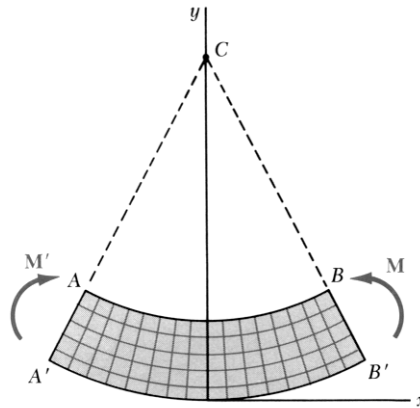


Figure 2-1 Bernoulli's hypothesis: plane sections remain plane.

The line AB , which was originally a straight line, will be transformed into an arc of center C , and so will line $A'B'$. It follows that any cross section perpendicular to the axis of the member remains plane.

The application of an axial load produces a uniform deformation. Applied in combination with a bending moment, plane sections still remain planar. As long as the stresses remain in the elastic range of the material, the maximum stress can be determined using the elastic flexure formula (Equation 2.1) as illustrated in Figure 2-2.

$$f_{max} = \frac{P}{A} \pm \frac{M \cdot c}{I} = \frac{F_o}{A} \pm \frac{F_o \cdot e \cdot c}{I} \quad (2-1)$$

Where,

M = Moment

c = Distance from neutral axis to extreme fiber

e = Eccentricity of prestressing force

I = Moment of inertia

P = Axial load

F = Force due to prestressing

A = Cross - sectional area

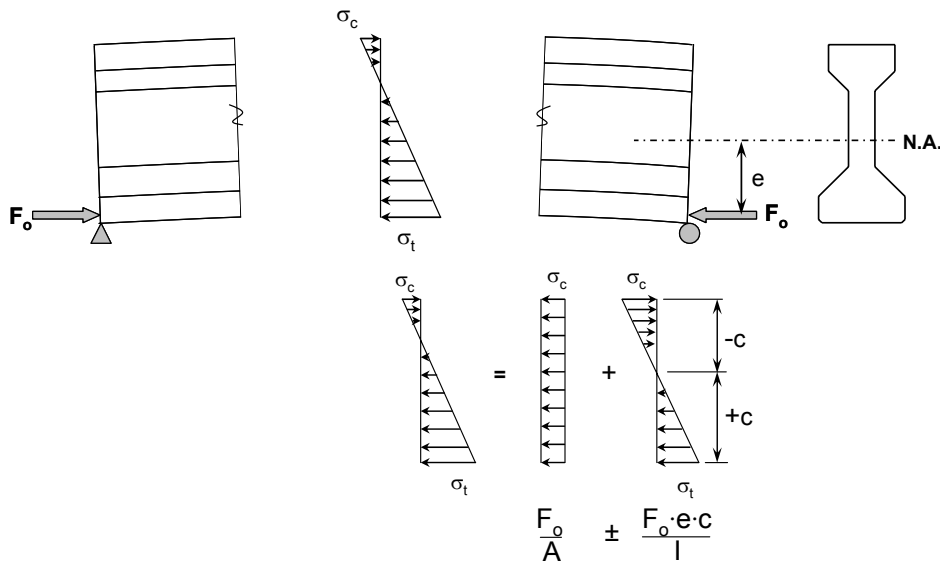


Figure 2-2 AASHTO Type IV beam loaded eccentrically, linear elastic stress distribution.

Regions of a member where Bernoulli's hypothesis is valid are referred to as "B-regions". The above method is not applicable where the strain distribution is significantly nonlinear; such as regions near concentrated loads, corners, bends, and other geometric discontinuities. These regions are referred to as "D-regions". To help illustrate the boundary between B and D-regions, consider the elastic stress trajectories of the Type IV beam shown in Figure 2-2. Loads on one side of the structure must find their counterpart on the other (Figure 2-3). The loads begin and end at the center of gravity of the corresponding stress diagram and tend to take the shortest possible streamlined way in between. Within this region of discontinuity, plane sections do not remain plane (Figure 2-3 b).

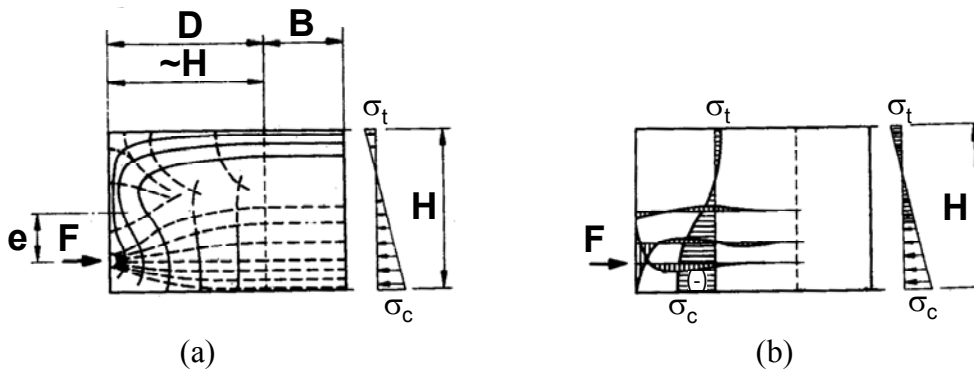


Figure 2-3 Typical D-region (a) elastic stress trajectories; (b) elastic stresses (Schlaich et al. 1987)

Typically, the length of a D-region is assumed to extend approximately a distance, H from a discontinuity (54-inches in the case of a Type IV beam). Figure 2-3 illustrates that at a distance H and greater, from the end of the beam, stresses are distributed in a linear manner. At a distance $H/2$, stresses are still distributed fairly linearly despite being located within the D-region. However, at a distance less than $H/2$, stresses are not flowing linearly. They are deviating significantly from the linear stress distribution and are certainly not remaining planar.

As a result, seven full-scale beam specimens were fabricated and instrumented in order to evaluate the extent of their D-regions and its contribution to the cracking problem. Cracks that had been observed in the field were typically located at a distance of 4-feet from the beam's end. Note that such a distance may possibly be located within the D-region of a 54-inch deep beam. It is important to understand the role that the "plane sections remain plane" assumption may contribute to the cracking problem.

2.3 BACKGROUND ON PRESTRESSED CONCRETE

In order to understand the fundamentals of prestressed concrete it is first necessary to understand some key concepts about concrete in general. Concrete is strong in compression but weak in tension. Its tensile strength varies from 8 to 14-percent of its compressive strength. Due to such low tensile strength, a conventionally reinforced member will develop flexural cracks at an early stage of loading. In order to reduce or prevent such cracks from developing in prestressed members, a compressive force is imposed in the longitudinal direction of the structural element. The purpose of precompressing a member's tension zone is to eliminate or reduce the tensile stresses experienced at service loads.

In prestressed concrete construction, high-strength reinforcement ($f_{pu} = 270$ -ksi) is used and this reinforcement is tensioned prior to the application of external loads. The application of an external load is resisted by a member's internal equilibrium of forces. Prior to the application of an external load a large compressive stress exists in pretensioned concrete. As an external load is applied, the resulting internal equilibrium of forces will transfer compressive stress from the bottom to the top fiber until the bottom fiber reaches its cracking stress. The bottom fiber of a conventionally reinforced member will experience its cracking stress under the application of a

relatively small external load. Figures 2-4 and 2-5 illustrate the equilibrium of forces in a conventionally reinforced and pretensioned member. The ultimate capacity of a prestressed member is the same as a non-prestressed member because the internal forces are essentially constant as soon as the reinforcement has yielded. By prestressing the reinforcement the engineer can actively control the stress in the reinforcement and the deformation of the structure without adversely affecting the member (Collins and Mitchell 1997).

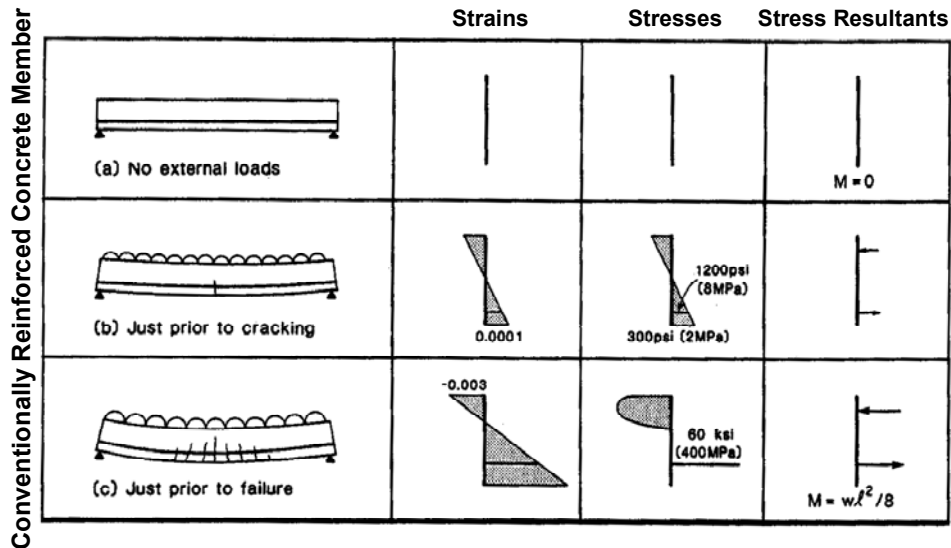


Figure 2-4 Behavior of a conventionally reinforced concrete beam. (Collins and Mitchell 1997)

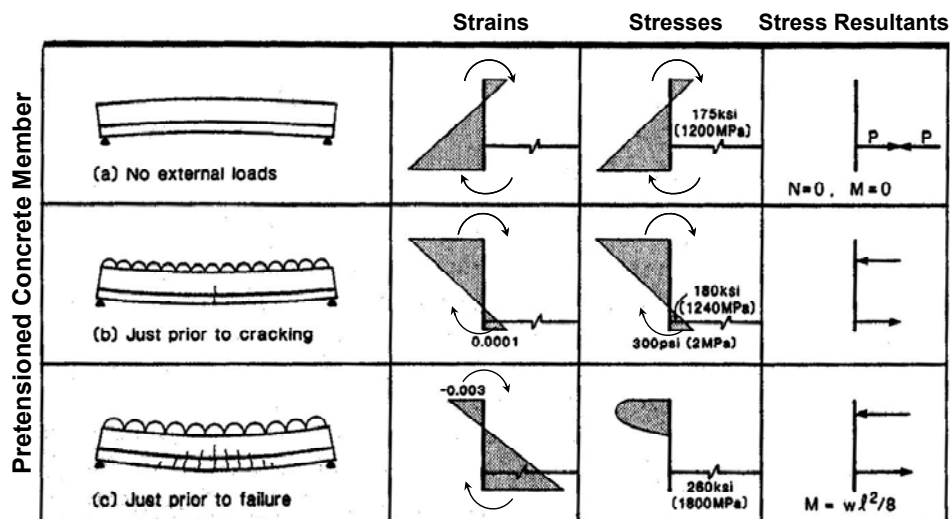


Figure 2-5 Behavior of a pretensioned concrete beam. (Collins and Mitchell 1997)

It is important to recognize that the cracking stress is solely a function of concrete's cracking capacity. Reinforcing steel does not prevent concrete from cracking. It controls cracks from widening once they have formed.

Since prestressing can be used to minimize or eliminate cracking at service loads and control deflections, it results in more slender structures. For example, a prestressed one way floor

slab can have a span-to-depth ratio of 45 to 1 which is about 60% more than the ratio possible with a non-prestressed one-way floor slab (Collins and Mitchell 1997).

However, the risk involved when prestressing a member is that other unwanted tensile stresses may be induced into the system. It is most effective to apply a prestressing force to a section with some eccentricity. A properly stressed member will utilize eccentricity to induce compression on the bottom surface and little to no tension on the top surface. The problem with loading a concrete member eccentrically is that tensile stresses on the top surface may exceed the tensile strength. Since concrete is weak in tension it takes a relatively small amount of stress to reach the cracking capacity. This phenomenon is what some prestressed beam manufacturers are experiencing in Texas: cracking at release due to tensile stresses caused by eccentricity.

When designing a pretensioned concrete member, it is necessary to understand the mechanics of stress transfer and material properties. An engineer must be able to specify the strength of concrete depending on the magnitude of stress applied at a cross section. Extensive research has been conducted on this topic over the last century. The expressions used by design engineers to define geometric properties and material behavior have been well established and evaluated. For example, the relationship between the compressive and tensile strength of concrete has been extensively studied in order to simplify the design process. After all, it is more convenient for an engineer to require verification of one material property, concrete compressive strength, rather than two. As it turns out, the applicability of this relationship is an important aspect of the current research project.

There are many variables affecting the results attained during research; including specimen geometry, boundary conditions, mix design, curing and preparation methods. Therefore, previous research that has formulated current design provisions will be evaluated in detail and used as a basis of comparison for the current experimental program.

2.4 PREVIOUS RESEARCH OF THE TENSILE STRENGTH LIMIT

Prediction of the tensile stress at which concrete cracks is an important aspect of this research project. A tensile stress limit can only be established if the tensile strength of concrete can be predicted reliably. As a result, unwanted cracking can be prevented. Typically an engineer will assume concrete's tensile strength based on an empirical relationship with its compressive strength. There are many variables that are not included in the empirical relationship between tensile and compressive strength. Even tests of cylinders prepared from identical mix designs under similar conditions exhibit a fair amount of variability. It is important to identify the maximum amount of variability expected so that engineers can determine whether or not a structure will crack. Accordingly, they can either design the structure to resist cracking or specify sufficient reinforcement to control cracking.

Concrete tensile strength can be measured three different ways: (i) direct tensile strength (non-standard); (ii) splitting tensile strength (ASTM C496); (iii) or flexural tensile strength also referred to as modulus of rupture (ASTM C78) (Figure 2-6).

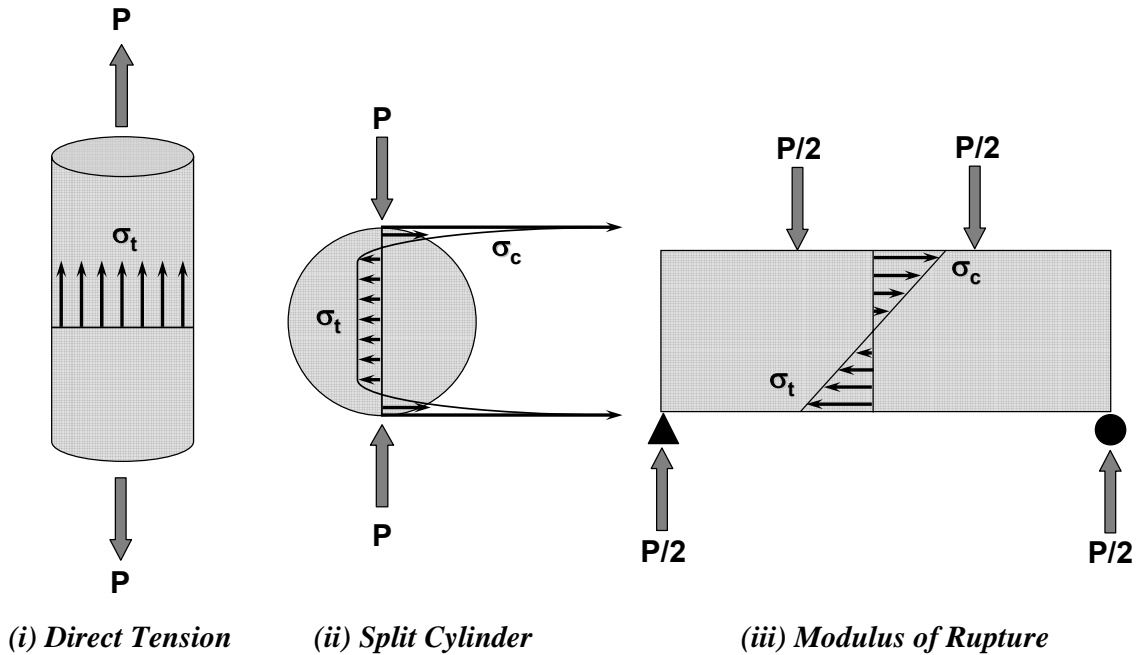


Figure 2-6 Tensile strength of concrete.

Depending on which method is used, the maximum stress at which concrete fails in tension varies significantly. The average stress at which concrete fails is generally assumed to be $4\sqrt{f'_c}$, $6\sqrt{f'_c}$, and $7.5\sqrt{f'_c}$ for the direct tension, split cylinder, and modulus of rupture tests respectively. The reason that there is such a varied difference in the strength values is due to the differences in the strain gradients. Take for example the strain gradients shown in Figure 2-6. The tensile strength of a concrete specimen decreases as the volume of the concrete that is highly stressed in tension increases. It can be concluded that when the size of a modulus of rupture (MOR) beam specimen becomes very large the strain gradient diminishes and the MOR strength approaches the direct tensile strength. Compare the strain gradient for a standard MOR beam to that of a Type IV girder (Figure 2-7).

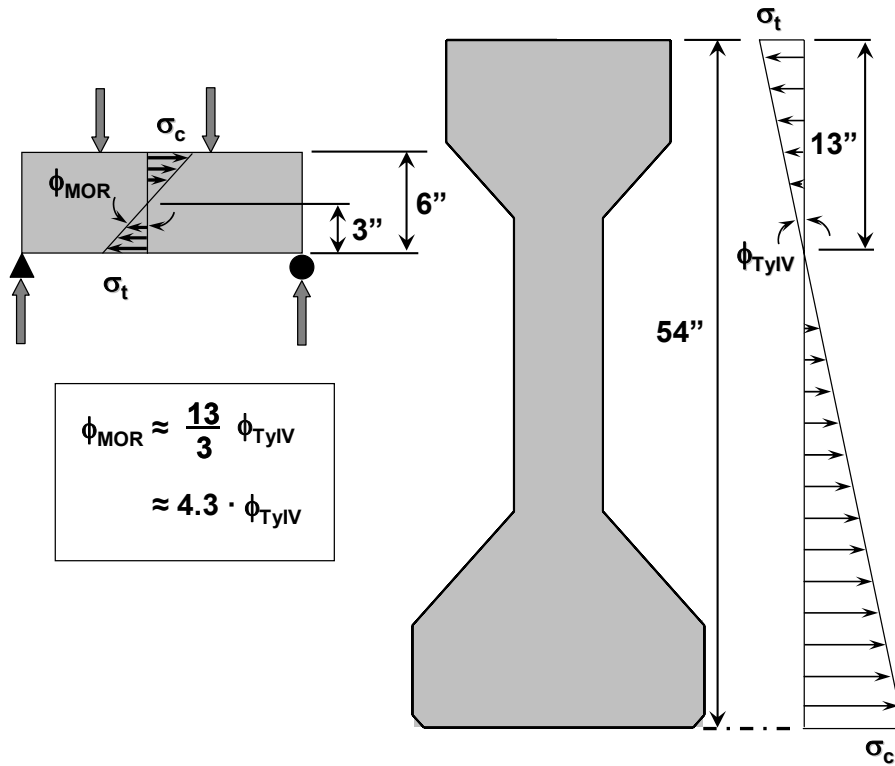


Figure 2-7 Difference in tensile strain gradient for standard 6" beam and pretensioned Type IV girder.

Within the end region, the height of a Type IV girder that is in tension is approximately 13-inches; resulting in a strain gradient over 4-times shallower (Figure 2-7). Thus, the strain gradient of a Type IV girder is approaching the uniform strain profile associated with a direct tension test. So, it can be theorized that the average extreme fiber tensile strength of a Type IV beam specimen is less than $7.5 \sqrt{f'_c}$ yet greater than $4 \sqrt{f'_c}$.

Because the short Type IV beams that cracked did so due to inadequate flexural-tensile capacity, experimental data that comprises the body of knowledge on the flexural-tensile capacity of concrete is examined.

Most tests are performed at the standard time of 28-days on 6x6x21-inch beam specimens (MOR test). As shown in Figure 2-3, the load is applied on the specimens at their third-points creating a region of constant moment in the middle third of the span. The Type IV beams that experienced cracking are 54-inches deep, between 20 and 60-ft long, I-shaped, have only cured for 24-hours or less, and the load is applied as a constant moment along almost the entire length. These differences likely affect the empirical relationship between the compressive and cracking stress of concrete. This relationship is very important as it influences the allowable compressive stress specified during design. In order to explore the affects of these variables a thorough literature search was conducted. A brief summary of the previous research carried out to determine the influence of compressive strength on the tensile strength is given below.

Gonnerman and Shuman (1928) tested 1760 6-inch cylinders and 7x10x38-inch plain concrete beams with average compressive strengths varying from 200 to 9200-psi (included in

Figure 2-8). It was concluded that moist-cured specimens had a higher value of modulus of rupture than air-dried specimens.

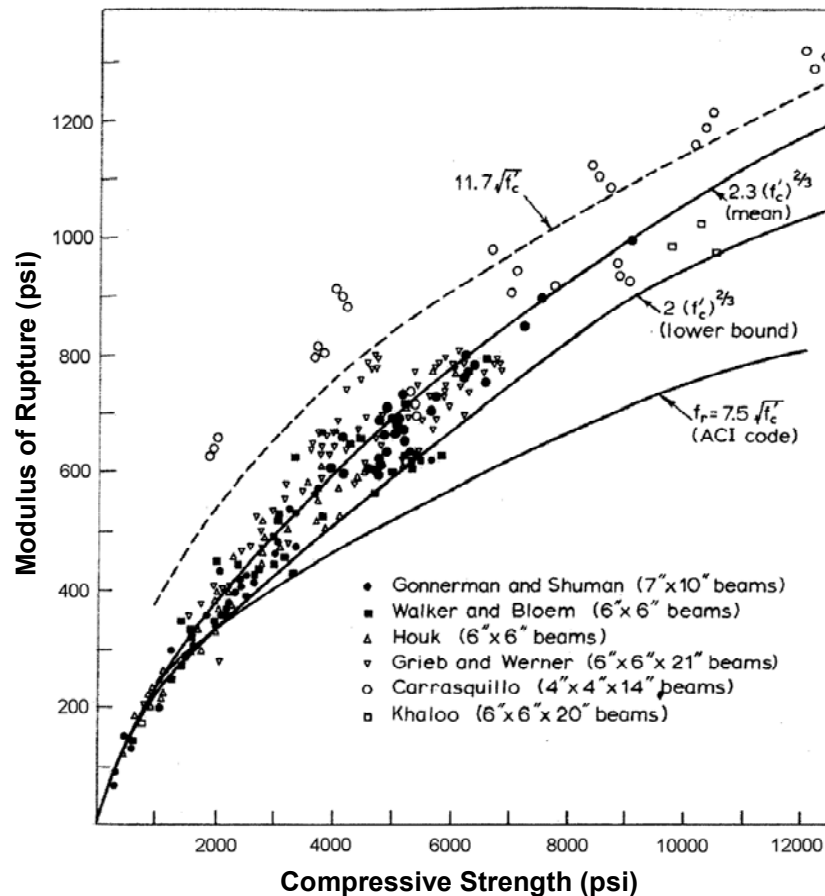


Figure 2-8 Beam flexural tensile strength vs. compressive strength (Shah and Ahmad 1985).

Kaplan (1959) tested 114 4x4x20-inch concrete beams (Figure 2-9). Mixture designs varied cement to aggregate ratios and were comprised of 13 different types of coarse aggregates. The beam specimens of each mix were tested at 7, 28, and 91-days. The 28-day concrete compressive strengths varied from 1880 to 11,460-psi. He reported that the aggregate properties affecting the flexural-tensile strength of concrete were shape, surface texture, and modulus of elasticity with modulus being the single most important factor affecting flexural strength. Although for concrete with the greatest flexural strength, surface texture had the predominating influence. He theorized that the increase in exposed surface area associated with a rougher surface texture resulted in a greater adhesive force between the cement matrix and aggregate; resulting in a higher concrete flexural strength. The aggregates used were generally stronger than the concrete and no relationship between the strength of coarse aggregate and the strength of concrete was established. The upper limit to the flexural strength of the concrete was set by the strength of the mortar. Presence of coarse aggregate generally reduced the flexural strength of concrete to below that of the mortar. Yet, concrete compressive strength was generally greater than that of the mortar; the presence of coarse aggregate therefore contributed to the compressive

strength of concrete. Depending on the aggregate type, a 40-percent difference in flexural strength was found for the same concrete mix.

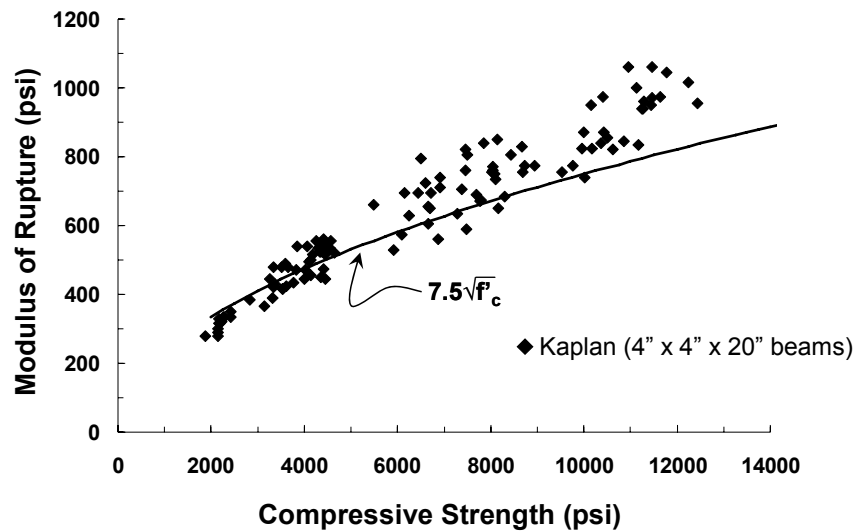


Figure 2-9 Beam flexural tensile strength vs. compressive strength (Kaplan 1959).

Walker and Bloem (1960) tested 128 moist-cured 6x6x36-inch concrete beams and 6x12-inch cylinders comprised of various water cement ratios and sizes of coarse aggregate (Figure 2-10). All specimens were moist cured and tested at 7, 28 and 91-days. Cement content varied between 4 and 8-sacks per cubic yard. Aggregate size varied between 3/8 and 2.5-inches. They showed that the size of the coarse aggregate exerted an influence on the concrete strength independent of the water-cement ratio. For a given water cement ratio, little or no strength advantage is gained from use of aggregate larger than 3/4-inch. The decrease in strength resulting from the use of large-sized aggregate was most pronounced in the concretes of higher cement ratios. Tests at 7, 28, and 91-days revealed a relatively small effect of age on the size vs. strength relationship in spite of differences in strength with age.

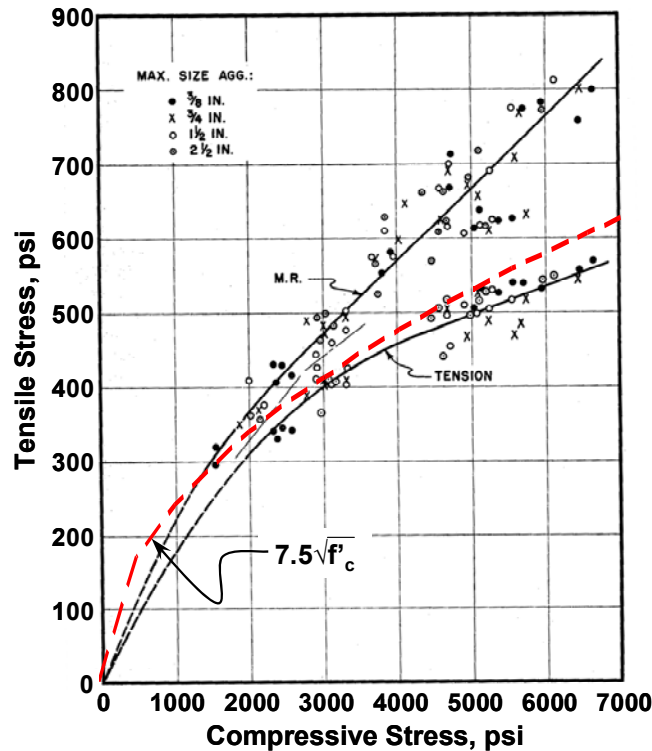


Figure 2-10 Splitting and beam flexural tensile stress vs. compressive stress (Walker and Bloem 1960)

Grieb and Werner (1962) tested more than 600 specimens made during a 10-year period using concrete made of natural, crushed, or lightweight aggregates with a 1.5-inch maximum size (included in Figure 2-8). Compression and split cylinder tests were conducted with 6x12-inch cylinders and flexural specimens were 6x6x21-inch beams. It was observed that the tensile strength was affected more by a change in the curing conditions (dry vs. moist-curing) than by a change in the compressive strength.

Carsquillo et al. (1981) tested 27 4x4x14-inch flexural beam specimens with compressive strengths ranging from 3000 to 12,000 psi (Figure 2-11). The maximum aggregate size was 3/4-inch and all mixes contained Type I cement. Specimens were moist cured between 7 to 28-days and tested between 7 to 95-days. Carsquillo et al. (1981) suggested that the modulus of rupture for concrete to be calculated as $11.7\sqrt{f'_c}$. For high-strength specimens, a maximum reduction of 26-percent in the 28-day modulus of rupture was observed when the specimens were subjected to drying after 7 days of moist-curing. In general, a better correlation between the modulus of rupture and the compressive strength was obtained at later test ages (28 and 95-days). It was also reported that the tensile strength of high-strength concrete is more sensitive to drying than normal-strength concrete.

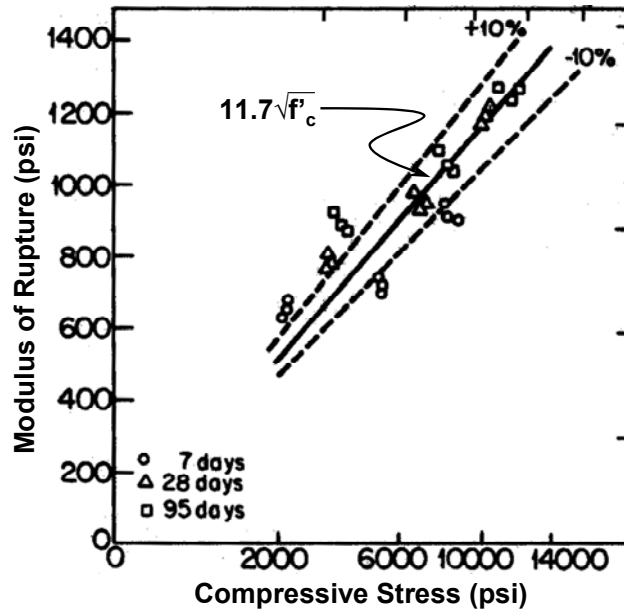


Figure 2-11 Beam flexural tensile stress vs. compressive stress (Carasquillo et al. 1981)

Mirza et al. (1979) examined 588 sets of compression cylinders and flexural beams (Figure 2-12). Based on a regression analysis, Mirza et al. (1979) proposed the mean modulus of rupture be taken as $8.3\sqrt{f'_c}$ with 20-percent variability. Specimens were made with Type I and Type III cements, with a water-cement ratio between 0.39 and 0.74, and an aggregate size of 3/8 to 1.5-inch. The data points presented by Mirza et al., on average, are lower and more scattered than data presented by other researchers. The overlying theme of the research conducted by Mirza et al. (1979) was to statistically model the differences between the strengths of in-situ and control specimen concrete. Variables included differences in volume, placement, and rate of loading.

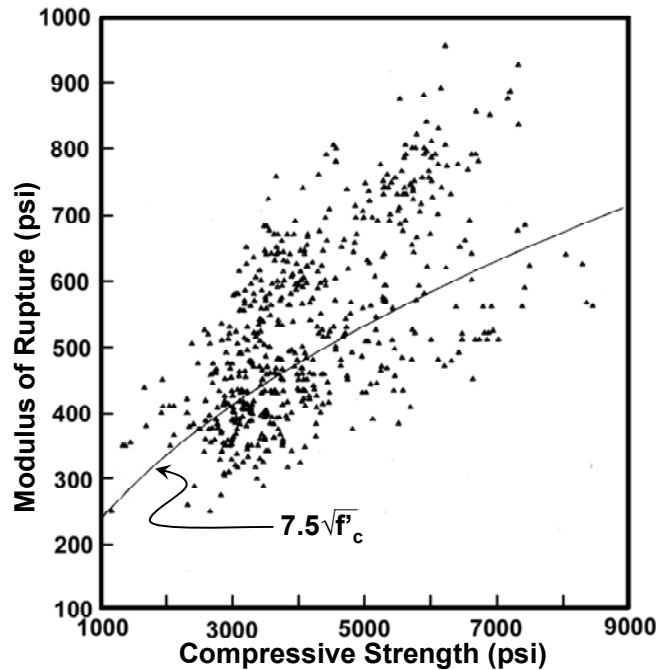


Figure 2-12 Beam flexural tensile strength vs. compressive strength (Mirza et al. 1979).

Raphael (1984) examined 12,000 individual results from direct tension, split cylinder, and modulus of rupture tests. The tests he examined were conducted by Gonnerman and Shuman (1928), Walker and Bloem (1960), Grieb and Werner (1962), and Houk (1965) (Figure 2-8). He proposed that the modulus of rupture be taken as $2.3(f'_c)^{2/3}$ (f'_c in psi); much higher than $7.5\sqrt{f'_c}$ (Figure 2-8). This relationship was proposed for concrete compressive strengths up to 9000-psi. The same relationship was recommended by Shah and Ahmad (1985) for predicting the modulus of rupture in terms of concrete compressive strengths up to 12,000-psi.

Khan et al. (1996) tested 4x4x16-inch beam specimens and 4x8-inch cylinders (Figure 2-13). Tests were performed from very early ages (less than 24 hours) until 91-days. Concrete strengths varied from 4300 to 14,500-psi. Specimens were temperature match cured in a water bath, seal cured with three layers of polyethylene, or air dry cured under ambient conditions. The compression and modulus of rupture tests were carried out at frequent intervals during the first 3-days to determine the compressive and tensile strength gains with age. For a given concrete mix, specimens that had been temperature match-cured typically resulted in significantly greater flexural strengths than specimens that had been sealed or air-dried cured. This was particularly apparent during the first 3-days. Khan et al. (1996) concluded that the current ACI Code expression for the modulus of rupture overestimates the modulus of rupture for very early-age concrete with compressive strengths less than 4000-psi and underestimates the modulus of rupture for compressive strengths greater than 4000-psi.

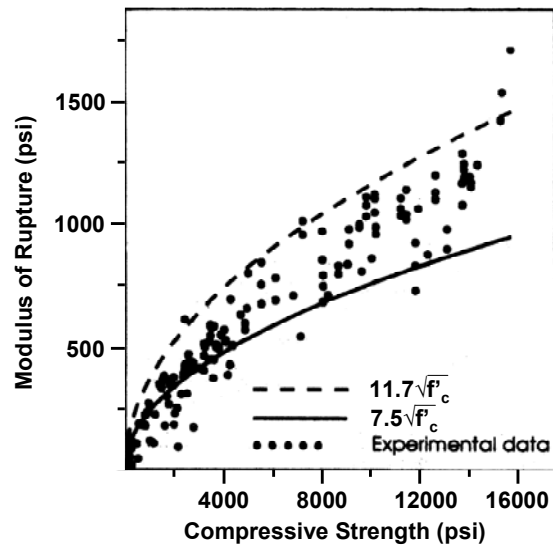


Figure 2-13 Beam flexural tensile strength vs. compressive strength (Khan et al. 1996)

Mokhtarzadeh and French (2000) tested a total of 280 6x6x24-inch flexural beam specimens from 90 high strength concrete mixes (Figure 2-14). The 28-day compressive strengths ranged from 7500 to 15,360-psi. The concrete mixtures designs contained either Type I or Type III cement and the admixtures used included silica fume, fly ash, and high range water reducer (superplasticizer). Six different types of coarse aggregate were investigated including two types of limestone, round river gravel, partially crushed river gravel, and granite. Specimens were either heat-cured or moist-cured. The heat-curing process was simulated using an electronically controlled environmental chamber programmed according to the curing procedure followed by precast prestressed concrete beam manufacturers. Moist-cured specimens were placed into lime saturated water immediately after casting. Mokhtarzadeh and French (2000) reported that the type of curing had a significant effect on the modulus of rupture tests with the moist-cured specimens exhibiting higher flexural tensile strengths. Taking into account the large amount of scatter in the data, the average modulus of rupture of moist-cured specimens appears to be approximately 30-percent larger than that of heat-cured specimens. Mokhtarzadeh and French (2000) suggested that the drying shrinkage strains in heat-cured beams added to the flexural tensile strains causing the heat-cured beams to fail at a lower load. Tensile strength values were between 5 and 8-percent of the compressive strength indicating the brittle nature of high strength concrete.

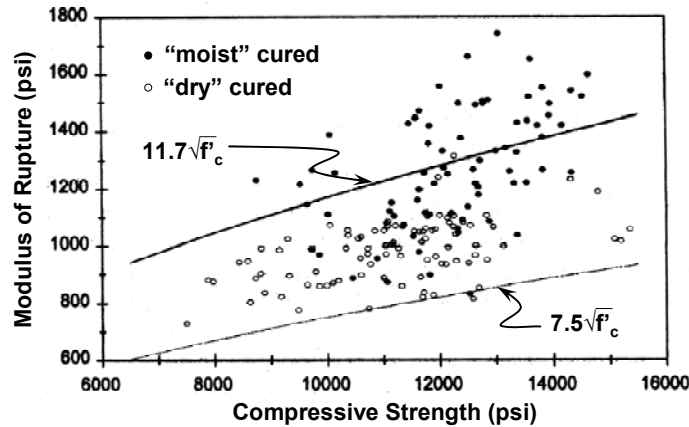


Figure 2-14 Beam flexural tensile strength vs. compressive strength (Mokhtarzadeh and French 2000)

Hueste et al. (2004) tested the modulus of rupture of 35 6x6x20-in beam specimens as part of a research project sponsored by TxDOT (Figure 2-15). Specimens were collected from three geographically different precasters in Texas; considered to be representative of the eight precasters in Texas that produce prestressed precast bridge members. Concrete compressive strengths varied from 5900 to 9200-psi. After cast, specimens were covered with wet burlap and plastic tarp to supply moisture during the first 24-hours. Approximately 24-hours after cast specimens were transported back to the laboratory for final curing and testing. Immediately on arrival at the laboratory, specimens were removed from their molds, labeled, and stored in a moist room for final curing. Laboratory tests were conducted at the age of 7, 28, and 56-days. They reported that the allowable tensile stress permitted in the AASHTO LRFD Bridge Design Specification may be too conservative. The best fit to their data was $10\sqrt{f'_{ci}}$. However, they cite the fact that the cracking stress of an actual structural member could be less than the MOR of laboratory samples due to the difference in curing conditions between the field and the laboratory.

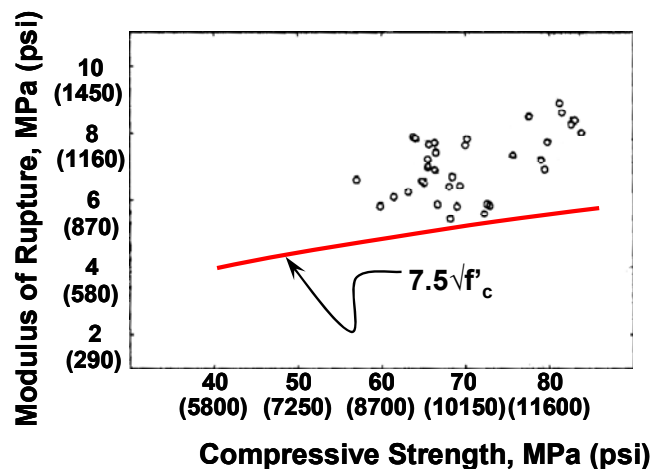


Figure 2-15 Beam flexural tensile strength vs. compressive strength (Hueste et al. 2004)

The flexural tensile strength versus compressive strength relationship is summarized and presented on one graph for all of the previously discussed research (Figure 2-16).

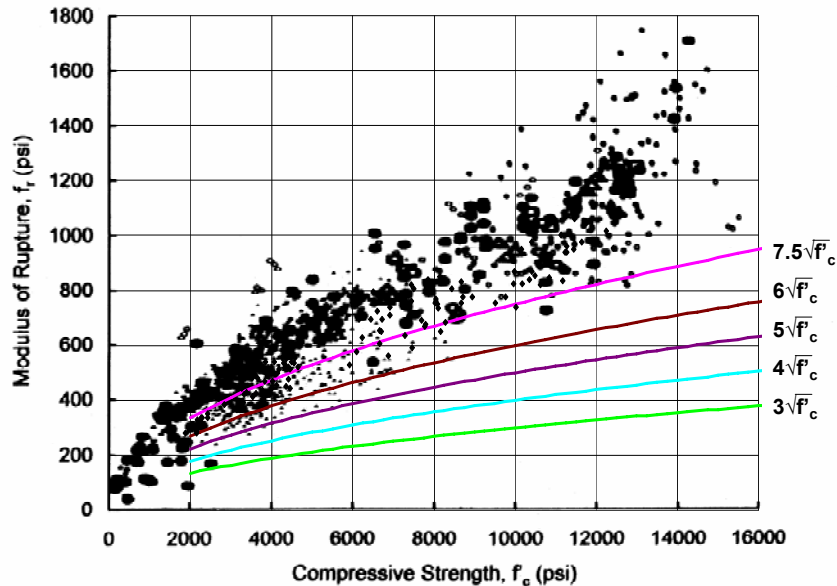


Figure 2-16 Summary of flexural tensile strength vs. compressive strength relationship (1330 data points).

As shown on the composite plot (Figure 2-16), a tensile strength equal to $7.5\sqrt{f'_c}$ is not necessarily a lower bound value, specifically for concrete compressive strengths in the range of 8000-psi and less. Data collected by Kaplan 1959 (Figure 2-9), Walker and Bloem 1960 (Figure 2-10), Mirza et al. 1979 (Figure 2-12), and Khan et al. 1996 (Figure 2-13) are the main contributors to the low tensile values shown in Figure 2.12. Recall that the research conducted by Mirza et al. (1979) intended to replicate in-situ conditions; and this resulted in relatively lower values than specimens fabricated in a laboratory. The data gathered by Khan et al. (1996) also resulted in relatively low values when those specimens were tested at very early ages (less than 24-hours). The research conducted by Kaplan (1959) and Walker and Bloem (1960) are similar to one another in the fact that they both considered the affects of different sizes of aggregate.

2.5 HISTORICAL DEVELOPMENT OF CONCRETE TENSILE STRENGTH LIMITS

2.5.1 Conventionally Reinforced Concrete

The modulus of rupture of concrete is an important property when determining a member's behavior under short-duration loads (instantaneous or service load deflections). In 1966, ACI Committee 435 (Deflections of Reinforced Concrete Flexural Members) suggested that the modulus of rupture value used to calculate deflections be between $7.5\sqrt{f'_c}$ and $12\sqrt{f'_c}$. The committee suggested the smaller factor 7.5 for general use.

Prior to that, not much emphasis was placed on the tensile strength of concrete. Similarly, not much emphasis was placed on the deformation behavior of concrete sections. Deflections were determined based on the properties of an uncracked section. Until 1967, ACI Committee 318 (Building Code Requirements for Reinforced Concrete) only required the tensile stress of concrete to be checked in unreinforced footings and walls. In ACI 318-67, the allowable tensile stress in flexure was limited to $1.6\sqrt{f'_c}$ (approximately 3% of the compressive strength for normal strength concrete).

In the 1971 version of the building code, ACI 318 saw the first major change in the procedure used to calculate deflections. Deflections were allowed to be calculated assuming that beam members were partially cracked along their length. The cracking moment used in making this calculation is determined using a modulus of rupture of concrete equal to $7.5\sqrt{f'_c}$. This procedure is identical to that which is specified today.

Along with the change to the procedure for determining deflections came a change in the allowable tensile strength of concrete. The tensile strength of concrete is typically neglected except it is allowed to be accounted for when the requirements prescribed in Chapter 18 of ACI 318 are met. Chapter 18 contains specifications for the design of prestressed concrete. A description of the history of allowable stresses for prestressed concrete follows.

2.5.2 Prestressed Concrete

The early development of the requirements of prestressed concrete saw opposing opinions on the importance of cracking. At the First United States Conference on Prestressed Concrete in 1951, the 600 participants heard considerable discussion as to the significance of cracking. Collins and Mitchell (1997) cite the following quotes heard at the conference:

It is my belief that the cracking point in a prestressed concrete beam should be accorded a respect similar to that shown for the yield point in structural steel design.

- W. Dean, Bridge Engineer, Florida State Road Department

[The cracking load should be called the transformation load since] at this load a normal prestressed girder is transformed into an ordinary reinforced girder.

- M. Fornerod, Chief Engineer, Preload Company

... a completely crackless concrete member is only better for a specific purpose if the presence of minute cracks is detrimental to its use.

- L. H. Corning, Portland Cement Association

... cracking load computed for prestressed concrete has practically no real significance except that it marks the spot where the stress and deflection curves begin to change their slope.

- T. Germundson, Portland Cement Association

In 1958, ACI-ASCE Committee 323 (ACI-ASCE 323), "Tentative Recommendations for Prestressed Concrete" suggested the following tensile stress limits before losses due to creep and shrinkage:

For members without non-prestressed reinforcement: $3\sqrt{f'_{ci}}$

For members with non-prestressed reinforcement provided to resist the tensile force in concrete; computed on the basis of an uncracked section: $6\sqrt{f'_{ci}}$

ACI Committee 318 (ACI 318-63) adopted the recommendations of ACI-ASCE Committee 423 (formerly ACI-ASCE 323) after introducing some minor modifications as follows:

Allowable tension stress in members without auxiliary reinforcement (unprestressed or prestressed) in the tension zone. $3\sqrt{f'_{ci}}$

Where the calculated tension stress exceeds this value $[3\sqrt{f'_{ci}}]$, reinforcement shall be provided to resist the total tension force in the concrete computed on the assumption of an uncracked section.

The allowable tensile stress limit for prestressed concrete changed slightly in the 1977 update to the ACI building code (ACI 318-77). Since then, the allowable tensile stress limits have remained essentially unchanged.

- (a) *Extreme fiber stress in compression* $0.6f'_{ci}$
- (b) *Extreme fiber stress in tension except as permitted in (c)* $3\sqrt{f'_{ci}}$
- (c) *Extreme fiber stress in tension at ends of simply supported members* $6\sqrt{f'_{ci}}$

Where computed tensile stresses exceed these values, bonded auxiliary reinforcement (non-prestressed or prestressed) shall be provided in the tensile zone to resist the total tensile force in concrete computed with the assumption of an uncracked section.

It is not explicitly stated why the allowable tensile stress was increased at the ends of simply supported members. Possibly, the consequence of cracking was determined to be less significant at the ends. Usually, engineers will either drape or debond tendons in order to decrease end eccentricity and meet allowable tensile limits. Debonding tendons may reduce the shear strength at the end of a beam. Therefore, it is possible that the allowable tensile strength limit was increased at the ends of beams in order to counteract the adverse effects of debonding.

An examination of the current AASHTO Bridge Design Specifications for Highway Bridges (AASHTO 2002) indicates that the 1958 ACI-ASCE Committee 423 recommendations were adopted and have remained virtually unchanged. With the exception of a slight modification to the tensile stress limit allowed when auxiliary bonded reinforcement is provided.

The extreme fiber tensile stress allowed before losses due to creep and shrinkage are prescribed by AASHTO as follows:

For members without bonded reinforcement: $200 \text{ psi or } 3\sqrt{f'_{ci}}$

For members with bonded reinforcement provided to resist the tensile force in concrete; computed on the basis of an uncracked section: $7.5\sqrt{f'_{ci}}$

Even though it is not explicitly stated, it can be safely assumed that the bonded reinforcement requirement is intended to control cracking at release for extreme fiber tensile stresses above $3\sqrt{f'_{ci}}$.

2.6 PREVIOUS RESEARCH ON THE MODULUS OF ELASTICITY

For the purposes of this research project, the modulus of elasticity is necessary in estimating stresses. More specifically, concrete strains are measured experimentally and the corresponding stress is inferred using Hooke's Law ($\sigma = E \cdot \epsilon$). This assumption is valid provided the stresses remain within concrete's proportional limit. The modulus is also crucial for estimating prestress loss due to elastic shortening. For high strength concrete a number of empirical relationships relating the modulus of elasticity to compressive strength have been proposed by various researchers. However, there is not much data relating the modulus of elasticity of high-early strength concrete to its compressive strength within the first 24-hours of curing. A brief summary of the research done to determine the influence of compressive strength and curing conditions on the modulus of elasticity is given below.

Pauw (1960) compiled applicable existing data from previous modulus of elasticity research (Figure 2-17). He proposed that the modulus of elasticity be expressed as a function of concrete's dry unit weight (ω) and compressive strength. At the time a standard test had not been adopted for determining the static modulus of elasticity. He proposed the modulus of elasticity to be taken to be:

$$E_c = 33 \cdot \omega^{3/2} \sqrt{f'_c} \quad (2-2)$$

$$(E_c = 57000 \sqrt{f'_c} \text{ for normal weight concrete})$$

Where,

E_c = Modulus of Elasticity of Concrete, psi

ω = air dry weight of concrete, pcf

f'_c = compressive strength of concrete

The equation he recommended was adopted in the 1963 version of the ACI 318 code and has since remained unchanged. He analyzed data for structural light-weight and normal-weight concrete mixes with compressive strengths ranging between 2000 and 7000-psi.

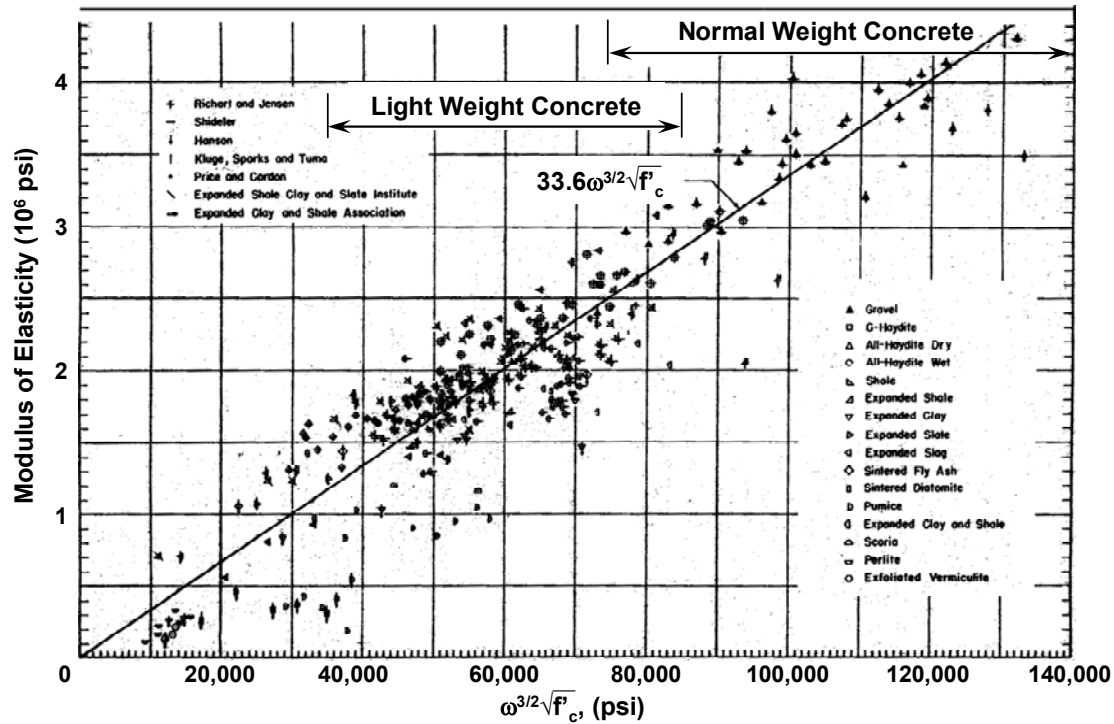


Figure 2-17 Modulus of elasticity of concrete as affected by density (Pauw 1960)

Mirza et al. (1979) analyzed 45 modulus of elasticity tests of normal weight concrete tested at the Portland Cement Association (Figure 2-18). Based on a regression analysis of this limited amount of data they determined that the secant modulus at 30-percent of maximum compressive strength to be taken as $60,400 \sqrt{f'_c}$. They also concluded that there was no significant statistical difference between the modulus of elasticity in tension and compression.

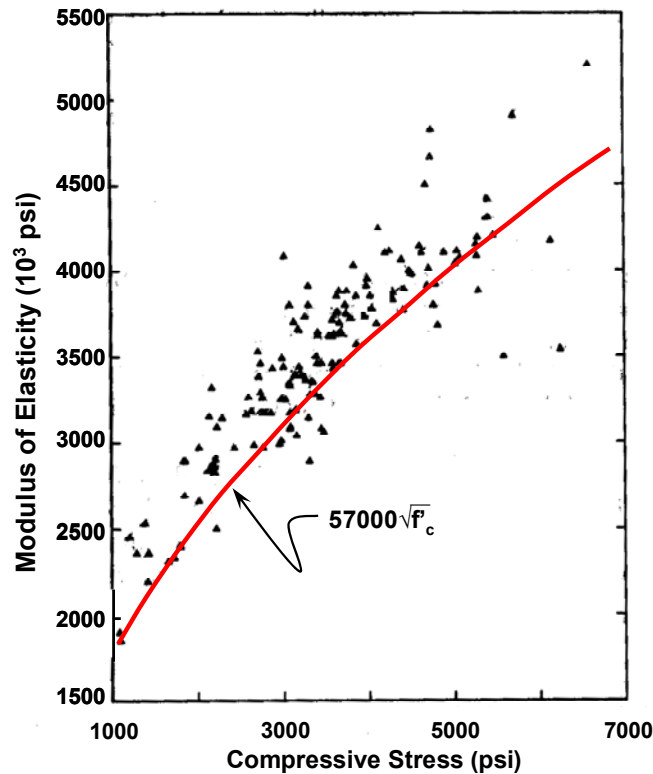


Figure 2-18 Modulus of elasticity vs. compressive stress (Mirza et al. 1979)

Carasquillo et al. (1981) reported modulus of elasticity values for 4x8-inch concrete cylinders tested at 53-days (Figure 2-19). Compressive strengths ranged between 4570 and 11,100-psi. Specimens were moist-cured for either 7-days followed by 50-percent relative humidity curing for an additional 21-days, or moist-cured for 28-days followed by 50-percent relative humidity for an additional 67-days. For concrete with compressive strengths greater than 6000-psi, Carasquillo et al. (1981) proposed that the modulus of elasticity be calculated using Equation 2.2.

$$E_c = 40,000 \sqrt{f'_c} + 1,000,000\text{-psi} \quad (2-3)$$

The same equation is recommended by ACI Committee 363 “State of the Art Report on High Strength Concrete”. Carasquillo et al. (1981) observed that the modulus of elasticity for high strength concrete is attributed to the stiffness of its mortar and its mortar-aggregate bond. They suggested that the behavior of high strength concrete is in many aspects similar to that of an intact rock specimen.

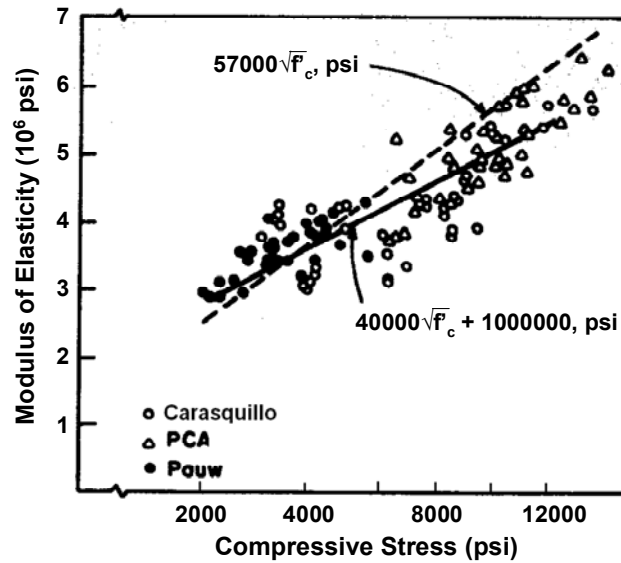


Figure 2-19 Modulus of elasticity vs. compressive stress (Carasquillo et al. 1981).

Mokhtarzadeh and French (2000) performed modulus of elasticity tests on 98 high strength concrete mixtures (Figure 2-20 and Figure 2-21). Specimens tested were 4x8 and 6x12-inch cylinders. 28-day compressive strengths ranged between 6000 and 19,500-psi. Of the 98 concrete mixtures, Type III cement was used in 90 and Type I cement was used in the other eight. Six different types of coarse aggregate were investigated; two types of limestone, round river gravel, partially crushed river gravel, and two types of granite. Several different curing conditions were examined for the specimens including: heat-cured and tested dry at 1, 28, 182, and 365-days; initial heat-cure followed by 1 to 3 day moist-cure; and moist-cured 7, 14, 28, 182, and 365-days. Mokhtarzadeh and French (2000) reported that the results from 314 sets of heat-cured specimens indicate that at 1 day, the modulus of elasticity was approximately 98-percent of its 28-day value. They concluded that the ACI 318 expression (Equation 2-2) overestimates the measured modulus of elasticity of 6x12-inch cylinders. The ACI 363 expression (Equation 2.3) was a better predictor for moist-cured specimens (Figure 2-20) and overestimated heat-cured test results (Figure 2-21).

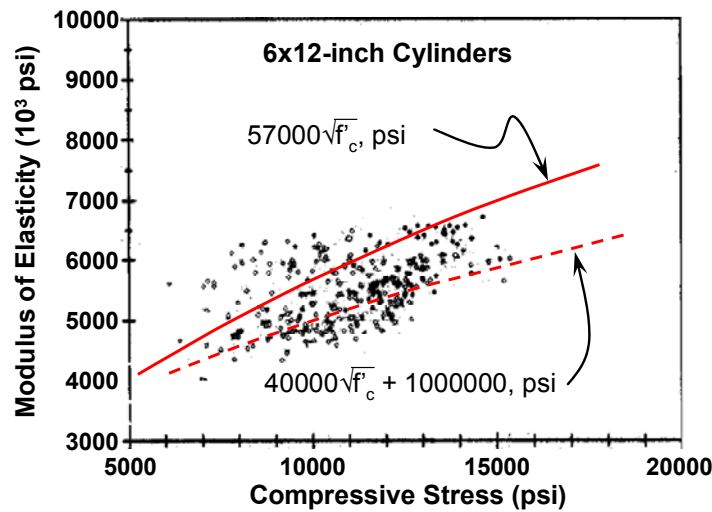


Figure 2-20 Modulus of elasticity vs. compressive stress, 6x12-inch moist-cured cylinders (Mokhtarzadeh and French 2000)

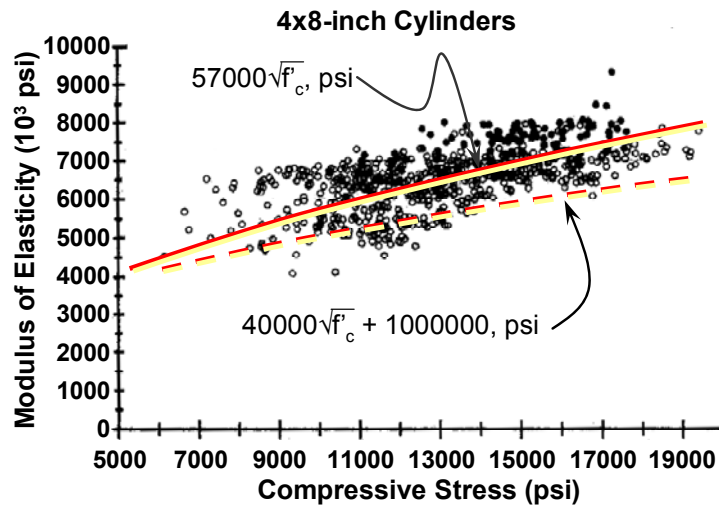


Figure 2-21 Modulus of elasticity vs. compressive stress, 4x8-inch heat-cured cylinders (Mokhtarzadeh and French 2000)

Hueste et al. (2004) tested the modulus of elasticity of 32 4x8-inch cylinders as part of a research project sponsored by TxDOT. Specimens were collected from three geographically different precasters in Texas; considered to be representative of the eight precasters in Texas that produce prestressed precast bridge members. Concrete compressive strengths varied from 5900 to 9200-psi. Specimens were cast in plastic molds and covered with plastic lids. Approximately 24-hours after cast specimens were transported back to the laboratory for final curing and testing. Immediately on arrival at the laboratory, specimens were removed from their molds, labeled, and stored in a moist room for final curing. Laboratory tests were conducted at the age of 7, 28, and

56-days. They determined that the modulus of elasticity was well predicted using the ACI 318 equation (Equation 2-2) and under predicted using the ACI 363 equation (Equation 2-3). They also found the modulus of elasticity to be highly dependent on the type of aggregate used in the production. Concrete made from crushed river gravel tended to have a higher MOE than concrete made from crushed limestone.

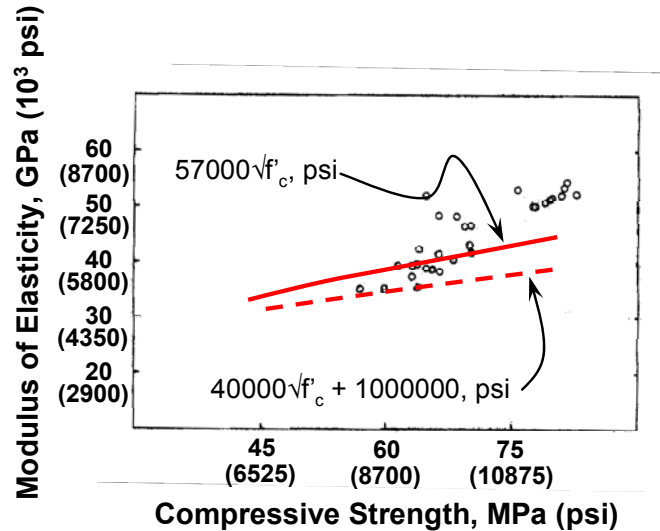


Figure 2-22 Modulus of elasticity vs. compressive stress, 4x8-inch cylinders (Hueste et al. 2004).

The modulus of elasticity versus compressive strength relationship is summarized and presented on one graph for all of the previously discussed research (Figure 2-23).

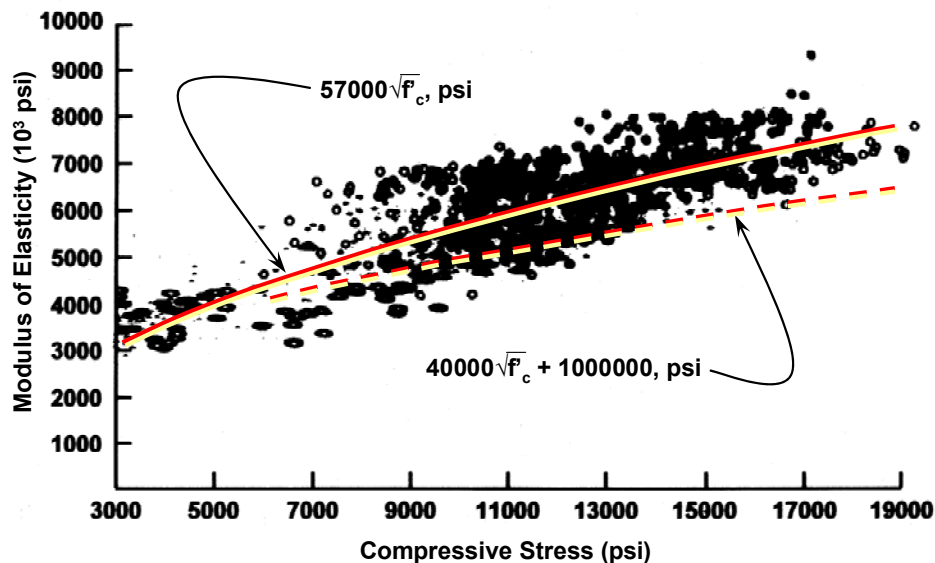


Figure 2-23 Summary of modulus of elasticity relationship.

As shown on Figure 2-23, the ACI 318 equation (Equation 2-2) appears to be a better predictor of the modulus of elasticity of concrete. The cloud of data is heavily influenced by the

4x8-inch cylinder data collected by Mokhtarzadeh and French (2000) (Figure 2-21). Mokhtarzadeh and French (2000) concluded that the ACI 318 equation underestimates the modulus of elasticity; but they were basing their conclusion on the 6x12-inch cylinder data. The ACI 363 equation was proposed by Carasquillo et al. (1981). Their research was based on modulus of elasticity data measured from 4x8-inch cylinders. So, it can be concluded that the size of the cylinder is not the sole contributor to the difference. Curing conditions are probably another influential factor. Cylinders that were used to formulate the ACI 363 expression (Equation 2-3) were comprised of Type I cement and were moist-cured for at least 7-days; followed by curing with 50-percent relative humidity until testing. Cylinders tested by (Mokhtarzadeh and French 2000) were often comprised of Type III cement and either heat-cured or dry-cured. Therefore, it can be theorized that heat-curing in addition to concrete mixtures containing Type III cement may result in a higher modulus of elasticity compared to a specimen consisting Type I cement that has been moist-cured for at least 7-days.

2.7 PREVIOUS RESEARCH ON THE USE OF MATCH CURING TECHNOLOGY

Match curing technology allows precast beam manufacturers to test cylinders that better represent the strength of their precast members. In general, a cylinder that is heated while curing will gain compressive strength faster than a cylinder that is cured without heat. An electronically controlled match-cured cylinder will cure at the same time vs. temperature profile as determined by a thermocouple located within a beam specimen. Through the course of the research project, it was brought to the attention of the research team that different precast manufacturers locate thermocouples in different locations based on variances in fabrication methodologies. Typically, manufacturers locate thermocouples at relatively cool locations within a precast element in order to conservatively determine the strength of concrete. However, very little information exists comparing the directly measured strength of a matched-cured cylinder with the strength of the in-situ concrete. In order to properly predict the tensile strength of concrete, it is relevant to understand the accuracy with which the strength of a match-cured cylinder represents the strength of in-situ concrete. The in-situ strength of concrete depends on many factors including curing conditions, mix proportions, size of element, compaction, and moisture state. Following is a discussion of the previous research on the match-curing of concrete.

Cannon (1986) tested 6-inch cubes that had been cured at a constant 68- °F. Additionally, he matched the curing temperature of a different set of cubes using a thermocouple located 2-inches below the surface of a 1-foot thick wall. Depending on the composition, he observed that the compressive strength of a match cured cube is approximately 50 to 100-percent greater than the strength of a cube cured at 68-°F up until 7-days. After seven days, the compressive strength of a match-cured cube was occasionally less than one cured at 68-°F. Finally, after 28-days the compressive strength of a match cured specimen was consistently 20 to 30-percent less than one cured at 68- °F.

Kehl and Carasquillo (1998) tested electronically match-cured and ambient air cured 4-inch cylinders of both normal and high strength concrete mixes. They used an electronic control system to model time vs. temperature curves representing various locations within AASHTO Type IV girders. The three locations they investigated were in the upper flange, lower flange, and the web. Maximum temperatures ranged between approximately 85 to 210-°F depending on the time of the year that the specimens were fabricated (Figure 2-24). The information shown in

Figure 2-24 is for a specimen that was fabricated in February. Therefore, due to the cool ambient air temperature, its maximum temperature was only about 150-°F.

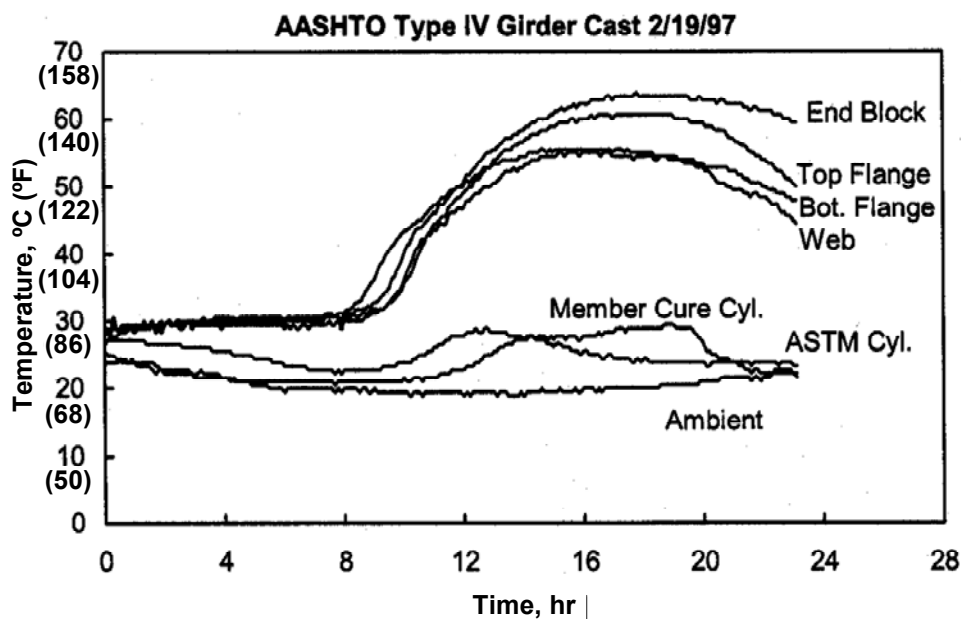


Figure 2-24 Curing temperature variation of a Type IV girder (Kehl and Carasquillo 1998).

Test specimens were both moist and dry (or “air”) cured. They found that the coolest spot in a section was in the web. They observed that the compressive strength of concrete begins to decrease as the maximum curing temperature exceeds 160 to 180-°F. Also, they observed that the modulus of elasticity of high performance concrete was affected very little by curing temperature. Finally, they concluded that specimens that were match-cured were more representative of the concrete in the member than were the control cylinders that had been cured next to the beam.

2.8 SUMMARY

Extensive research has been conducted in order to evaluate the mechanical properties of concrete. Variables that have been evaluated include: high-strength and normal-strength mixtures, various aggregate strengths and sizes, different cement types, maturity, and curing conditions. Even though there is not much data reported on the properties of high-strength concrete at very early ages, there is plenty of data available on mature concrete. Such information is useful as a basis of comparison with current results. More information regarding the early-age properties of concrete, specifically those which contain Type III Portland cement, is necessary in order to properly design precast prestressed structures. This material data is very important because in precast beam manufacturing operations engineers rely on concrete strengths to be developed as quickly as 12 to 18-hours after batching. It is a goal of the research team to better understand the differences between high-early strength and typical concrete mixture designs; including differences observed in the field as opposed to those in the laboratory.

Another variable that deserves more attention is the difference found between in-situ concrete and representative test specimens. The concrete strength attained from a test can vary

by as much as 20-percent depending on the level of quality control (Mirza et al. 1979). Mirza et al. (1979) cite factors such as segregation of aggregate and bleeding of water as two occurrences in deep members that result in a larger degree of uncertainty in in-situ concrete strengths. Raphael (1984) suggested that differential drying of a large mass of concrete may restrain shrinkage, thus inducing surface-level tensile stresses and lowering the in-situ tensile strength. Mohktarzadeh and French (2000) also observed lower flexural tensile strengths associated with dry-curing. Raphael (1984) cited a dam project where the tensile strengths of cores were sometimes 50-percent lower than the tensile strengths of laboratory specimens.

It is a goal of the research team to be able to identify the source of the Type IV cracking problem through systematic research. Therefore, it is necessary to be able to place data collected in the laboratory in the context of other historically gathered data. The allowable tensile stress limits prescribed by AASHTO are derived from vast amounts of previously conducted research.

Recommendations that remedy the end region cracking problem require complete understanding of the tensile stress limit. This knowledge will enable the research team to assess the validity of possible solutions. When using a model code, it is important to consider where the empirical formulas come from; what are the assumptions built into them; and how do they apply to the problem at hand. Also, previous research measuring the material properties of concrete will form a basis of comparison for the data collected as part of the current project. Finally, evaluating the different fabrication methods used by manufacturers of Type IV beams allows the research team to understand the assumptions being made in the field and how those assumptions may contribute to the cracking problem. All of these factors will be considered in the evaluation of the information collected as part of this research program.

CHAPTER 3

Experimental Program

3.1 INTRODUCTION

Design of test specimens, design of the prestressing facility, material testing, and instrumentation used to monitor the behavior of specimens are discussed in this chapter. The experimental program includes a series of full-scale pretensioned girders fabricated and tested at the Phil M. Ferguson Structural Engineering Laboratory at the University of Texas at Austin. This report details the results from seven full-scale beams fabricated at the Ferguson Laboratory.

3.2 BACKGROUND

The intent of the experimental program is to identify the cause of cracking in the end regions of short-span AASHTO Type IV beams and recommend practical solutions to eliminate the cracks or reduce the crack widths. An AASHTO Type IV beam is a 54-inch deep standard I-shaped section used by the Texas Department of Transportation (TxDOT). A TxDOT standard detail showing the geometry and reinforcing details for an AASHTO Type IV beam is located in Appendix A. Beams that exhibit cracking have a relatively short span length and highly eccentric strand locations. The span lengths vary between 20 and 60-feet and the strands are located approximately 23-inches from the center of gravity of the section (Figure 3-5). The cracking occurs immediately after release when the beams are lifted from the casting bed. The cracks are vertical, starting at the top flange, at a distance approximately 4-feet from the beam end. Cracking has been observed in beams both with and without block-out details (Figure 3-1 and Figure 3-2). The block-out is 4-foot long by 1.5-inch deep and is located at the ends of the top flanges. The purpose of the block-out is to accommodate a thickened slab along the end of a bridge deck at an expansion joint.



Figure 3-1 Cracking in the end of a Type IV beam, without block-out.

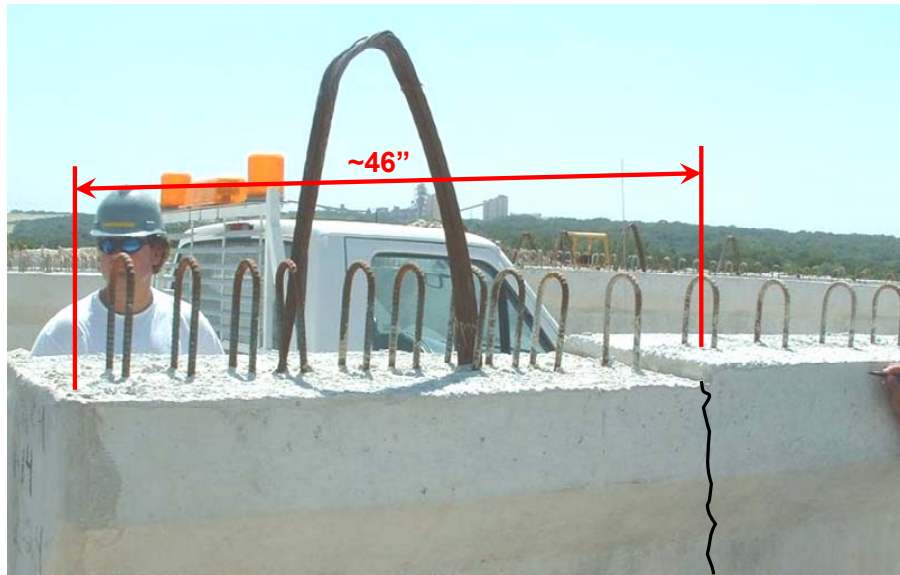


Figure 3-2 Cracking in the end of a Type IV beam, with block-out.

At release, calculated tensile stresses located in the end regions of short-span Type IV beams used in Texas are very close to the nominal tensile strength of concrete ($7.5\sqrt{f'_c}$). The tensile strength of concrete at an early-age can not be defined with empirical relationships derived from 28-day old concrete. Early-age material testing and a detailed literature review were conducted in order to better quantify the variability of the tensile strength of concrete. Early-age material testing that was conducted as part of this research project is discussed in Section 3.2.4.

What was also required was an investigation into the mechanics of stress transfer in the end regions of Type IV beams. Within these regions designers assume that plane sections remain

plane and the stress profile of a concrete section can be defined by the “ $P/A \pm Mc/I$ ” expression (Equation 3-2). This expression may or may not be valid within the zone of prestress transfer. One of the goals of the research team is to experimentally evaluate the validity of the expression in the end region of short Type IV beams with high eccentricities. A series of full-scale specimens were fabricated and tested at the Ferguson Laboratory. These specimens establish a comparison between experimentally measured and theoretically determined strain profiles. As a result, the degree of accuracy inherent in the “plane sections remain plane” assumption was evaluated (Section 4.6.2). Following is a detailed discussion of the theory that is used to determine the mechanics of prestress transfer.

3.2.1 Transfer Length of Prestressing Force

The force in a prestressing strand is transferred into the beam by the bond between the concrete and the strand. The length required to transfer the full prestressing force is called the “transfer length.” According to ACI 318 §12.9 (ACI 318-05) and AASHTO LRFD §5.11.4.2 (AASHTO 2004), the development length of seven-wire strand shall not be less than that required by Equation 3-1.

$$l_d = \left(\frac{f_{se}}{3} \right) \cdot d_b + (f_{ps} - f_{se}) \cdot d_b \quad (3-1)$$

Where,

f_{se} = Stress in prestressed reinforcement
after initial losses, ksi

f_{ps} = Stress in prestressed reinforcement
at nominal strength, ksi

d_b = Strand diameter, in.

l_d = Transfer length

The first term in the equation is the transfer length and the second term is the additional length required for the stress increase corresponding to the nominal strength. In lieu of more accurate information, the effective stress in the strand after initial losses, f_{se} can be taken to be equal to 170-ksi. Therefore, for 0.5-inch strand the transfer length of the prestress force is calculated as follows:

$$l_d = \left(\frac{170\text{ksi}}{3\text{ksi}} \right) \cdot (0.5\text{in}) = 28\text{in}$$

The prestressing force varies linearly from zero at the end of the beam to the full prestressing force after elastic shortening at the point of full transfer (Figure 3-3). When predicting the strain profile located at a distance less than the transfer length, it is necessary to reduce the applied force accordingly.

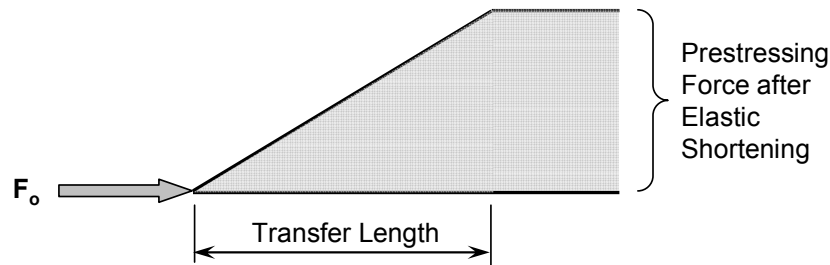


Figure 3-3 Prestressing Strand Transfer Length

Losses in prestressing force associated with elastic shortening are discussed in detail in Section 3.2.3. For now, it is important to note that losses are indirectly proportional to the modulus of elasticity of concrete. Thus, if the modulus of elasticity, or stiffness, of a beam increases then the losses decrease. If the stress in prestressed reinforcement after losses, f_{se} shown in Equation 3-1 were to be calculated, rather than assumed, then the transfer length would vary depending on the stiffness of the beam.

3.2.2 Allowable Stress Method: Classical Beam Theory

The allowable stress design method, currently used by designers of pretensioned concrete beams, utilizes a linear analysis of concrete cross-sections (ACI 318-05). For uncracked sections, stresses calculated at the extreme fibers are based on the assumptions that plane sections remain plane, and the stress-strain relationship for concrete is linear (Figure 3-4). Given the prestress force, its eccentricity, and cross-sectional properties, one can easily calculate the extreme fiber stresses for a pretensioned member.

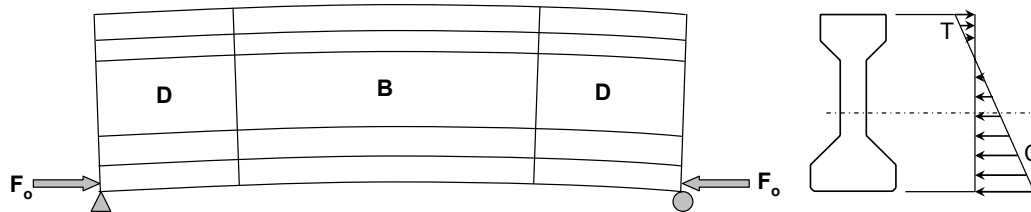


Figure 3-4 Linear-elastic stress distribution of pretensioned member

For example, consider the Type IV pretensioned beam shown in Figure 3-5. A typical section contains twelve low-relaxation strands, located two inches from the bottom of the beam. Assume that the force in each strand is 29-kips immediately after elastic shortening. For the sake of simplicity, disregard the dead weight of the beam. The top fiber tensile stress at transfer can be calculated as follows:

$$f_{top} = -\frac{F_o}{A_g} + \frac{F_o \cdot e \cdot y_t}{I_g} \quad (3-2)$$

Where,

F_o = Force in prestressing strands, kip

e = Eccentricity of strand force, in.

y_t = Distance from centroid to top fiber, in.

A_g = Area of gross section, in²

I_g = Moment of inertia of gross area, in⁴

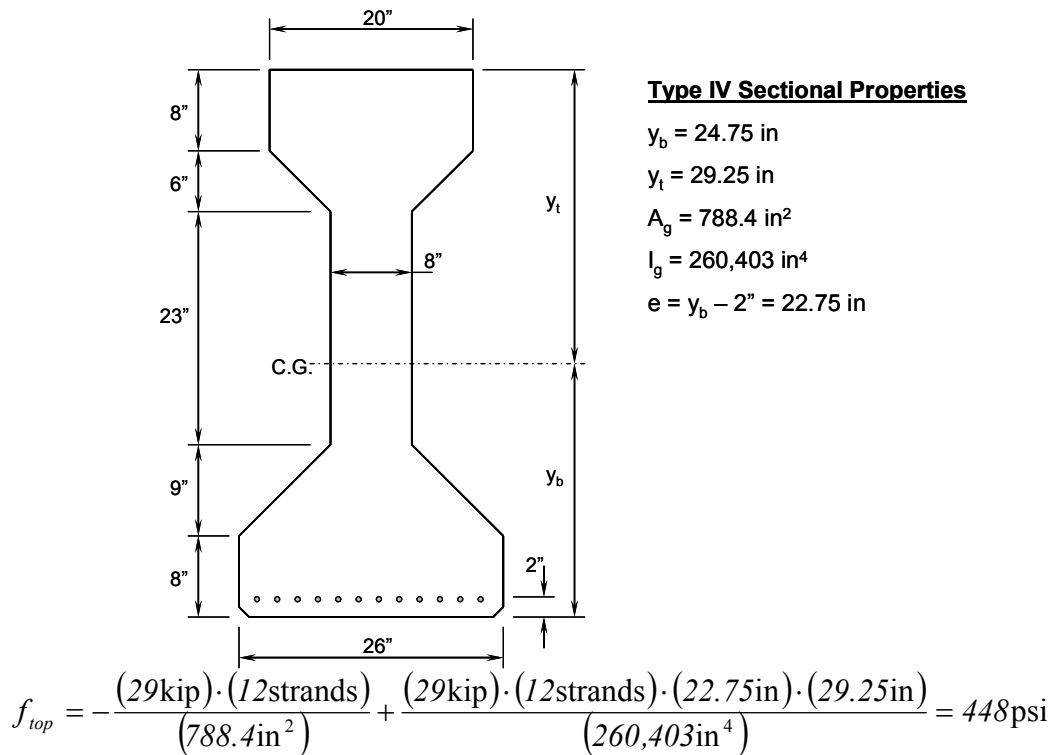


Figure 3-5 Type IV cross sectional properties and top fiber stress.

If cracking at release is unacceptable then a designer must specify the appropriate grade of concrete that is able to resist the applied tensile stress. For the previous example a designer would have to specify a tensile strength of concrete sufficient to resist 448-psi. If cracking is acceptable then a designer would specify the appropriate amount of reinforcement to control crack spacing and widths.

In reality, designers do not directly specify the tensile strength of concrete. The ACI 318 and AASHTO Bridge Design Specifications limit the concrete tensile strength based on an empirical relationship with the compressive strength (Table 3-2). The empirical relationship can be expressed as follows:

$$f_t = (TS) \cdot \sqrt{f'_c} \quad (3-3)$$

Where,

TS = Tensile strength factor

f_t = Tensile strength of concrete

f'_c = Compressive strength of concrete

The “tensile strength factor” is an empirically derived value. A goal of the research team is to evaluate this empirical relationship and its relation to the top fiber tensile stress of a Type IV girder. The historic background of the tensile strength factor is discussed in depth in Chapter 2.

Provisions included in current bridge design specifications and building codes are intended primarily to prevent cracking and excessive deflection. The current allowable tensile stress limits at transfer are presented in Table 3-1.

Table 3-1 Allowable concrete tensile stress limits at prestress transfer

American Association of State Highway and Transportation Officials (AASHTO LRFD) Pretensioned Members	
No bonded reinforcement	$200 \text{ psi or } 3\sqrt{f'_{ci}}$
With bonded reinforcement to resist the total tensile force in uncracked concrete section	$7.5\sqrt{f'_{ci}}$
American Concrete Institute (ACI 318-05) Pretensioned and Post-tensioned Flexural Members	
Extreme fiber stress in tension except at locations other than the ends of simply supported members	$3\sqrt{f'_{ci}}$
Extreme fiber stress in tension at ends of simply supported members	$6\sqrt{f'_{ci}}$

AASHTO allows a minimum tensile stress equal to $7.5\sqrt{f'_{ci}}$ when bonded reinforcement is provided to resist tensile forces. If the intent is to absolutely prevent cracking at transfer the allowable tensile stress is a minimum of $3\sqrt{f'_{ci}}$ or 200-psi according to AASHTO and $6\sqrt{f'_{ci}}$ according to ACI. The ACI limit was increased in the 1977 version of ACI 318 from $3\sqrt{f'_{ci}}$ to $6\sqrt{f'_{ci}}$ (see Chapter 2 for more detailed information). In general, the serviceability requirements of AASHTO tend to be more stringent than those of ACI due to the cyclic nature of moving loads.

Consider the previous Type IV beam example (Figure 3-5). Recall that the extreme fiber tensile stress at transfer is predicted to be equal to 448-psi. According to the provisions summarized in Table 3-1, if cracking is unacceptable then the required compressive strength of concrete at release would have to be equal to an unrealistic 22,300-psi according to AASHTO ($3\sqrt{22,300\text{psi}} = 448\text{psi}$) or 5,575-psi according to ACI ($6\sqrt{5,575\text{psi}} = 448\text{psi}$).

3.2.3 Prestress Losses due to Elastic Shortening

The force in prestressing strands will decrease due to the losses associated with the axial and flexural deformations. According to AASHTO LRFD Bridge Design Provisions, § 9.16.2.1.2 (AASHTO 2004) the losses associated with the elastic shortening of a specimen can be expressed as follows:

$$\Delta f_{pES} = \frac{E_{ps}}{E_{ci}} \cdot f_{cir} \quad (3-4)$$

Where,

E_{ps} = Modulus of elasticity of prestressing strand, ksi

E_{ci} = Modulus of elasticity of concrete at the time of release, ksi

f_{cir} = Compressive stress of concrete at the centroid of the strand based on gross section properties, ksi

For example, consider the previous Type IV girder example. Suppose that the compressive strength of concrete at release is 5000-psi and the force per strand prior to release is 30-kips (196-ksi) per strand. The losses due to elastic shortening are calculated as follows:

$$E_{ps} = 29,000 \text{ ksi}$$

$$E_{ci} = 57,000 \cdot \sqrt{5000} = 4,031 \text{ ksi}$$

$$f_{cir} = -\frac{(30 \text{ kip}) \cdot (12 \text{ strand})}{788.4 \text{ in}^2} - \frac{(30 \text{ kip}) \cdot (12 \text{ strand}) \cdot (22.75 \text{ in})^2}{260,403 \text{ in}^4} = 1.17 \text{ ksi}$$

$$\Delta f_{pES} = \frac{29,000 \text{ ksi}}{4,031 \text{ ksi}} \cdot 1.17 \text{ ksi} = 8.43 \text{ ksi}$$

For this particular example the stress level in the strands will decrease from 196-ksi to 188-ksi or 1.3-kips per strand (4.1-percent loss due to elastic shortening).

3.2.4 Early-Age Mechanical Properties of Concrete

Due to the competitive nature of the precast beam industry, manufacturers typically release pretensioned members as soon as release strength requirements are met (12-18 hours after batching). The concrete continues to gain strength after release resulting in a 28-day strength much greater than the release strength. A substantial amount of experimental data gathered from previous research was examined as part of this research project (Chapter 2). While a wealth of information exists on the mechanical properties of mature concrete (age of 28-days or greater), very little information was encountered on the early-age properties of concrete; especially in mixture designs containing Type III cement. Therefore, there is no clear correlation between compressive strength and tensile strength or stiffness for early-age concrete.

As part of the scope of the research project a preliminary investigation was conducted on the early-age material properties of concrete. The purpose of this preliminary investigation was to determine whether or not full-scale beam specimens were necessary. Four similar mixes from four different precast manufacturers were tested. Of the four precast manufacturers selected two had experienced cracking problems in the past and two had not. The precast manufacturers prepared approximately sixty 4-inch standard cylinders from the same batch of concrete used to cast a Type IV girder. Table 3-2 presents a summary of the four mixture designs tested. Plants A and B are the two manufacturers that had previously experienced cracking problems.

Table 3-2 Summary of Mixture Designs

	Plant A	Plant B	Plant C	Plant D
Course Aggregate	1781 lb/cy River Rock	1726 lb/cy Crushed Limestone	1992 lb/cy River Rock	1951 lb/cy River Rock
Fine Aggregate	1453 lb/cy	1468 lb/cy	1359 lb/cy	1403 lb/cy
Type III Cement	611 lb/cy	658 lb/cy	564 lb/cy	564 lb/cy
Water	211 lb/cy	251 lb/cy	192 lb/cy	205 lb/cy
Water/Cement Ratio	0.35	0.38	0.34	0.36
HRWR Admixture	3-16 oz/Cwt	20 oz/Cwt	21 oz/Cwt	12 oz/Cwt
Retarder	0 oz/Cwt	3.5 oz/Cwt	3 oz/Cwt	0.75 oz/Cwt

The research team picked up the cylinders on separate occasions from the precast manufacturers as soon as they had initially set (about 4 to 5 hours after batch). The team then transported the cylinders to the Ferguson Laboratory and conducted a series of tests. Three cylinders were tested each in compression and tension about every two hours over a period of 24-hours.

In addition to the preliminary material tests, whenever a Type IV beam specimen was cast in the Lab a series of cylinders were prepared and tested. Three different curing conditions were tested and compared to one another. One set of cylinders were match-cured using an electronic controller to match cylinder curing temperatures with those measured by a thermocouple embedded within the beam. These cylinders will be referred to as the “match-cured cylinders”. Match-curing and its affect on concrete maturity are discussed in further detail in Section 3.3. Another set of cylinders were match-cured next to a curing beam. These cylinders will be referred to as the “next-to-beam cylinders”. Finally, a set of cylinders were cured away from a heat source under the ambient temperature conditions in the lab. These cylinders will be referred to as the “ambient cylinders.” Following is a discussion of the tests conducted to determine the mechanical properties of the concrete.

3.2.4.1 ASTM C39 Standard Test Method for Compressive Strength of Cylindrical Concrete Specimens

A 600-kip hydraulically actuated universal testing machine was used to test the compressive strength of a standard 4x8-inch concrete cylinder (Figure 3-6). The cylinder was capped at each end with an unbonded neoprene pad, talcum powder and steel retaining ring as stipulated per ASTM C39. The load was applied by the testing machine’s steel base. A stationary

steel spherical head provided the reaction. The compressive strength of the concrete cylinders was determined per ASTM C39 (Equation 3-5):

$$f'_c = \frac{4 \cdot P}{\pi \cdot D^2} \quad (3-5)$$

Where,

P = Ultimate load

D = Diameter of cylinder



Figure 3-6 ASTM C39 Standard test method for determining the compressive strength of concrete.

3.2.4.2 *ASTM C496 Standard Test Method for Splitting Tensile Strength of Cylindrical Concrete Specimens*

A 60-kip hydraulically actuated testing machine was used to test the splitting tensile strength of a standard 4x8-inch concrete cylinder (Figure 3-7). The load was applied by the testing machine's steel base. A stationary 4x4-inch steel bar provided the reaction. A compressible barrier between the concrete and steel surfaces was formed with 1/8-inch thick plywood strips. The splitting tensile strength of a concrete cylinder was determined per ASTM C496 (Equation 3-6).

$$f_{sp} = \frac{2 \cdot P}{\pi \cdot l \cdot D} \quad (3-6)$$

Where,

P = Ultimate load

D = Diameter of cylinder

l = Length of cylinder

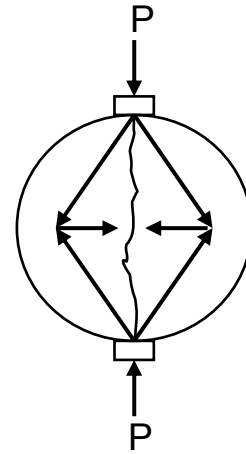


Figure 3-7 ASTM C496 Standard test method for determining the splitting tensile strength of concrete.

3.2.4.3 ASTM C78 Standard Test Method for Flexural Strength of Concrete (Using Simple Beam with Third-Point Loading)

A 60-kip hydraulically actuated testing machine was used to test the flexural strength of a standard 6x6x21-inch concrete beam (Figure 3-8). Specimens span 18-inches, are supported on steel rollers and loaded at the third points. The load was applied by the testing machine's steel base. A rigid plate provided the reaction. Ball bearings and rollers were provided at all supports and load points in order to reduce longitudinal restraint. The flexural strength of a 6x6x21-inch concrete beam was determined per ASTM C78 and can be calculated by using to Equation 3-7.

$$f_r = \frac{P}{12in^2} \quad (3-7)$$

Where,

P = Ultimate load



Figure 3-8 ASTM C78 Standard test method for determining the flexural strength of concrete.

3.2.4.4 ASTM C469 Standard Test Method for Static Modulus of Elasticity and Poisson's Ratio of Concrete in Compression

A 600-kip hydraulically actuated universal testing machine was used to apply compression to either a 4x8-inch or 6x54-inch concrete cylinder (Figure 3-9). Standard compressometers were used to measure the concrete strains. First, the ultimate compressive strength of concrete was determined by testing a standard 4x8-inch cylinder per ASTM C39. Then, the modulus of elasticity specimen was loaded to 40 percent of the established ultimate strength. The applied load was recorded when the measured strain is 0.05 millistrain. Finally, the elastic deformation was recorded when the applied load equaled 40-percent of the cylinder's ultimate strength. The 6x54-inch cylinder was designed to be the same height as a Type IV beam in order to measure differences in stiffness between the top and bottom of a beam caused by segregation. Despite the use of a non-standard cylinder size, the modulus of elasticity was determined in accordance with ASTM C469. The modulus of elasticity is expressed according to Equation 3-8.

$$E_c = \frac{4 \cdot (P_{40\%} - P_{0.00005})}{\pi \cdot D^2 \cdot (\epsilon_{40\%} - 0.00005)} \quad (3-8)$$

Where,

$P_{40\%}$ = 40% of ultimate load

$P_{0.00005}$ = Load when strain equals 0.00005

D = Diameter of cylinder

$\epsilon_{40\%}$ = Strain corresponding to $P_{40\%}$



Figure 3-9 6x54-inch cylinder. Modulus of Elasticity measured at top and bottom in accordance with ASTM C469

3.3 MATCH CURING TECHNOLOGY

The concept of match curing technology is a direct application of the concrete maturity theory. Temperature is an important factor in the strength development of concrete, especially within the first 24 hours. The maturity of concrete is determined by multiplying an interval of time by the temperature of the concrete (Figure 3-10). Maturity has been shown to be an excellent indication of the development of the strength concrete (Kehl and Carasquillo 1998). Figure 3-10 illustrates the concept of maturity. Concrete cured under a higher temperature will reach the same maturity (i.e. strength) sooner than concrete cured under a lower temperature.

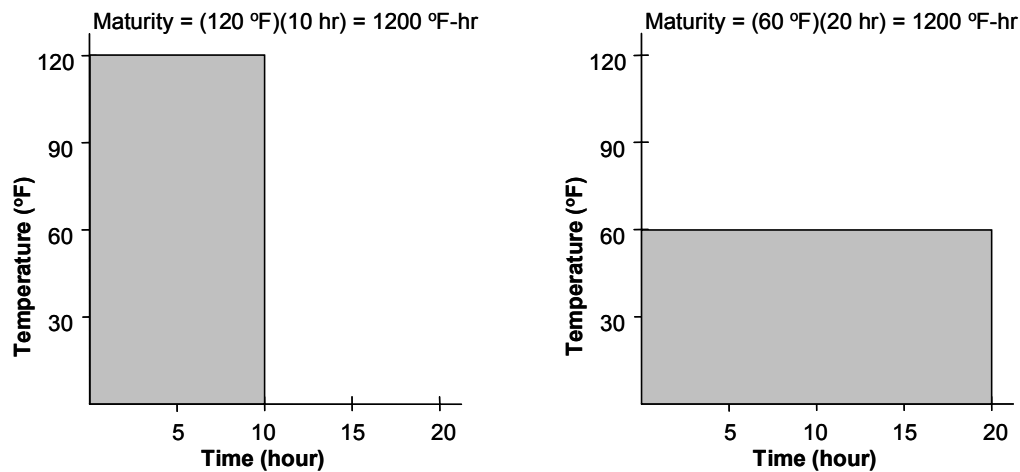


Figure 3-10 Concrete maturity is accelerated by temperature.

A Type IV beam has a much larger mass than a standard 4x8-inch cylinder and; therefore, cures at a much higher temperature. In order to better represent the concrete in the beam specimens with that in a standard cylinder it was necessary that the time-temperature

profiles match one another. One method of match-curing is the placement of control cylinders next to the beam such that they are cured with the heat generated from the beam. The temperature next to the beam is less than a location within the beam; therefore the curing temperature of a next-to-beam cylinder would be less than or equal to the coldest curing temperature within a beam. It follows that the strength of a control cylinder cured next to a beam would be a lower bound value of the in-situ strength. A more accurate method is the use of an electronic controller (Figure 3-11).



Figure 3-11 Electronic match-curing controller and insulated cylinder molds.

The *Sure Cure* system monitors temperatures in the beam and standard 4x8 cylinders; and uses an electronic controller to match the time-temperature profiles. Type-T thermocouples are used to read temperature values (Section 3.7.1.3). A schematic illustrating the electronic match-curing process is shown in Figure 3-12.

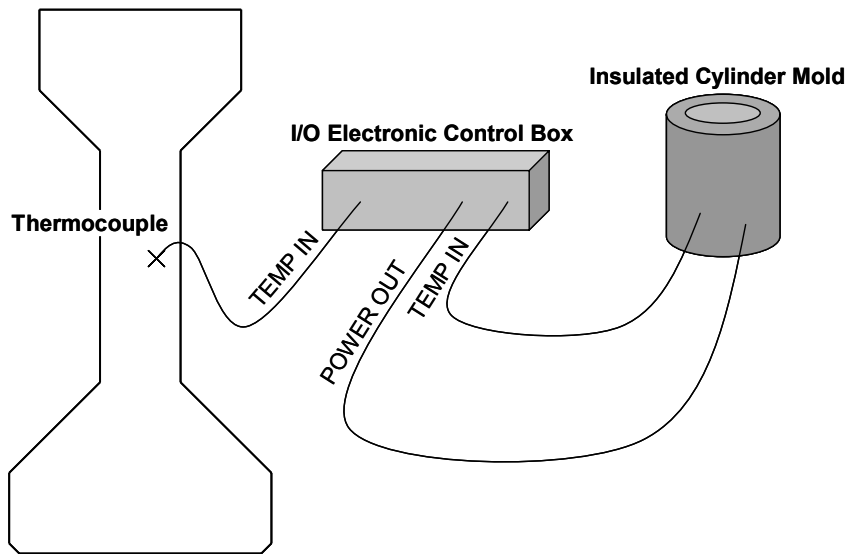


Figure 3-12 Electrically Controlled Match Curing System

Cylinder temperatures are increased depending on the temperature at the thermocouple location. Precast manufacturers typically locate thermocouples at a “relatively cool” location in the beam. There are many variables in locating the “relatively cool” location. This results in a wide range of differences between thermocouple locations depending on variability in insulation, geometries, and time of measurement.

3.4 PRESTRESSING FACILITY

The prestressing facility used for this project was originally constructed for TxDOT Project 1210 (Russell 1992) and then later modified for TxDOT Project 4086 (Rogers 2002) (Figures 3-13 and 3-14). The prestressing facility was originally designed to accommodate 3 bays of specimens up to 40-feet in length.

The prestressing facility is a steel reaction frame comprised of stationary bulkheads that are tied down to the laboratory floor with high strength 1-inch diameter steel threaded rods. The rods prevent overturning of the frame. Steel compression members (12x12-inch tubes) prevent the frame from sliding and shearing the rods. The current research project utilized the two exterior bays and only one beam was prestressed at a time. Slight modifications were made to the bulkhead in order to accommodate different strand patterns. The current project required a change in the prestressing loads and strand eccentricities. Therefore, the existing steel frame and floor tie-down connections were analyzed to check their adequacy (Table 3.3). The results in Table 3.3 show that the structure is able to resist the applied loads.



Figure 3-13 Prestressing Facility



Figure 3-14 AASHTO Type IV beam during fabrication.

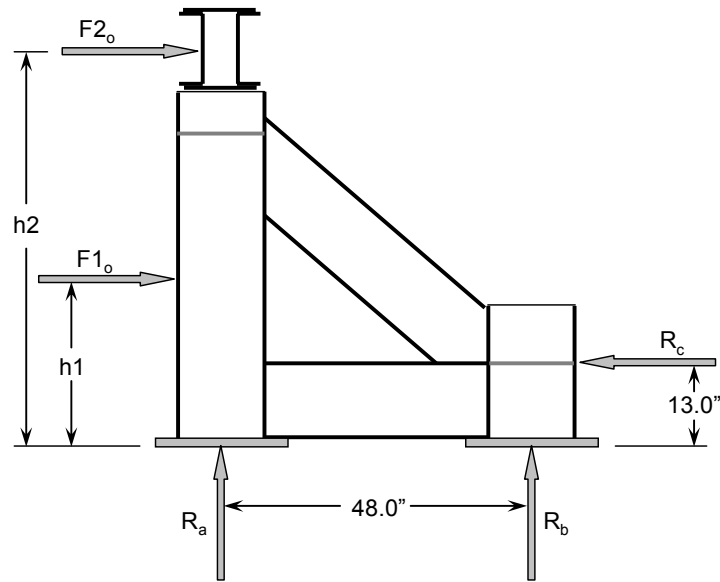


Figure 3-15 Free-body diagram of steel bulkheads subjected to prestressing forces.

Table 3.3 Elastic Analysis of Prestressing Bed

TxDOT Research Project 4086							
	h1	h2	F1 _o	F2 _o	R _a	R _b	R _c
Required Values	25.8"	0	240 k	0	-72 k	72 k	211 k
Capacity	-	-	-	-	-120 k	-	>450 k
Comment					OK		OK
TxDOT Research Project 5197							
Beam 1	h1	h2	F1 _o	F2 _o	R _a	R _b	R _c
Required Values	27.5"	0	372 k	0	- 78 k	78 k	123 k
Capacity	-	-	-	-	-120 k	-	>450 k
Comment					OK		OK
Beam 4	h1	h2	F1 _o	F2 _o	R _a	R _b	R _c
Required Values	27.5"	52"	310 k	124 k	-111 k	111 k	167 k
Capacity	-	-	-	-	-120 k	-	>450 k
Comment					OK		OK

3.5 STRAND PROPERTIES

Standard Low-Relaxation Grade 270 0.5-inch prestressing strands were used for this project. It was crucial to be able to accurately measure the force in the strand during the tensioning and release operations. Typically, in the field, this would be verified by measuring the elongation of the strand and verifying against the pressure applied by a hydraulic tensioning ram.

Then, general assumptions are made on seating losses in order to determine the final force per strand. This field method provides a conservative estimate of the concrete stresses at release. The research team was interested in a more accurate method of measurement of the force per strand. This was accomplished by using strain gauges to directly measure the strain in the strands. In addition to measuring the force per strand using strain gauges, the hydraulic pressures were also recorded in order to validate strain values.

Strain gauges were affixed to the prestressing strands along individual wires (Figure 3-16). Because the wires twist at an angle of approximately 9° the stress vs. strain relationship had to be modified accordingly. The research team conducted a series of tensile tests on 3-foot lengths of instrumented strands in order to directly relate the applied load to the measured strain. The same mechanical wedges that were used during prestressing operations were also used during these tests. A load vs. strain curve was developed and used to associate the measured strain to a force in the strand. These calibration curves were established for the linear elastic range of strands as the post-yield region was not applicable for this project. Strands used to fabricate the first beam specimen came from a different spool than strand for the other beam specimens. Calibration curves were established for each separate spool of strand. Figure 3-17 is an example of one of the calibration curves that was used for this project. Calibration curves for both spools are located in Appendix B.

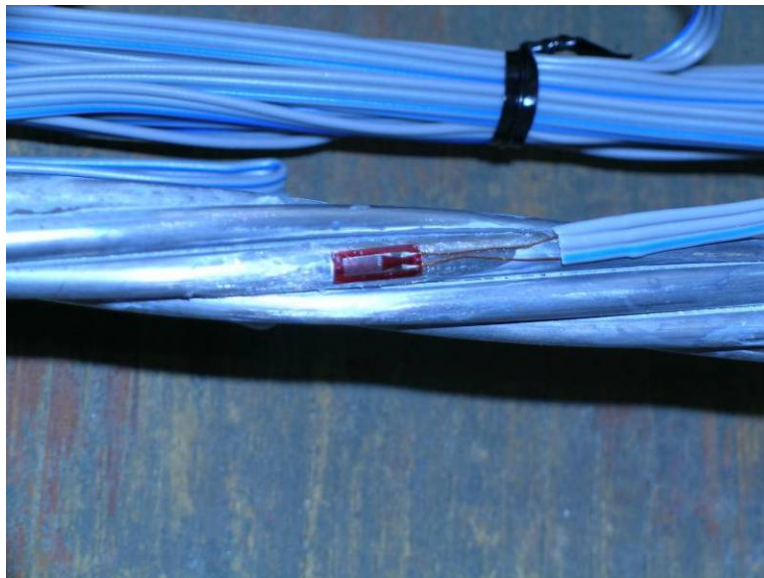


Figure 3-16 Strain gauge affixed to strand wire.

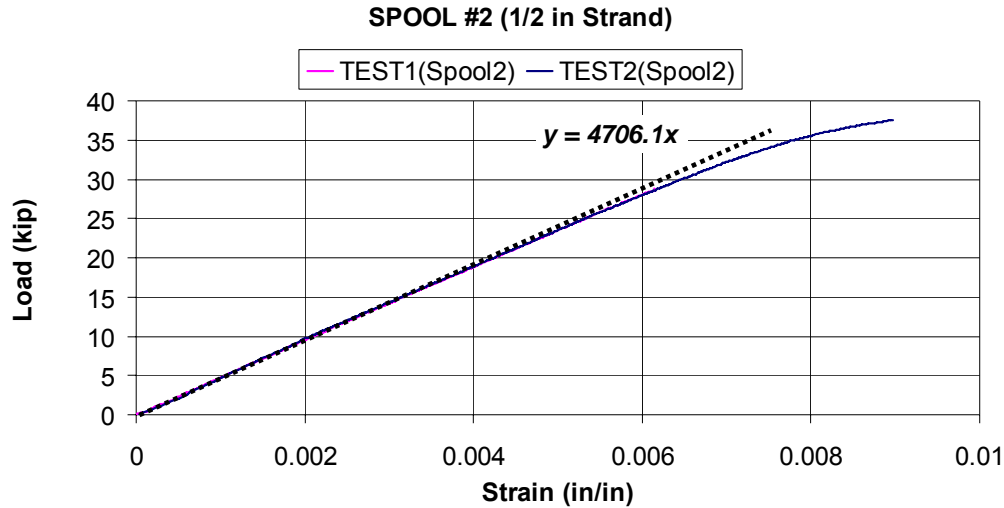


Figure 3-17 Calibration curve for estimating applied force in strand

3.6 STEEL REINFORCEMENT PROPERTIES

Steel reinforcement was standard Grade 60 deformed bars meeting the requirements of ASTM A615. Cross sectional dimensions were assumed per the nominal sizes given in ASTM A615. The modulus of elasticity was 29,000-ksi.

3.7 INSTRUMENTATION

3.7.1 General

Approximately 60 to 100 strain gauges were used per each specimen. Strain gauges were used to measure the change in deformation of prestressing strand, reinforcing steel, and concrete. A data acquisition system was used to collect the data. A computer software program was used to manage and convert the data from voltages into strains.

Temperature values were monitored using type T thermocouples. Thermocouples produce a voltage that is proportional to temperature. A separate *Sure Cure* system was used to control the match-curing of a series of 4-inch cylinders. An 8-channel data logger and the *Sure Cure* system were both used to monitor and record concrete curing temperatures.

3.7.1.1 Strain Measurements, Steel

The same gauges that were used to calibrate the Load vs. Strain curve (Figure 3-17) were used in the specimens. During testing, gauges were used to measure the change in strain in the strand and in reinforcement. The gauges used are identified as FLA-3-11-3LT manufactured by the Japanese company Tokyo Sokki Kenkyujo Co. These gauges are intended for general purpose mild steel applications. The gauges have a resistance of $120\Omega (\pm 0.5)$, and have a 1.5 by 3-mm dimensions.

To install the gauge, first the steel surface was sanded with very fine grit sandpaper until shiny and smooth. Then the surface was cleaned with a mild phosphoric acid immediately

followed with an ammonia based solvent to neutralize any chemical reaction. Once the surface had been cleaned the gauge was affixed using a cyanoacrylate adhesive. After the gauge was securely bonded to the steel it was coated with an air-drying toluene based acrylic. The acrylic formed a hard thin waterproof coating capable of high elongation. Finally, a piece of neoprene rubber was affixed over the gauge with foil tape. The neoprene and foil tape provided a final layer of protection from the placement of concrete.

3.7.1.2 Strain Measurements, Concrete

The gauges used to measure concrete strains are identified as PL-60-11-3LT manufactured by the Japanese company Tokyo Sokki Kenkyujo Co. These gauges are intended for general purpose concrete surface applications. The gauges have a resistance of $120\Omega (\pm 0.5)$, and have an 8 by 60-mm dimensions.

To install the gauge, first the concrete surface was lightly ground. The intention of the grinding was to remove the exterior cement paste layer thus exposing the aggregate. Next the exterior surface was cleaned of dust. A thin layer of epoxy adhesive was applied to fill the voids and provide a smooth bonding surface. Once dry, the surface was cleaned with a mild phosphoric acid immediately followed with an ammonia-based solvent to neutralize any chemical reaction. Once the surface had been cleaned the gauge was affixed using a cyanoacrylate adhesive. After the gauge was securely bonded to the concrete it was protected with a coating of an epoxy adhesive.

3.7.1.3 Temperature Measurements

Temperatures were monitored using Type T thermocouples. Type T thermocouples have a positive copper wire and a negative Constantan wire. They are commonly used for moist monitoring applications because of their ability to resist corrosion. Thermocouples that were used to match-cure cylinders were located at relatively cool locations of each specimen (Figure 3-18). Where a manufacturer locates this “relatively cool” location varies depending on differences in curing methodology and operations. For the most part, the cool location used by manufacturers is near the bottom of the bottom flange by the end of a beam. For beams fabricated in the laboratory, the coolest location was discovered to be located both in the middle of the web or the very top of the top flange. The difference in temperature between both locations was minimal. Thermocouples were also located along the height of the Type IV beams in order to record time vs. temperature variations during curing.

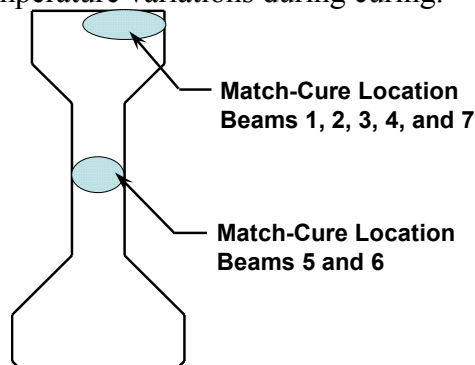


Figure 3-18 Thermocouple locations used to match-cure control cylinders.

3.7.2 Steel Reinforcement Gauges vs. Concrete Gauges

The background of the first beam specimen and its role in determining the location of future instrumentation is discussed in this section. Data collected from the first specimen was used to locate strain gauges for all subsequent test specimens.

Strain compatibility requires that steel reinforcing bars embedded in structural concrete experience the same elastic deformations as the concrete. Therefore, it can be inferred that strains measured in the rebar will be equal to the strains measured in the concrete. Data collected from the first specimen was used to verify the validity of this assumption. Strain readings from surface mounted gauges were compared with data from embedded steel gauges.

Additionally, the end regions of the first specimen were instrumented along its full height (Figures 3-19 and 3-20). The purpose was to determine the linearity of the strain profile in the region where prestress force was being transferred. Data points from the first beam specimen showed that the strain profile does in fact remain linear (Figure 3-21); however, the measured profile did not necessarily match the theoretical profile at a distance less than 2-feet from the beam's end. Subsequent tests measured strain at the top and bottom of the cross section and assumed a linear profile in between.

It was also discovered that locating the instrumented bar within the middle of the section's width resulted in the damage of numerous gauges while vibrating the concrete. Therefore, subsequent specimens were instrumented in the bells of the top and bottom flanges through the use of reinforcing bars embedded in concrete (Figure 3-23). The strain profile was assumed to be a straight line connecting the data points.

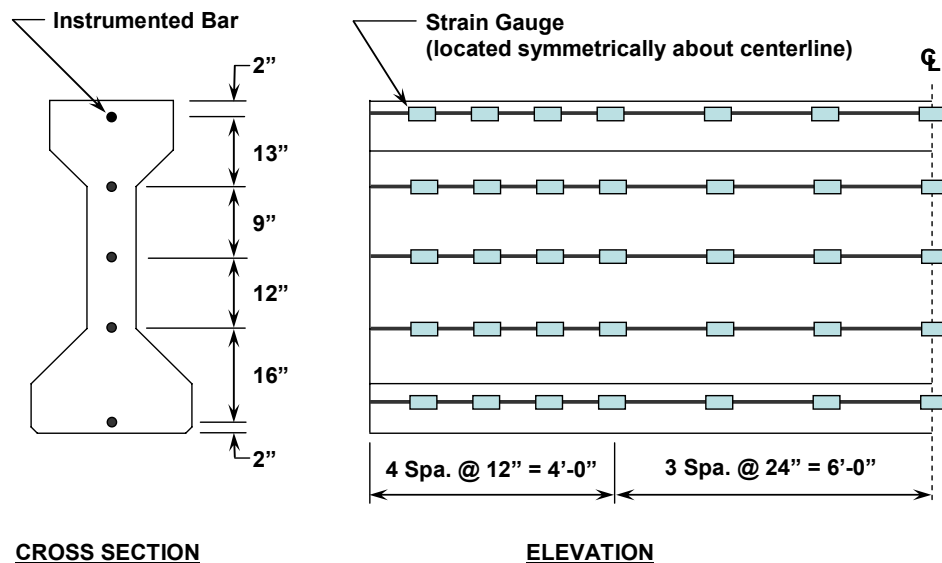


Figure 3-19 Location of embedded steel strain gauges, Beam 1

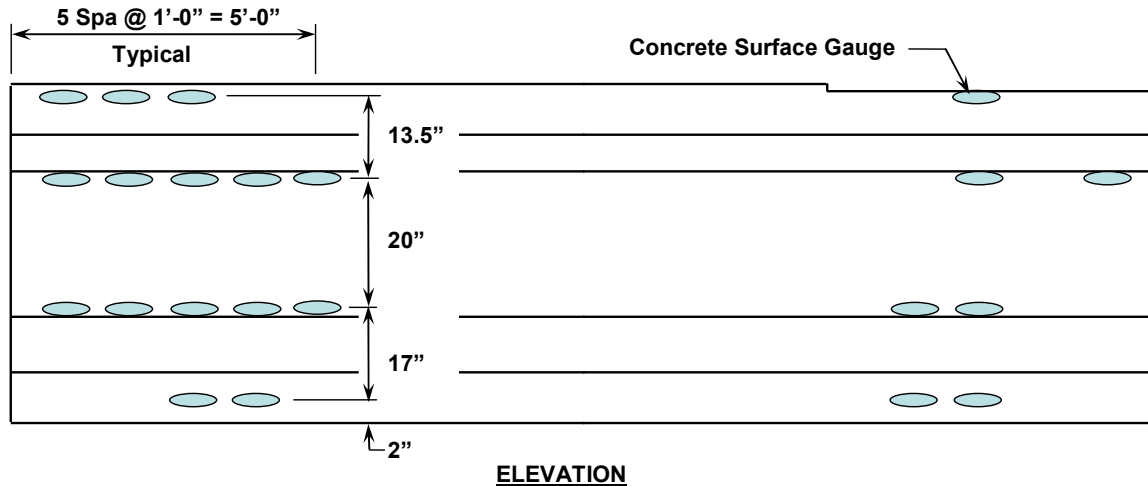


Figure 3-20 Location of concrete surface gauges, Beam 1

3.7.2.1 Compatibility between Steel and Concrete Gauges

Based on the scope of this project, the ability to cast a specimen and release within a short time frame (12 to 24-hours) was extremely important. The amount of time required to attach a concrete surface gauge after the concrete has reached sufficient strength does not allow for a quick release. In order to facilitate a quick release it was necessary to have all of the instrumentation in place and operating prior to placing of concrete. Therefore, it was deemed necessary to use embedded strain gauges attached to the steel reinforcement. For the first beam specimen, the research team compared the strain values from embedded steel gauges to concrete surfaces gauges. The measured strains from both types of gauges were compared to the theoretical strains (Figure 3-21). For the most part, strains between both types of gauges matched the theoretical profile. There was no discernible difference in accuracy between either of the two types of gauges. Therefore, for future tests strain gauges were affixed solely to embedded reinforcement in order to measure the strain profile during release (Section 3.7.4).

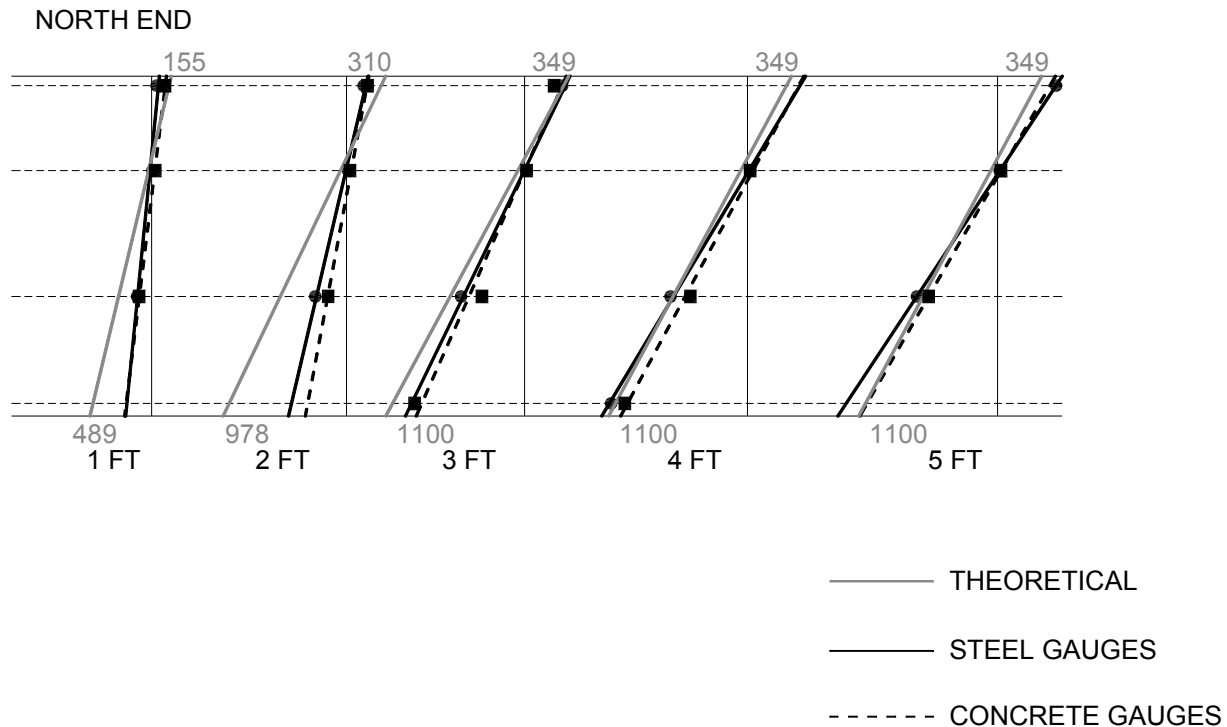


Figure 3-21 Experimentally measured strain profiles from steel and concrete strain gauges.

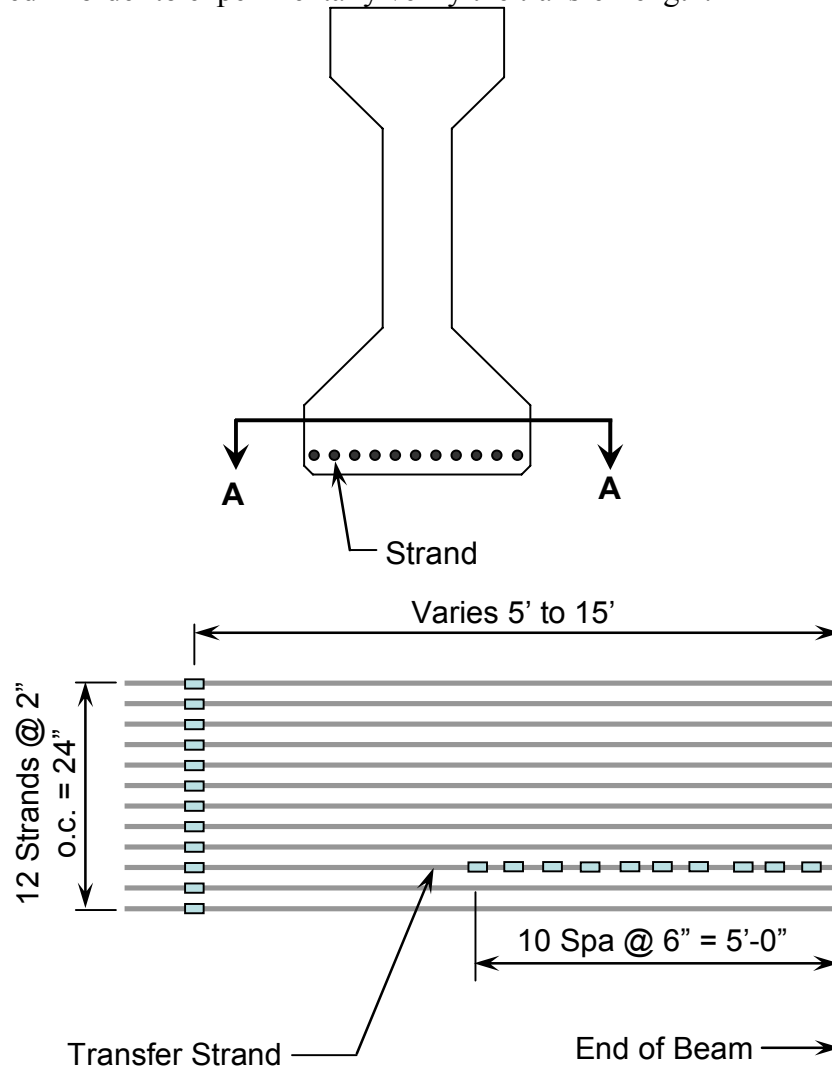
3.7.2.2 Verification of the Linear Strain Profile

In addition to verifying compatibility between gauges, it was important to verify if a linear variation in strains could be expected within the end region of a Type IV girder. Assuming that the strain profile is linear makes for ease of instrumentation; because only two data points are needed to define the straight line profile. There were some discrepancies for planar sections one and two feet from the end (Figure 3-21). However, this was to be expected for a 54-inch deep member. It was not surprising that plane sections did not remain plane less than 2-feet within the transfer region. Also, the consolidation problem experienced with Beam 1 may have contributed to the discrepancy within the first two feet of the end region. This information was not as significant to the project because the cracking that was being studied had occurred at a distance of approximately 4-feet from the beam's end. Data points from the first beam specimen showed that the strain profile does in fact remain relatively linear; particularly at sections where cracking was observed in the field (4-feet from the end).

3.7.3 Instrumentation of Prestressing Strand

Each strand was instrumented with a strain gauge in order to measure the strain, thus determine the force during stressing and release operations (Figures 3-22 and 3-24). Dimensions shown in these figures are given for the final position of the gauge. When determining the final location of a gauge affixed to a strand, it was necessary to take into account the anticipated axial

elongation. One strain gauge was affixed to each strand in order to represent its respective force. These strain gauges were generally located within the middle 10-feet of each specimen. Additionally, one strand per specimen was instrumented every 6-inches starting from the end of the beam for a total distance of 5-feet. Referred to as the “transfer strand” the strains along this strand were measured in order to experimentally verify the transfer length.



SECTION A-A

Figure 3-22 Prestressing strand gauge locations.

3.7.4 Instrumentation of Steel Reinforcement

Once it was determined that the strain profile was essentially linear (Section 3.7.2), subsequent gauges were located in more optimal locations for Beams 2 through 7 (Figures 3-23 and 3-24). Assuming that plane sections remain plane allowed the research team to use the strain readings at the top and bottom of each specimen to form a straight-line profile. For Beams 2

through 7 strain gauges were located at each end of a beam, every 1-foot on center for a total distance of 5-feet. Two #5 bars in the top flange were instrumented and located 52-inches from the bottom of the beam. Two #4 bars in the bottom flange were instrumented and located 6-inches from the bottom of the beam.

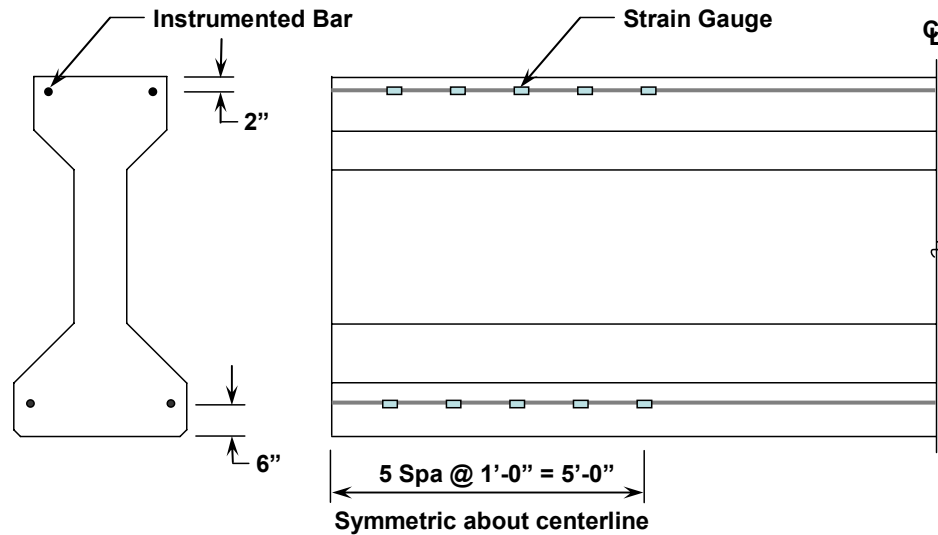


Figure 3-23 Reinforcing bar strain gauge locations (Beams 2 through 7)



Figure 3-24 End of specimen illustrating gauge locations.

3.7.5 Temperature Instrumentation

Thermocouples were located at various locations along the height and width of each specimen in order to evaluate the temperature gradient realized during curing. Temperature readings that were taken at a distance of 5-feet from the end of a beam are shown in Figure 3-25. Other temperature readings were taken 4-inches from the bottom of the beam at distances of 6-

inches, 2-feet 6-inches, 4-feet, and 5-feet in order to get a representation of the temperature variation along the beam's length.

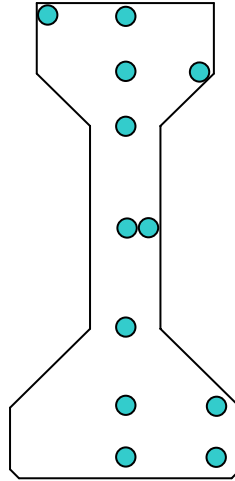


Figure 3-25 Thermocouple locations, 5'-0" from end of beam

3.8 FABRICATION OF TEST SPECIMENS

The tasks completed during the fabrication of seven test specimens are discussed in this chapter. Some of the tasks and procedures evolved through the course of the research project. This is due to the nature of experimental research. As new questions arise during the course of the research, procedures are updated accordingly. These changes were minor yet pertinent to the scope of the research.

3.8.1 Prestressing of Strands

The strands were individually stressed using a single strand hydraulic ram and pump (Figure 3-26).



Figure 3-26 Single strand stressing operation.

Strands were initially stressed to 15 to 30-ksi (2 to 5-kips per strand). This allowed for an easier fabrication of the rebar cages. After the strands had been lightly stressed, strain gauges were affixed as described in Section 3.7.3. The initial preload had to be accounted for during the prestressing operations. Because strain gauges were affixed to preloaded strands, the measured force in the strands was 2 to 5-kips lower than the hydraulic force in the tensioning ram. This was accounted for in the final force calculations. Prior to seating the wedges, the strain gauge and hydraulic pressure gauge values were recorded. The average difference between the two values was added to the final strand force after seating and elastic shortening losses. Detailed calculations of strand forces are located in Appendix C. For this particular setup it was observed that additional significant losses due to the deformation of the prestressing bed also occurred. In order to compensate for these initial seating and deformation losses each strand was stressed to a value approximately 10% higher than the desired final value. 34-kips was considered the maximum limiting force per strand in order prevent yielding of the strands or failure at the anchorages.

3.8.2 Casting of Concrete

All specimens were cast using the same 6.5-sack mix design (Table 3-4)

Table 3-4 6.5-Sack Type III Cement Mix Design

<i>Coarse Aggregate</i> (Crushed Limestone)	<i>1840 lb/cy</i>
<i>Fine Aggregate</i>	<i>1430 lb/cy</i>
<i>Type III Cement</i>	<i>611 lb/cy</i>
<i>Water</i>	<i>214 lb/cy</i>
<i>Water/Cement Ratio</i>	<i>0.35</i>
<i>HRWR Admixture</i> (Sika Viscocrete 2100)	<i>8 oz/Cwt</i>
<i>Retarder (Sika Plastiment)</i>	<i>4 oz/Cwt</i>

The coarse and fine aggregate were supplied by a local precast manufacturer and delivered in a ready-mix truck. 90-percent of the water was added to the aggregates followed by all of the cement. The admixtures were diluted into the remaining 10-percent of the water and added last. Finally, the drum of the ready-mix truck was rotated approximately 200 times. Type III cement, water, and admixtures were added at the Phil M. Ferguson Laboratory. For the first specimen, 90% of the water was delivered in the ready-mix truck along with the coarse and fine aggregate. For subsequent specimens, all of the water was metered and added at the laboratory. A hopper was used to manually add the cement to the truck (Figure 3-27). The hopper could only hold half the required cement at a time so two loads were required.



Figure 3-27 Type III cement being added to a ready mix truck.

For the first specimen, electric rod vibrators were solely used to consolidate the concrete. After pulling the forms, air voids were observed in the ends of the bottom flanges. For subsequent beam specimens, pneumatic vibrators attached to the forms were used to consolidate the concrete in each specimen (Figure 3-28). Rod vibrators were continued to be used to consolidate the concrete through internal vibration (Figure 3-29). The concurrent use of form vibrators and rod vibrators eliminated the consolidation problem experienced for Beam 1. Subsequent beams specimens did not have any consolidation problems.



Figure 3-28 Form vibrators used to consolidate concrete.

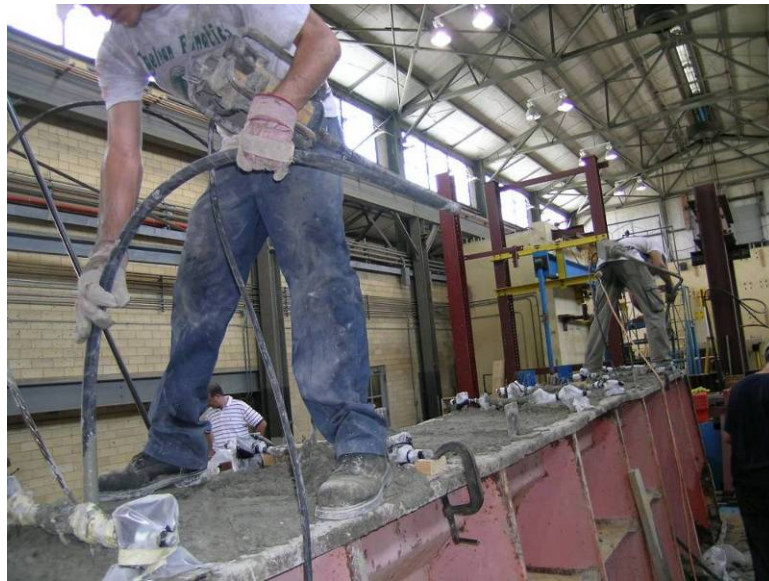


Figure 3-29 Rod vibrators used to consolidate concrete.

Beams 1 and 2 were cured covered with plastic. Beams 3 through 7 were cured covered with wet burlap and plastic (Figure 3-30).



Figure 3-30 Beam specimens were cured by covering with wet burlap and plastic.

3.8.3 Releasing of Strands

The strands were released by torch-cutting them one at a time (Figure 3-31). Strands were heated such that wires failed individually. The strands were heated slowly in order to minimize sudden movement of the beam specimens during release. Despite these efforts the beam still moved approximately 1 to 2-inches during release.



Figure 3-31 Torch-cutting prestressing strands.

After one or two strands had been completely cut, individual wires located on uncut strands began breaking on their own. As soon as all strands were cut the beam specimen was lifted with an overhead crane (Figure 3-32).



Figure 3-32 Beam specimen immediately prior to being lifted

The purpose of lifting the beams was to emulate the same loading condition that a beam would experience in the field. All beam specimens that cracked in the laboratory did so prior to being lifted by the overhead crane. Uncracked beams remained uncracked after being lifted by the overhead crane.

3.9 DESIGN OF BEAM SPECIMENS

Seven full-scale prestressed concrete Type IV beams were designed and reinforced in accordance with TxDOT's standard detail (Appendix A). Dimensions of an AASHTO Type IV beam are shown on Figure 3-5; general reinforcement layout is shown in Figure 3-33. The TxDOT detail requires bursting, shear and longitudinal top flange reinforcement. The shear reinforcement was omitted because shear resistance was not necessary for the purposes of this project.

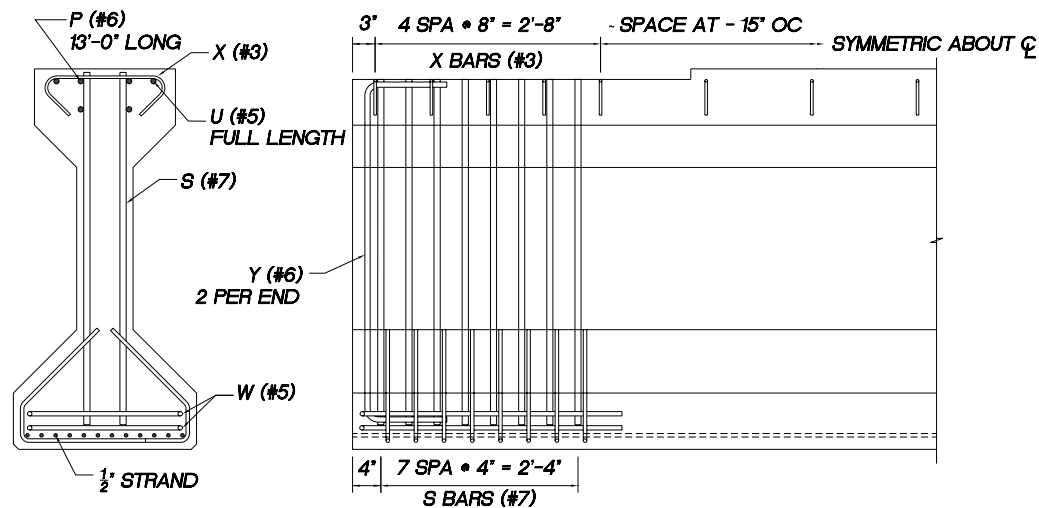


Figure 3-33 Reinforcement layout for typical beam specimen.

As discussed earlier, cracking problems at release were observed for short beams with highly eccentric prestressing force. “Short beams” is a term that is used for Type IV girders that are used to span a distance less than 20 to 60-feet. In order to represent a worst-case scenario, an uncommonly short length of 20-feet was selected for all specimens. It was not necessary to test a beam longer than 20-feet because the beam's end region was the only area of interest. Therefore, each beam specimen provided two end regions for a total of 14 tests.

Currently TxDOT requires 2.4-in² of compression steel in the top flange; this detail is referred to as TxDOT's “new design” (Figure 3-34). In the past, the #6-P bars shown in Figure 3-33 were not required. Therefore, only 0.6-in² was provided in the top flange; this detail is referred to as TxDOT's “old design”. It was of interest to the research team to examine the affects of the “new” and “old” designs on cracking and crack control. Therefore, each beam specimen was reinforced according to the “new” design along one half of the length and the “old” design along the other.

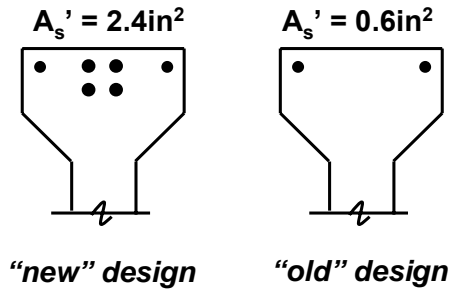


Figure 3-34 TxDOT “new” design vs. “old” design: Top flange of Type IV beam

Additionally, a 4-foot long by 20-inch wide by 1.5-inch deep block-out was provided at both ends of the specimens (Figures 3-1 and 3-2); except Beam 1 which only had a block-out at one end. Recall that cracking at release has been observed in specimens with and without block-outs. However, after Beam 1 was tested the research team determined that the blocked-out region was of greater interest. All subsequent beam specimens were fabricated with the block-out at each end. When analyzing a section linear-elastically, the block-out reduces the sectional area and moment of inertia resulting in slightly higher stresses.

All 7 of the fabricated beam specimens and 14 test regions are shown in Figures 3-35 through 3-37. Key parameters are summarized in Table 3.5. The maximum tensile stress will be slightly different for seemingly similar specimens due to differences in prestress loss. Losses due to elastic shortening are inversely proportional to the modulus of elasticity of concrete (Equation 3-4). Therefore, the amount of prestress force lost due to elastic shortening decreases as the stiffness of concrete increases.

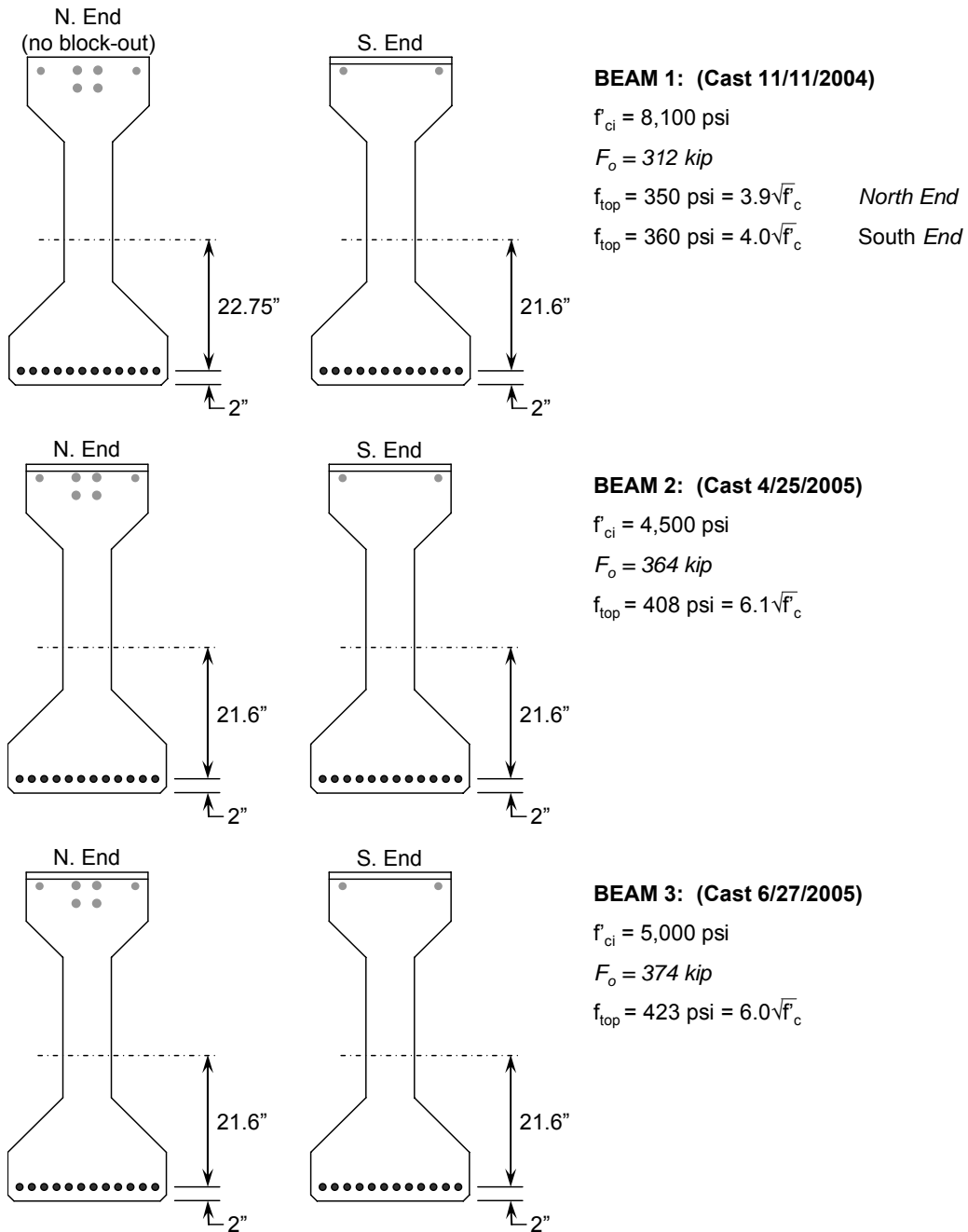


Figure 3-35 Beam specimens 1 through 3.

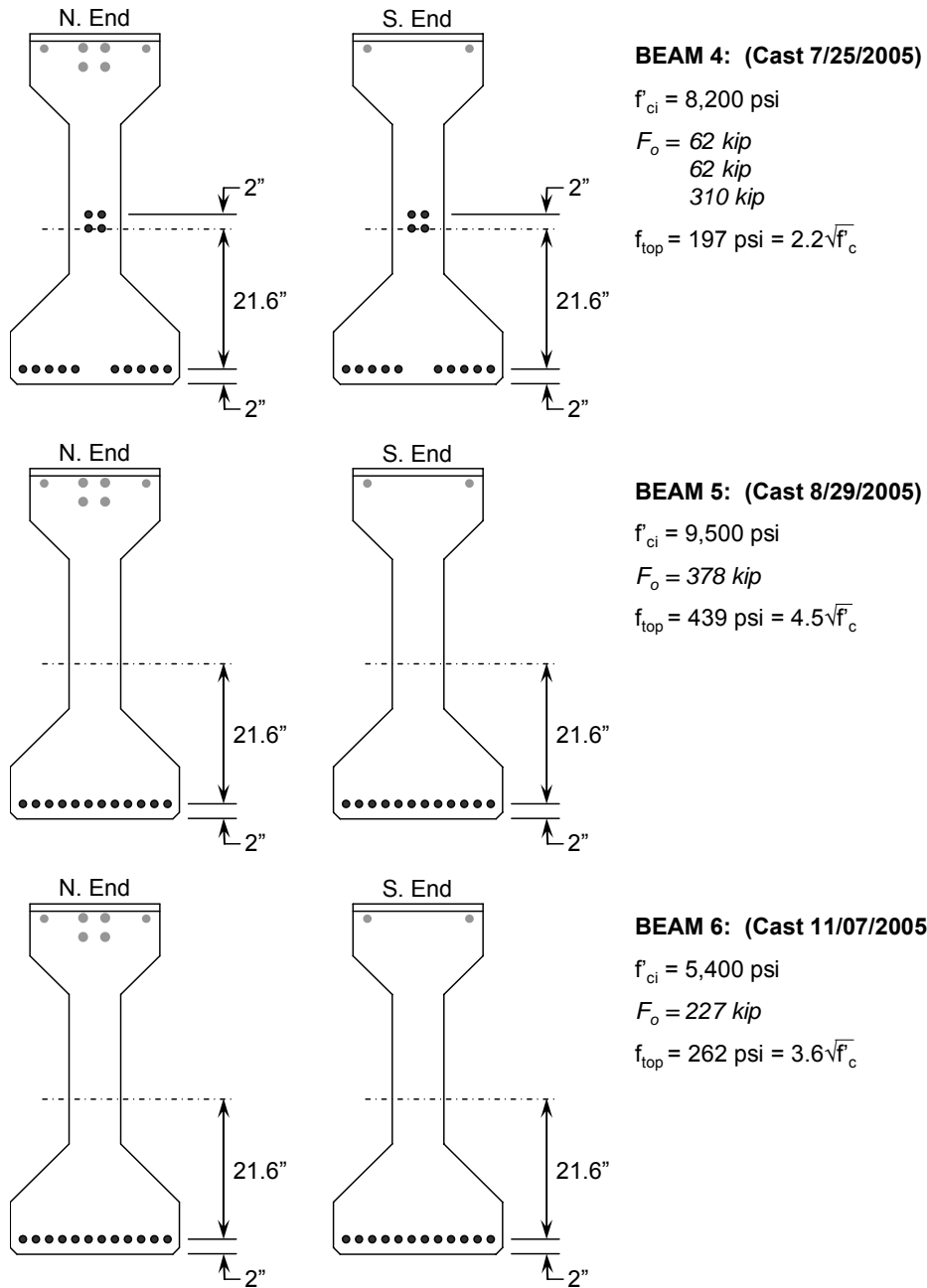


Figure 3-36 Beam specimens 4 through 6.

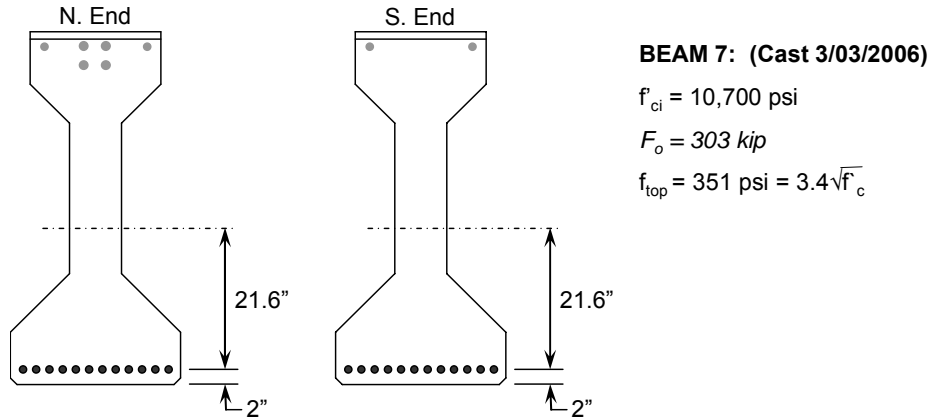


Figure 3-37 Beam specimen 7.

Table 3-5 Summary of Test Specimens

Specimens	Release Time	F_{strand} (kip)	Eccentricity	f'_{ci} (psi)		f_{top}	$f_{top} / \sqrt{f'_{ci}}$	
				Target	Actual		Target	Actual
Beam 1	38-days	26.0	21.6"	> 8000	8100	359	< 7.5	4.0
Beam 2	10-hrs	30.3	21.6"	4000	4500	408	< 7.5	6.1
Beam 3	8-hrs	31.2	21.6"	5000	5000	427	< 7.5	6.0
Beam 4	17-hrs	31.0	15.1"	> 8000	8200	197	< 3.0	2.2
Beam 5	3-days	31.5	21.6"	> 8000	9500	439	< 6.0	4.5
Beam 6	10-hrs	18.9	21.6"	5000	5400	262	3.0	3.6
Beam 7	5-days	25.3	21.6"	> 8000	10700	351	3.0	3.4

The purpose of Beam 1 was to establish the strain gauge arrangement for subsequent beams as well as format the testing procedure. Initially, it was the goal of the research team to release each beam specimen with a compressive strength of 4000-psi and an extreme fiber tensile stress less than $7.5\sqrt{f'_{ci}}$. In order to represent the worst-case conditions present in the field. All beam specimens were reinforced with the TxDOT “new design” on their north end and the TxDOT “old design” on their south end. This, in effect, provided two testing regions per beam specimen. Beam specimens 2 and 3 cracked immediately at release. Therefore, the top fiber tensile stresses were limited in subsequent beam specimens. This was accomplished either by lowering the eccentricity (Beam 4), reducing the force in the strands (Beams 6 and 7), or releasing strands after concrete had reached full strength (Beam 5). In summary, beams 2 and 3 cracked immediately at release. Beam 5 cracked on the south end (“old design”) and remained uncracked on the north end (“new design”). Beams 1, 4, 6 and 7 did not crack at release.

CHAPTER 4

Discussion of Results

4.1 INTRODUCTION

From the onset of the research project it was theorized that cracking at release is due to one of two phenomena: insufficient material strength or a lack of understanding of structural mechanics within the transfer region. Results from a series of material tests and 14 beam region tests are discussed in this chapter.

Material tests were conducted during the initial stages of the research program in order to shed light on to the importance that material/mixture design contributes to the cracking problem. After the preliminary material tests, the next stage of the research program involved the fabrication of full scale Type IV girders. The girders were instrumented and strains were measured. Stresses inferred from the strain readings were compared with values calculated using classic beam theory ($P/A \pm Mc/I$).

Additional material tests were conducted in conjunction with the fabrication of the full scale specimens. Approximately 40 cylinders were fabricated per beam specimen in order to evaluate the early-age properties of Class H concrete used in prestressed beam fabrication.

Finally, in order to better understand the role that curing temperature plays in the strength of concrete, internal temperature readings were recorded and evaluated at multiple locations within the cross-section of each beam specimen. A relatively cool location was used to control the curing temperature of control specimens. Additionally, a series of compression and tension tests were conducted on cylinders match-cured from the hottest and coldest points found in a curing Type IV beam.

Results from these series of material and beam tests are further discussed.

4.2 PRELIMINARY CONCRETE MATERIAL TESTING

During the initial stages of the research project a series of preliminary material tests were conducted at the Phil M. Ferguson Structural Engineering Laboratory. The information collected from these tests provided the research team with valuable information that was used in planning the subsequent tests. Concrete that was used to make Type IV girders was collected from four different precast manufacturers. Plants A and B had experienced cracking problems at release; Plants C and D did not. The mix designs varied slightly from plant to plant. However, they were similar in the fact that they were 6 to 7-sack mixes without the inclusion of fly ash. After initial set (approximately 4-hours) over 240 cylinders (60 cylinders per plant) were transported from the precast plants to the Ferguson Laboratory and tested every two hours over a period of 24 hours in order to determine their strength gain with time. In order to verify that the movement of 4-hour old concrete cylinders would not adversely affect their compressive or tensile strengths a series of twelve 4x8-inch cylinders were fabricated at the Ferguson Laboratory; six were left undisturbed in the laboratory while the other six were loaded on a truck as soon as they had initially set (4-hours after batching). Then, the cylinders were subjected to an hour of truck movement on the local highways. After an hour, they were returned to the Ferguson Laboratory and tested in conjunction with the undisturbed cylinders. Three were tested in compression

(ASTM C39) and three were tested in tension (ASTM C496) for each set. As a result, there was no significant statistical difference in the compressive or tensile strengths. Therefore, it was concluded that the cylinders could be transported from the precasters to the Ferguson Lab as soon as the concrete had initially set.

The differences in mix designs between the four prestressed precast beam manufacturers are summarized in Table 4-1.

Table 4-1 Summary of Mix Designs

	<i>Plant A</i>	<i>Plant B</i>	<i>Plant C</i>	<i>Plant D</i>
<i>Course Aggregate</i>	1781 lb/cy River Gravel	1726 lb/cy Crushed Limestone	1992 lb/cy River Gravel	1951 lb/cy River Gravel
<i>Fine Aggregate</i>	1453 lb/cy	1468 lb/cy	1359 lb/cy	1403 lb/cy
<i>Type III Cement</i>	611 lb/cy	658 lb/cy	564 lb/cy	564 lb/cy
<i>Water</i>	211 lb/cy	251 lb/cy	192 lb/cy	205 lb/cy
<i>Water/Cement Ratio</i>	0.35	0.38	0.34	0.36
<i>HRWR Admixture</i>	3-16 oz/Cwt	20 oz/Cwt	21 oz/Cwt	12 oz/Cwt
<i>Retarder</i>	0 oz/Cwt	3.5 oz/Cwt	3 oz/Cwt	0.75 oz/Cwt

4.2.1 Compressive Strength

Compressive tests were conducted in accordance with ASTM C39. The compressive strength is the only criterion used by precast prestressed beam manufacturers when determining whether or not the concrete used in their beams is mature enough to release.

Typically, manufacturers will match-cure their cylinders in order to accelerate their maturity; either with an electronically controlled system or by setting the cylinders next to a curing beam. It was not possible to match-cure the cylinders collected by the research team. Therefore there were some differences in the magnitude of strength gains recorded by the manufacturers at the time of release with those recorded by the research team. Nonetheless, the data collected provided a general basis of comparison between the different material properties of concrete. Cylinders were collected between the months of January and April; they cured in their molds under the ambient air temperature in the laboratory. Figure 4-1 summarizes the compressive strength gain over time for the four different mixes.

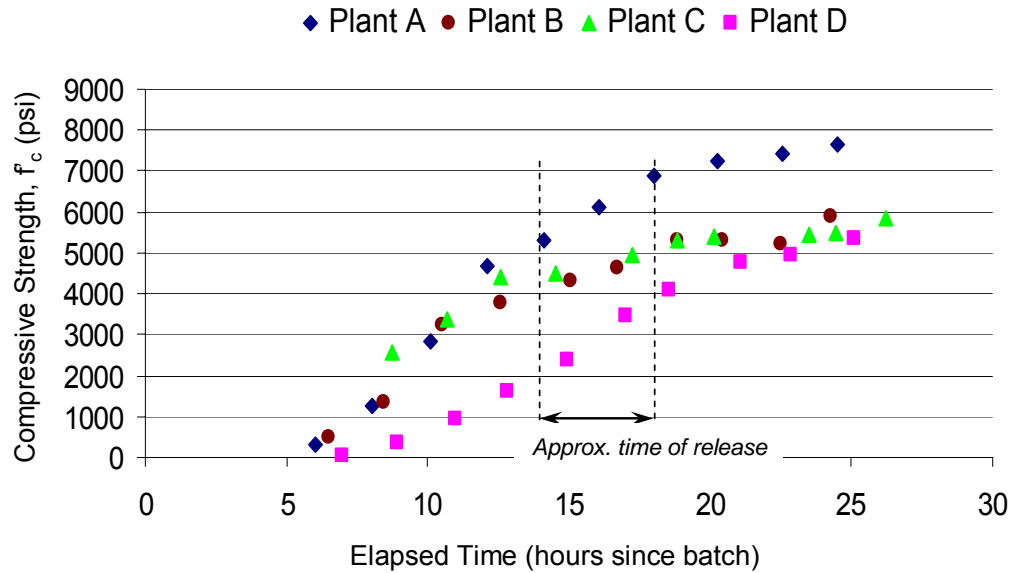


Figure 4-1 Compressive strength vs. time from different manufacturers.

Typically the minimum required release strength, f_{ci}' is equal to 4000-psi. Beams that had exhibited cracking in the field were fabricated with 4000 to 5000-psi mixes. By the time of release all of the mixture designs tested at Ferguson Lab had reached their minimum required compressive strength. Results of the compressive stress tests conducted at the precast plants were approximately 500 to 1000-psi higher due to warmer curing temperatures. Differences in compressive strengths between various mixture designs can likely be attributed to variations in aggregate stiffness and mix proportions.

4.2.2 Tensile Strength

For the determination of tensile strength, split cylinder tests were conducted in accordance with ASTM C496. At release, the design of a short Type IV girder with a high eccentricity of prestress force is controlled by the ability of the concrete in the top flange to resist cracking (i.e. its tensile strength). Cylinders were collected from four different precast manufacturers and tested at the Ferguson Laboratory. See Figure 4-2 for a tensile strength gain summary of the four mixes tested.

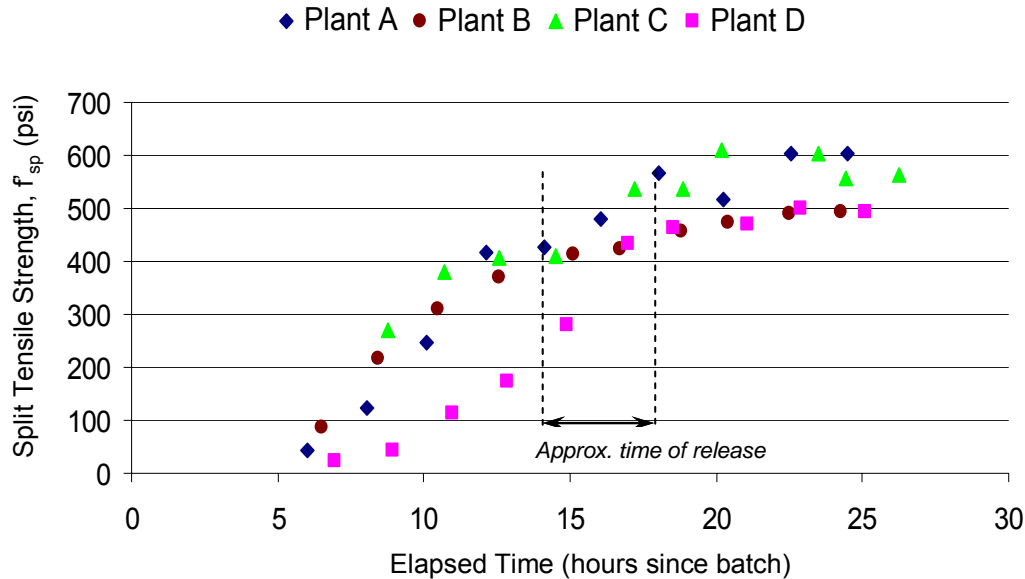


Figure 4-2 Tensile strength vs. time for four different manufacturers.

Except for the concrete collected from Plant D, the tensile strengths of the cylinders grew at almost identical rates. This is also true for the compressive strength growth rate of the concrete collected from Plant D (Figure 4-1). Of greater interest is a comparison of the growth of the tensile strength in relation to the compressive strength. This is discussed in further detail in the following section.

4.2.3 Tensile – Compressive Strength Relationship

As discussed in Chapter 3 the tensile strength of concrete is related to the compressive strength by an empirical relationship (Equation 4-1).

$$f_t = (TS) \cdot \sqrt{f'_c} \quad (4-1)$$

Where,

TS = Tensile strength factor

f'_c = Compressive strength of concrete

f_t = Tensile strength of concrete

The “tensile strength factor” has been empirically derived and well established for mature concrete. However the factor varies depending on the type of test being used (Section 2.3). Recall, for a split cylinder test, $6\sqrt{f'_c}$ is the value recommended by ACI. However the mode of failure of a split cylinder test is not flexural tension. Yet, the Type IV girders that have cracked did so due to flexural tension. For a direct flexural test (modulus of rupture), $7.5\sqrt{f'_c}$ is extreme fiber tensile capacity recommended by ACI. If a split cylinder test is used to evaluate the tensile capacity of concrete and the concrete has cracked in flexural tension; then the split cylinder

values must be factored by 1.25 ($7.5/6 = 1.25$) in order to correlate with the cracking capacity in flexure.

Figure 4-3 shows the gain of the tensile strength factor from the four different plant mixes. The values shown are from split cylinder tests. As can be seen, at the time of release the cylinders meet or exceed the ACI recommended value of $6\sqrt{f'_c}$. Applying the 1.25 factor, the predicted modulus of rupture would vary between 7.5 and $10.4\sqrt{f'_c}$.

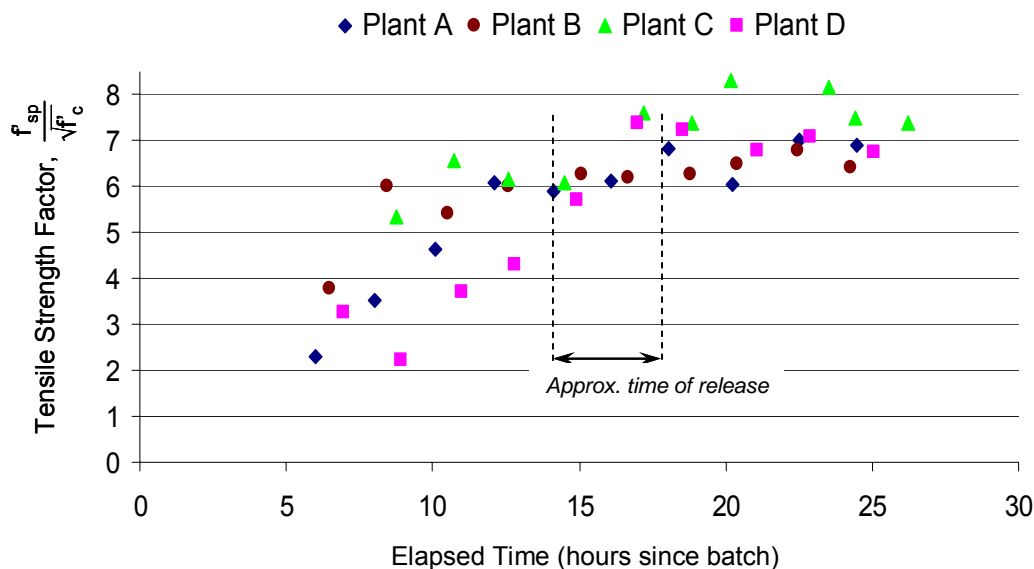


Figure 4-3 Tensile strength factor vs. time for four different manufacturers.

Notice that there is considerable scatter in the tensile strength factors just before the time of release. After 16 hours the values finally converge into a range between 6 and $8\sqrt{f'_c}$. The large difference in scatter is an indication of the immaturity or “greenness” of concrete during the early stages when hydration is taking place at its peak rate.

Suppose a precast manufacturer were to release strands during the very early stages of concrete’s maturity (less than 14 hours). Compressive strength may not be a reliable indicator of the tensile strength due to the large amount of scatter present in the data. For example, consider the strength gain of Plant A’s mix. The compressive strength attains 4000-psi within approximately 12-hours. At that time, the tensile strength of the mix is equal to 442-psi or $7\sqrt{f'_c}$. A similar comparison can be made for the other plants. The tensile strength of concrete when its corresponding compressive strength is equal to 4000-psi is presented in Figure 4-4.

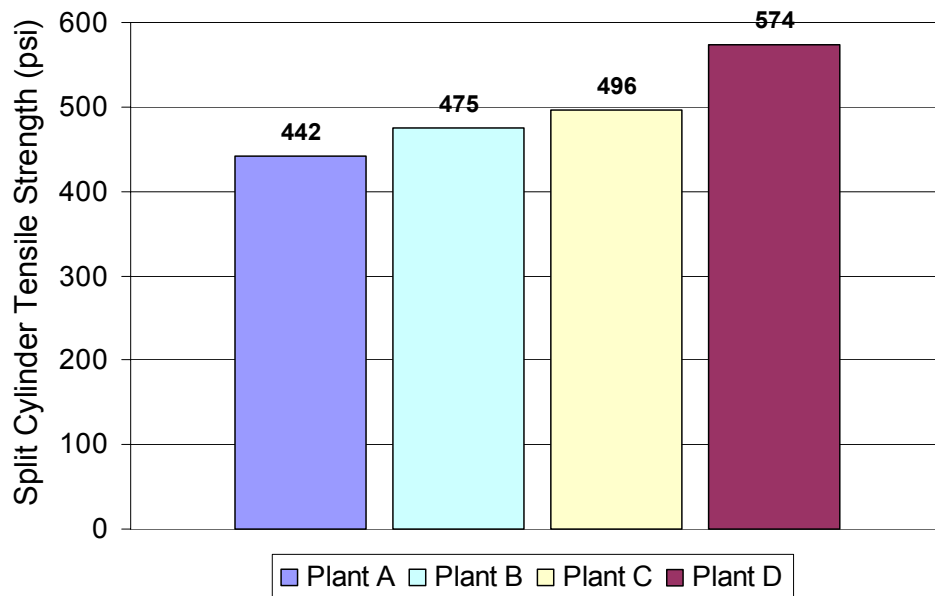


Figure 4-4 Tensile strength of concrete when compressive strength = 4000-psi.

The values shown are for split cylinder tests. Recall that the expected tensile strength of a split cylinder test is $6\sqrt{f'_c}$. It is important to note that $6\sqrt{4000\text{psi}} = 379\text{-psi}$ therefore all of the concrete mixes tested met or exceeded the expected value. Plants C and D used approximately 200-lb/cy more coarse aggregate than Plants A and B. This may have been a contributing factor to the higher tensile strengths. Also, the two plants that had previously experienced cracking problems (Plants A and B) are the two lowest of the group. This may be an indication of the immaturity of the concrete from Plants A and B when the measured compressive strength was 4000-psi. While this observation may not be the only piece of information needed to answer the question at hand, it may be considered a contributing factor to the Type IV beam cracking problem.

4.3 MATERIAL DATA ASSOCIATED WITH THE FABRICATION OF TYPE IV BEAM SPECIMENS

Along with the fabrication of each Type IV beam specimen, a series of 4x8-inch cylinders, 6x6x21-inch beams, and 6x54-inch cylinders were also prepared and tested. The purpose of these tests was to get a better understanding into material strength variations that may be experienced in the field and their impact on typical design assumptions.

4.3.1 Compressive Strength

Concrete compressive strength is the only criterion used to verify whether or not a beam is ready to be subjected to the loads associated with the release of prestressing strands. In the field, release strength is typically verified by testing three 4x8-inch cylinders. The cylinders have been match-cured to a “relatively cool” location within the cross-section.

Approximately 4 to 6-hours after fabrication of a Type IV beam specimen, the match-cure, next-to-beam, and ambient cylinders were tested in compression every two hours in order

to monitor compressive strength gain. Match-cure strengths were used to determine the beam's release strength. Two cylinder tests were used to establish the compressive strength of concrete at release. On the occasions when the strengths established from two tests were inconsistent with one another, a third cylinder was tested. Concrete compressive strengths at the time of release are presented in Table 4-2.

Table 4-2 Concrete Compressive Strengths at the time of Release

	<i>Time of Release</i>	<i>Match-Cure</i>	<i>Next to Beam</i>	<i>Ambient</i>
Beam 1	38 days	8,100 psi	NA	10,100 psi
Beam 2	10 hours	4,500 psi	NA	2,000 psi
Beam 3	8 hours	5,000 psi	5,000 psi	4,000 psi
Beam 4	17 hours	8,200 psi	8,200 psi	6,800 psi
Beam 5	3 days	9,500 psi	9,300 psi	9,300 psi
Beam 6	10 hours	5,400 psi	5,100 psi	2,500 psi
Beam 7	5 days	10,700 psi	NA	10,700 psi

4.3.2 Tensile Strength

Split cylinder tests were also conducted for the match-cure, next-to-beam, and ambient cylinders. The tensile strength of concrete at the time of release for Beams 1 and 2 was measured using split cylinder tests and factored by 1.25 in order to compare their values with MOR data. For Beams 3 through 7, a more direct measurement of the flexural tensile strength was achieved by testing 6x6x21-inch beams in flexure. Concrete tensile strengths at the time of release are presented in Table 4-3. A comparison of the modulus of rupture values within the context of historical data is presented in Figure 4-12.

Table 4-3 Concrete Tensile Strengths at the time of Release

	<i>Time of Release</i>	<i>Match-Cure</i>	<i>Next to Beam</i>	<i>MOR*</i>
Beam 1	38 days	690 psi	705 psi	862 psi**
Beam 2	10 hours	500 psi	425 psi	625 psi**
Beam 3	8 hours	475 psi	475 psi	534 psi
Beam 4	17 hours	640 psi	640 psi	689 psi
Beam 5	3 days	600 psi	595 psi	902 psi
Beam 6	10 hours	550 psi	600 psi	550 psi
Beam 7	5 days	650 psi	590 psi	987 psi

* *Modulus of Rupture*

** *Determined by multiplying match-cured split cylinder values by 1.25*

Concrete tensile strength values are presented within the context of historic values presented in Figure 4-10. As shown, the relationship between concrete compressive and tensile strength is reasonable considering the scatter of previously researched data. Therefore, based on results collected in the laboratory, the empirical relationship relating the compressive strength of a 4-inch cylinder to the flexural strength of a 6x6x21-inch beam is reasonable.

4.3.3 Modulus of Elasticity

Modulus of elasticity (MOE) tests were also conducted as described in Chapter 3. The modulus of elasticity was simultaneously measured at the top and bottom of the “tall” cylinders in order to determine if segregation would cause a significant difference in stiffness (Figure 4-5).

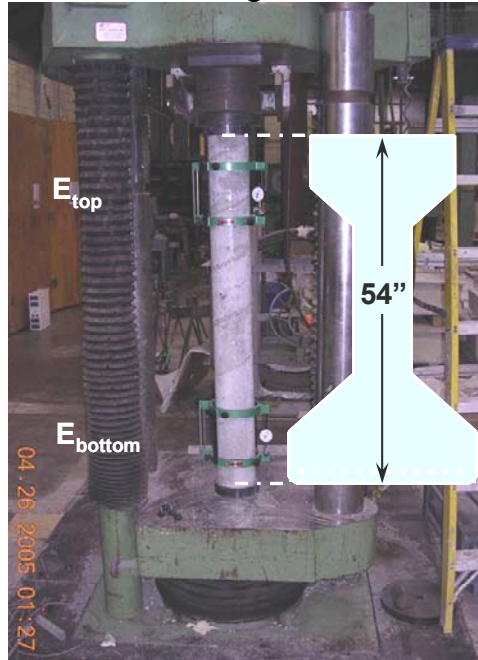


Figure 4-5 Modulus of elasticity of “tall” cylinders

The tall cylinders were tested when their strength was the same as the strength of a beam at the time of release. It was not possible to match-cure the tall cylinders; instead they cured under the ambient laboratory temperature. Therefore, the tall cylinders achieved the required “release strength” hours after the actual release of a beam specimen. The compressive strengths of the tall cylinders were verified based on the compressive strengths of ambient cylinders.

Table 4-4 presents the modulus of elasticity data obtained when the tall cylinders achieved release strength. A comparison is made between the measured value, ACI 318 recommended value, and the ACI 363 proposed value. The ACI 363 value is to be used for concrete compressive strengths greater than 6000-psi.

Table 4-4 Modulus of Elasticity at top and bottom of “tall” cylinders

E_c	Top	Bottom	% Diff ($E_b - E_t$)/ E_b	ACI 318*	ACI 363**
Beam 1	5,593 ksi	5,813 ksi	+ 3.8%	5,130 ksi	4,600 ksi
Beam 2	4,721 ksi	4,557 ksi	- 7.5%	3,824 ksi	NA
Beam 3	4,830 ksi	5,319 ksi	+ 9.2%	5,075 ksi	NA
Beam 4	5,050 ksi	5,494 ksi	+ 8.1%	5,162 ksi	4,622 ksi
Beam 5	6,007 ksi	6,440 ksi	+ 6.7%	5,556 ksi	4,899 ksi
Beam 6	6,029 ksi	6,058 ksi	+ 0.5%	4,189 ksi	NA
Beam 7	5,967 ksi	6,241 ksi	+ 4.4%	5,896 ksi	5,138 ksi

* $E_c = 57000 \sqrt{f'_c}$, (f'_c in psi)

** $E_c = 40000 \sqrt{f'_c} + 1000000$ when $f'_c \geq 6000$ psi, (f'_c in psi)

On average, the bottom of the tall cylinders had a modulus of elasticity 3% greater than the top. Such a small difference is considered statistically insignificant given the scatter associated with modulus of elasticity values. On average, the modulus of elasticity values predicted by ACI 318 were 19% less than measured; and the values predicted by ACI 363 were 22% less than measured. These seemingly large differences are still within the range of scatter associated with modulus of elasticity tests. Figure 4-6 illustrates a comparison of the current study with historical modulus of elasticity values.

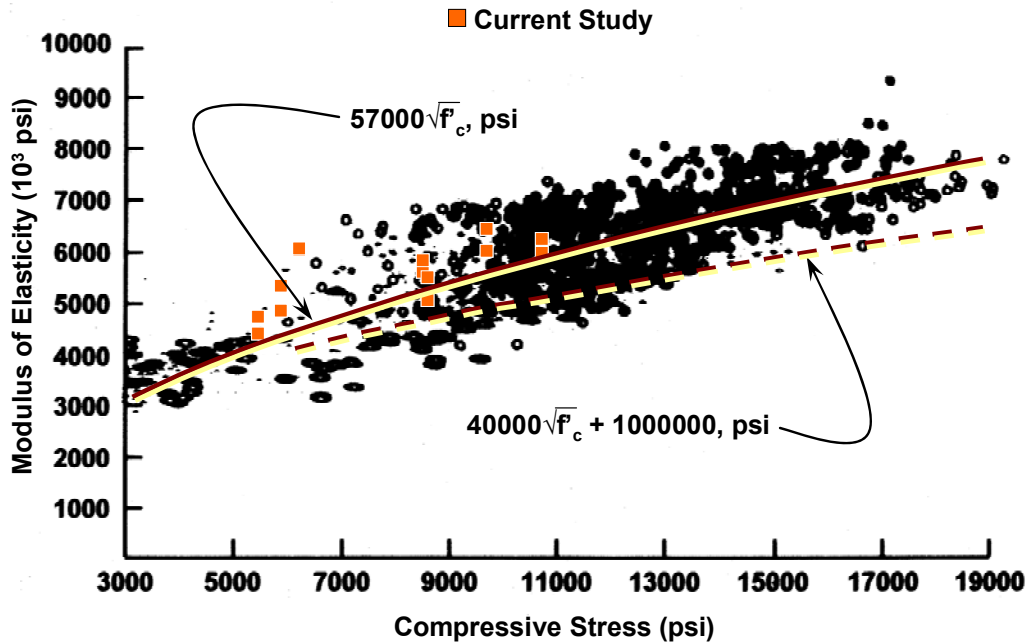


Figure 4-6 Modulus of elasticity in comparison with historical* data.

* (Mirza et al. 1979), (Carasquillo 1981), (Mokhtarzadeh and French 2000)

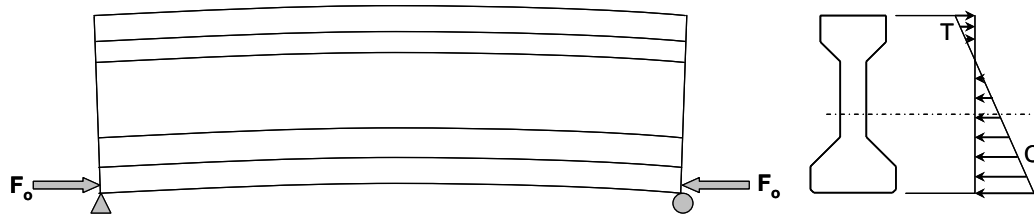
As can be seen in Figure 4-6, the modulus of elasticity values measured for each beam specimen lie within the general range of scatter of other results reported in the literature. Within the range of scatter, the ACI 318 equation provides a more reasonable estimate of the average modulus of elasticity. While the ACI 363 equation is a lower bound of the data cloud.

4.4 SECTIONAL ANALYSIS

Predicted stresses were calculated using typical linear-elastic assumptions. Actual material data such as modulus of elasticity and strand force was substituted for those that would normally be assumed. Detailed calculations are presented in the following section.

4.4.1 Linear-Elastic Analysis Considering Actual Material Data

Following is an example of how a designer may calculate tensile stresses at release based on a linear elastic analysis. Even though cracking had been observed 4-feet from the end of a beam, the maximum tensile stress was assumed to be located a distance from the end of a specimen equal to the transfer length (theoretical transfer lengths varied between 20 and 33-inches). Theoretically, this is where the most critical section should be located and was considered to be the worse-case scenario. On average, this assumption resulted in a maximum theoretical applied tensile stress about 5-percent greater than the stress located at a distance of 4-feet. Also, note that the section properties are reduced due to a 1.5-inch block out. Tensile stress calculations are shown in Table 4-5.



Material Properties

$$f'_{ci} = 9.5\text{ksi}$$

$$f_y = 60\text{ksi}$$

$$E_s = 29000\text{ksi}$$

$$A'_s = 2.38\text{in}^2$$

$$y'_s = 50\text{in}$$

$$A_{ps} = 0.153\text{in}^2$$

$$y_p = 2\text{in}$$

$$E_{ci} = 6224\text{ksi}$$

Section Properties (Block-Out)

$$L_o = 20\text{ft}$$

$$H = 52.5\text{in}$$

$$y_b = 23.62\text{in}$$

$$A_g = 758.4\text{in}^2$$

$$I_g = 235067\text{in}^4$$

$$F_o = 377.5\text{kip}$$

$$d_b = 0.5\text{in}$$

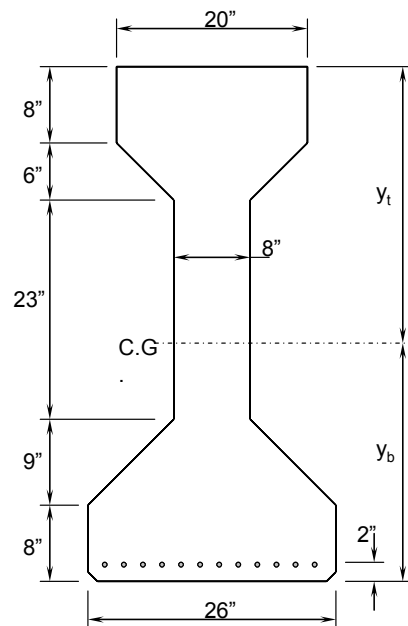


Figure 4-7 Properties used in determining concrete stresses at release.

Table 4-5 Calculations for Determining Top Fiber Tensile Stress

Transfer Length (AASHTO LRFD §5.11.4.2)	
$f_{se} = \frac{(F_o - \Delta F_{pES})}{12 \cdot A_{ps}}$	$f_{se} = 200.2 \text{ ksi}$
$l_d = \frac{f_{se}}{3} \cdot d_b$	$l_d = 33 \text{ in}$
Transformed Section Properties	
$n = \frac{E_s}{E_c}$	$n = 4.7$
$y_{btr} = \frac{A_g \cdot y_b + (n-1) \cdot (A'_s \cdot y'_s + 12 A_{ps} \cdot y_p)}{A_g + (n-1) \cdot (A'_s + 12 A_{ps})}$	$y_{btr} = 23.73 \text{ in}$
$A_{tr} = A_g + (n-1) \cdot (A'_s + 12 A_{ps})$	$A_{tr} = 774 \text{ in}^2$
$I_{tr} = I_g + A_g (y_b - y_{btr})^2 + (n-1) [A'_s (y'_s - y_{btr})^2 + 12 A_{ps} (y_p - y_{btr})^2]$	$I_{tr} = 244259 \text{ in}^4$
Losses due to Elastic Shortening (AASHTO LRFD §5.9.5.2.3)	
$f_{cir} = \frac{F_o}{A_g} + \frac{F_o (y_b - y_p)^2}{I_g}$	$f_{cir} = 1.25 \text{ ksi}$
$\Delta f_{pES} = n \cdot f_{cir}$	$\Delta f_{pES} = 5.82 \text{ ksi}$
$\Delta F_{pES} = \Delta f_{pES} \cdot A_{ps} \cdot 12$	$\Delta F_{pES} = 10.7 \text{ kip}$
Dead Load Moment due to Beam Selfweight	
$\omega_D = 0.145 \text{ kcf} \cdot A_g$	$\omega_D = 0.764 \text{ klf}$
$M_D = \frac{\omega_D \cdot l_d \cdot L_o}{2} - \frac{\omega_D \cdot l_d^2}{2}$	$M_D = 219 \text{ k} \cdot \text{in}$
Top Fiber Stress at Transfer	
$f_{top} = \frac{-(F_o - \Delta F_{pES})}{A_{tr}} + \frac{(F_o - \Delta F_{pES})(y_{btr} - y_p)(H - y_{btr})}{I_{tr}} - \frac{M_D(H - y_{btr})}{I_{tr}}$ $f_{top} = 439 \text{ psi}$ $= 4.5 \sqrt{f'_{ci}}$	

A similar analysis was conducted for all beam specimens. Detailed calculations are included in Appendix E. The predicted tensile stress values are summarized in Table 4-6.

Table 4-6 Predicted Maximum Tensile Stresses

	f_{top}	$f_{top}/\sqrt{f'_{ci}}$
<i>Beam 1</i>	359	4.0
<i>Beam 2</i>	408	6.1
<i>Beam 3</i>	427	6.0
<i>Beam 4</i>	197	2.2
<i>Beam 5</i>	439	4.5
<i>Beam 6</i>	262	3.6
<i>Beam 7</i>	351	3.4

4.5 TRANSFER LENGTH

One strand per specimen was instrumented every 6-inches starting from the end of the beam for a total distance of 5-feet. Referred to as the “transfer strand”, the strains along this strand were measured in order to experimentally verify the transfer length. The data collected from the transfer strand is shown in Figure 4-8.

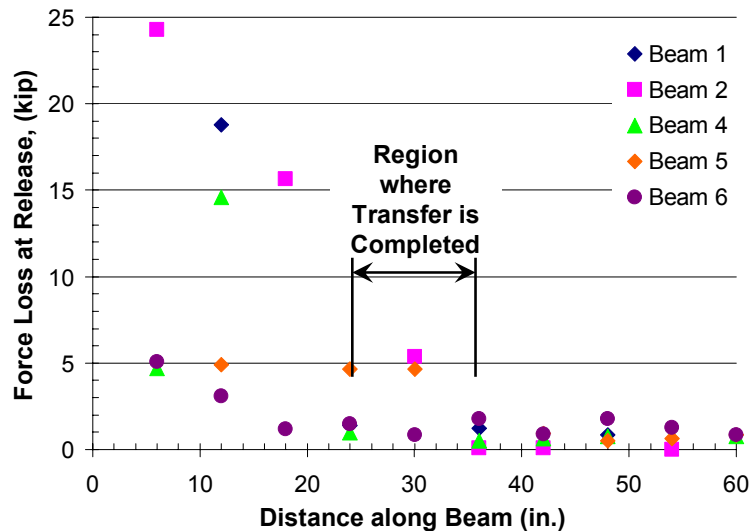


Figure 4-8 Loss of prestress force along strand.

The transfer length is defined as the distance required to develop the full prestressing force after elastic shortening losses. As shown in Figure 4-7, the force loss per strand was high near the end of the beam and then the loss decreased as the distance along the beam increased. Finally, the loss per strand leveled to a value between one and two kips. This loss was due to the elastic shortening of the beam. The loss per strand stabilized somewhere between 25 and 35-inches. The transfer lengths determined per AASHTO LRFD §5.11.4.2 also were between 25 and 35-inches depending on the amount of losses due to elastic shortening. Theoretical transfer length values are calculated for each beam specimen and included in Appendix E. The purpose of this research project was not to experimentally verify the theoretical transfer length. However, the data collected provided the research team with additional confidence when using AASHTO LRFD §5.11.4.2 to calculate the length necessary to develop prestressing strands.

4.6 CRACK CONTROL: NEW DESIGN VS. OLD DESIGN

According to the AASHTO Code (AASHTO 2002), a designer is allowed to limit the top fiber stress at release to $7.5\sqrt{f'_c}$; provided enough steel is provided in the tension region to resist the tensile forces of an uncracked section. TxDOT's "new" design (Figure 4-9) meets the requirements of the $7.5\sqrt{f'_c}$ limit in the AASHTO code (assuming working stress of steel is equal to 30-ksi). Comparison of the behavior of the test regions with the "new" design and the "old" design show that the new design does indeed do a better job of controlling crack widths and lengths (Figure 4-10). Cracks on the new design side of the cracked specimens are smaller, spaced closer and do not extend as far into the web. Also, Beam 5 cracked at one end ("old" design) and not at the other ("new" design). The effectiveness of the "new" and "old" design to control cracking is summarized in Figure 4-10.

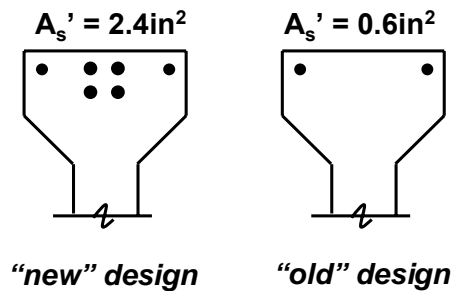


Figure 4-9 TxDOT's "new" design vs. "old" design (Top flange)

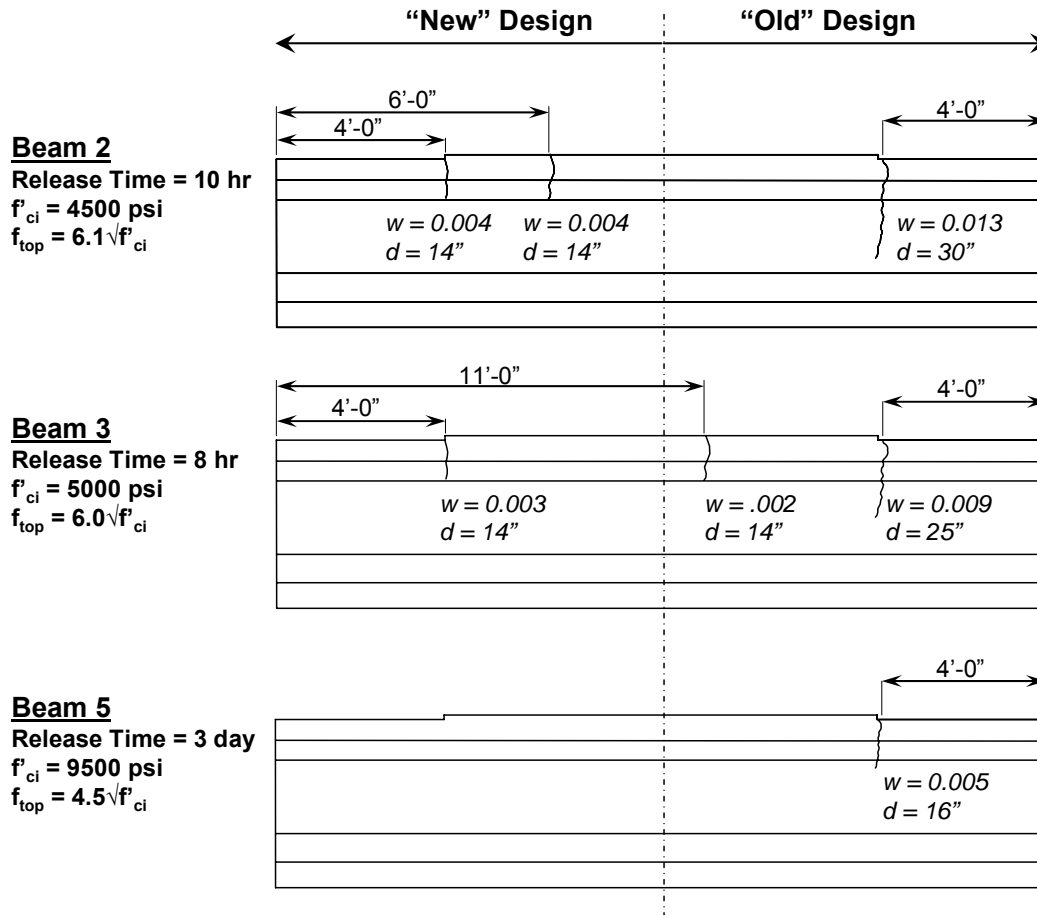


Figure 4-10 "New" vs. "Old" designs for specimens that cracked.

4.7 PREVENTING CRACKING AT RELEASE

Preventing short Type IV girders with high strand eccentricities from cracking at release depends on an engineer's ability to predict the following two physical events.

- 1.) Concrete material properties including strength and stiffness at the time of release.
- 2.) Mechanics of stress transfer in the end regions of a Type IV girder at the time of release.

The ability of a design engineer to predict cracking of short Type IV girders at release is discussed in this section.

4.7.1 Predicting Concrete Cracking Capacity

ACI 318, §18.4.1 limits the extreme fiber tensile stress applied immediately at release to $6\sqrt{f'_{ci}}$ unless reinforcement is provided. If reinforcement is not provided then only the concrete is relied upon to resist cracking. Therefore, the $6\sqrt{f'_{ci}}$ limit implies that cracking will be prevented, although it is not explicitly stated. AASHTO LRFD §5.9.4.1.2 limits the extreme fiber tensile stress applied immediately at release to $3\sqrt{f'_{ci}}$ when reinforcement is not provided.

Therefore, the $3\sqrt{f'_{ci}}$ limit also implies that cracking will be prevented, although this is not explicitly stated. The applied tensile stress at release for all beam specimens and the corresponding adequacy of the concrete to resist cracking is summarized in Figure 4-11.

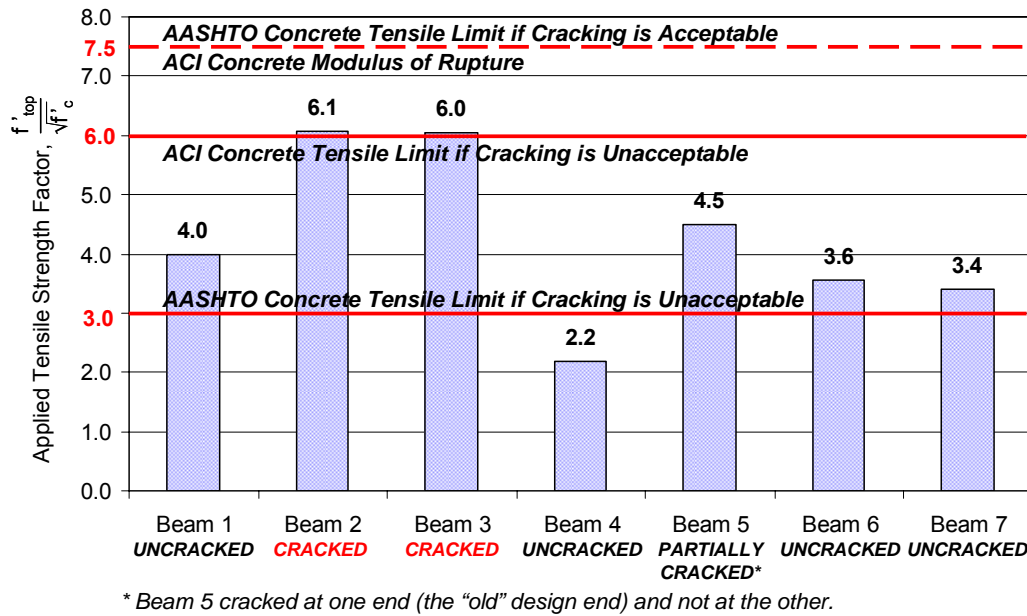


Figure 4-11 Applied tensile stress at release.

For the beams tested as part of this research program, two of them cracked despite efforts to prevent cracking; four of them did not crack; and one “partially cracked”. What is meant by “partially cracked” is that the “old design” end cracked and the “new design” end did not. Refer to Figure 4.9 for a mapping of cracks that occurred at release. Based on the data from these series of tests, the AASHTO tensile limit of $3\sqrt{f'_{ci}}$ is an adequate limit of the extreme fiber tensile strength if cracking is unacceptable. The ACI limit of $6\sqrt{f'_{ci}}$ is not adequate if cracking is unacceptable. Specimens tested as part of the research program exhibited cracking with an extreme fiber tensile stress as low as $4.5\sqrt{f'_{ci}}$ (Beam 5); significantly lower than the ACI limit of $6\sqrt{f'_{ci}}$. There are a number of contributing factors to the low cracking capacity of a short Type IV beam. These factors are discussed as follows.

Recall that the modulus of rupture of concrete is typically assumed to be equal to a minimum value of $7.5\sqrt{f'_{ci}}$. The data presented in Figure 4-12 is a composite plot of the historical data that formulates the tensile strength limit of concrete. Typically, the data was from 6x6-inch beams that were made with Type I cement and had cured for 28-days, often in a moist room for the first 7-days.

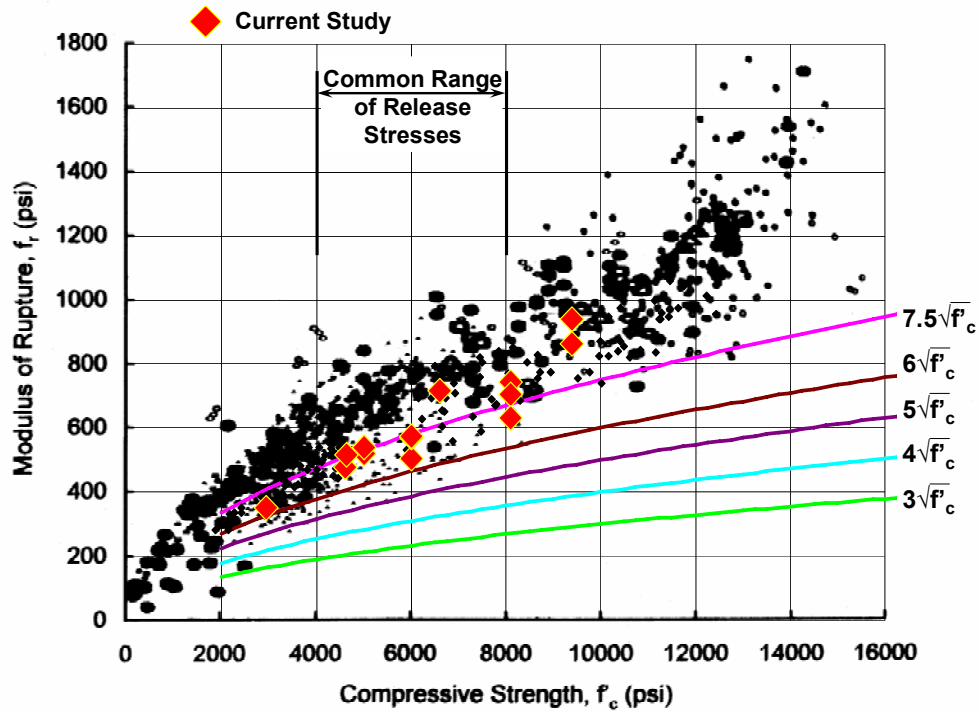


Figure 4-12 Summary of flexural tensile strength in comparison with historical* data. *(Kaplan 1959), (Carasquillo et al. 1981), (Shah and Ahmad 1985), (Khan et al. 1996), (Mokhtarzadeh and French 2000)

As can be observed in Figure 4-12, when concrete compressive strength is between 4000 and 5000-psi the lower bound to the data is approximately $5\sqrt{f'_{ci}}$. Beams 2 and 3 had release strengths of 4500 and 5000-psi respectively. Therefore, it was entirely possible that these beams could crack with an applied stress of $6\sqrt{f'_{ci}}$. Beam 3, however, had a release strength equal to 9500-psi yet it still cracked at one end with an applied tensile stress equal to $4.5\sqrt{f'_{ci}}$; somewhat lower than the lower bound to the historic data. Hence, the behavior of Beam 3 can not be explained solely with the data reported in the literature. As such, other contributing factors to the low tensile capacities will be further discussed.

Again, the data illustrated in Figure 4-12 is for flexural tests of 6x6x21-inch beams; not 54-inch deep by 20-foot long Type IV girders. The strain gradient is significantly less steep for a Type IV beam compared with a 6x6-inch beam (Figure 4-13).

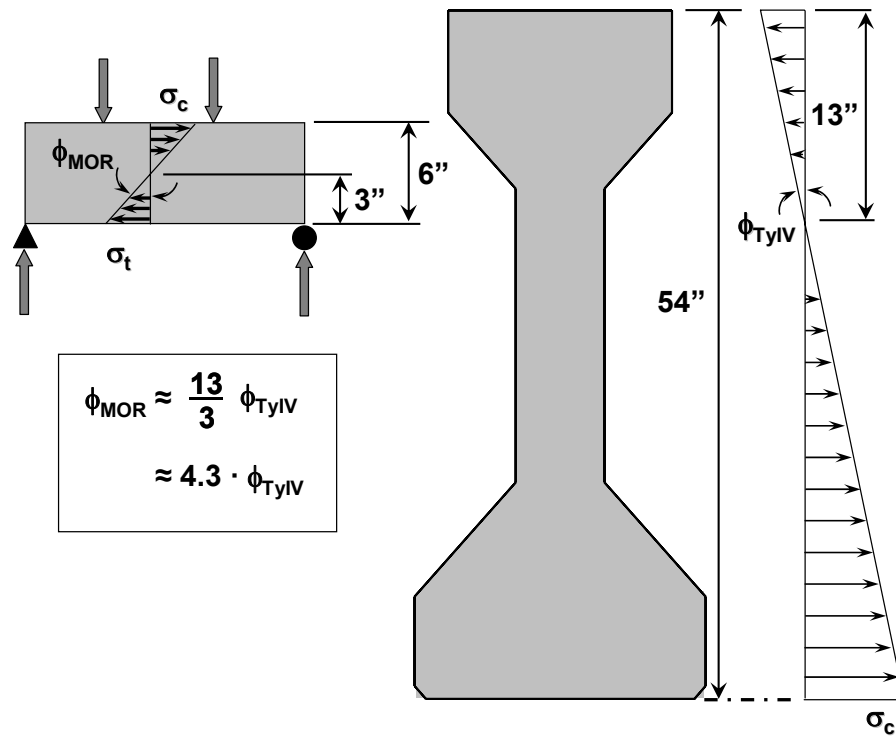


Figure 4-13 Difference in tensile strain gradient for 6x6-inch beam and Type IV girder.

As the strain gradient decreases, the measured tensile strength approaches that of a direct tensile test ($4\sqrt{f'_{ci}}$). The tensile strength of a concrete specimen decreases as the volume of the concrete that is highly stressed in tension increases. Therefore, another possible contributing factor to the cracking problem is the difference in strain gradients between an AASHTO Type IV and standard 6x6-21-inch beams.

The Type IV beam specimens fabricated in the laboratory were covered with wet burlap and plastic in order to attempt to control shrinkage strains. However, given the amount of heat of hydration associated with such a large mass of concrete it can be assumed that the amount of differential shrinkage of the Type IV beam specimens was larger than that of the 6x6-inch beams. Raphael (1984) discussed the tensile strength of over 500 cores taken from 14 concrete dams on the West Coast. The measured strength of field-placed concrete was 50-percent weaker than the measured strength of cylinder-placed concrete. The difference, he suggested, was in the curing history. He explained that differential drying induces tensile stresses in the concrete surface due to the restraining forces provided by shrinkage. Mohktarzadeh and French (2000) also reported a reduction in the flexural strength of concrete induced by drying and shrinkage.

Finally, the variability of concrete tensile tests is another factor to consider. Concrete is not a homogenous material. There are many variables that affect the strength and stiffness including, aggregate stiffness, water-cement ratio, aggregate size, etc. The top flanges of beam specimens fabricated as part of this research program were likely weaker in strength than indicated by material tests (i.e. MOR beams). Fabrication of a deep beam generally results in increased segregation and bleeding of water to the top. Most likely, the concrete that was placed in the top flange of a Type IV beam was weaker than the 6x6-inch beams. Therefore, the 6x6-

inch beams would indicate a somewhat higher tensile capacity than what is present in the top flange of a Type IV beam specimen.

No single factor is considered to be a sole contributor. However it is possible that all the variables taken together contribute to the significant difference observed in cracking capacities.

Further information regarding the differences in cracking capacities is presented in Figure 4-14. This figure provides a summary of the measured cracking capacity of concrete compared with the applied tensile stress for each beam specimen. Values are based on split cylinder tests for Beams 1 and 2 (factored by 1.25 for converting split-tensile stress to flexural-tensile stress) and MOR tests for Beams 3 through 7.

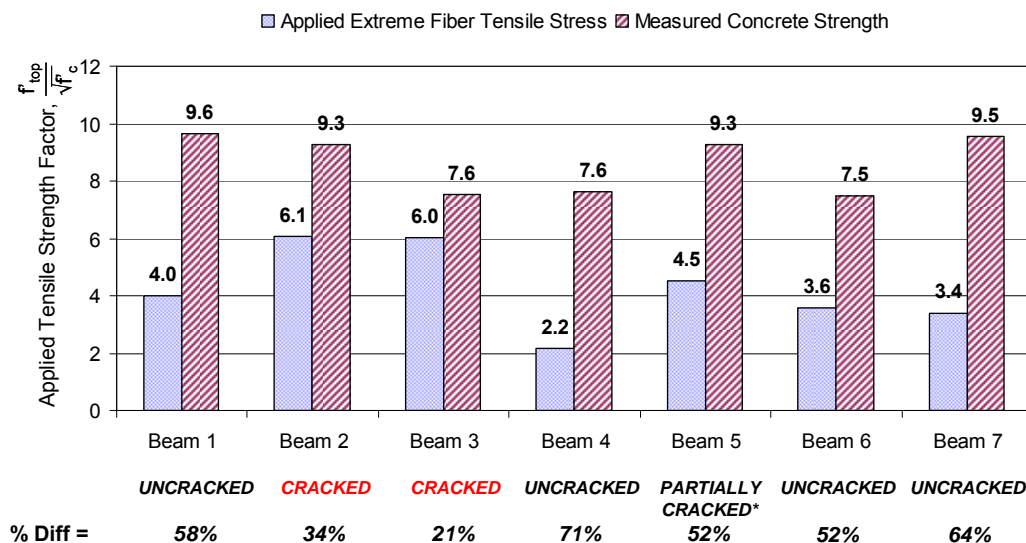


Figure 4-14 Measured concrete strength and corresponding predicted maximum tensile stress.

As illustrated in Figure 4-14 specimens that had measured concrete tensile strengths greater than the applied stress by 21 to 52-percent still exhibited cracking. This suggests that the concrete strength measured via a split cylinder or third-point flexural beam test is not a good indication of the tensile strength available in the outermost fiber of a full size Type IV beam.

Therefore, in order to absolutely prevent cracking, it appears that the maximum tensile stress applied to concrete should be limited to less than 50-percent of the tensile strength measured per a MOR specimen. This limit considers the contributing factors previously discussed: variability in tensile strength data; differences in quality of concrete due to a small amount of segregation and bleeding; tensile strains due to differential drying shrinkage; and differences in the applied strain gradient.

4.7.2 Mechanics of Stress Transfer

The stress profile at release was predicted using measured material properties as illustrated in Section 4.4. The predicted stress profiles are compared with the strain data for the specimens that did not crack (Beams 1, 4, north end of Beam 5, and Beams 6 and 7). When beams crack, “ $P/A \pm Mc/I$ ” is not valid for predicting stresses. Hence, only strain data from beams that did not crack is presented. Planar locations of strain gauges are summarized in Figure 4-15.

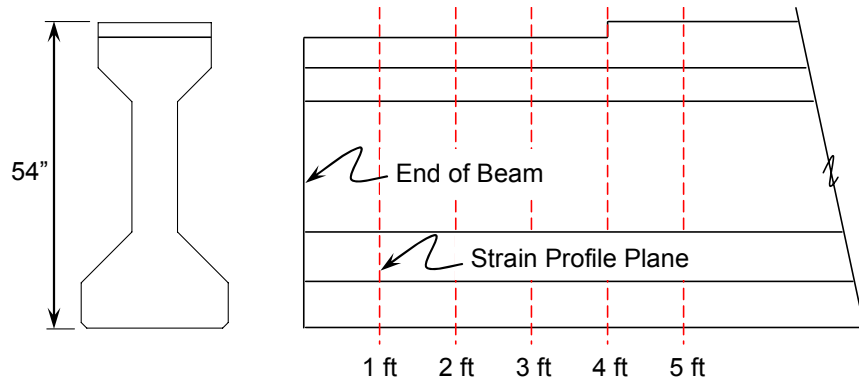


Figure 4-15 Planar location of experimentally measured strain profiles.

A summary of the theoretical vs. observed strain profiles measured 3-feet, 4-feet and 5-feet from the end of the beam are shown in Figures 4-16 through 4-18. Experimentally measured strain values are converted to stress values and compared with the “ $P/A \pm Mc/I$ ” stress profile line. For a distance from the beam end less than 2-feet, measured values did not correspond as well with predicted values. This is most likely due to invalid assumptions of the behavior of stresses within the transfer region. Differences between measured and predicted strain values less than 2-feet from a beam’s end were not considered to be relevant to the cracking problem. Cracking that had occurred in the field was consistently located approximately 4-feet from the end of a beam. Therefore, it was more important to the research team to be able to measure strain and predict behavior at the location where cracking had occurred. Details regarding all of the predicted vs. measured stress profiles can be found in Appendix F.

3'-0" from End of Beam

--- Best Fit Line
— Theoretical Line

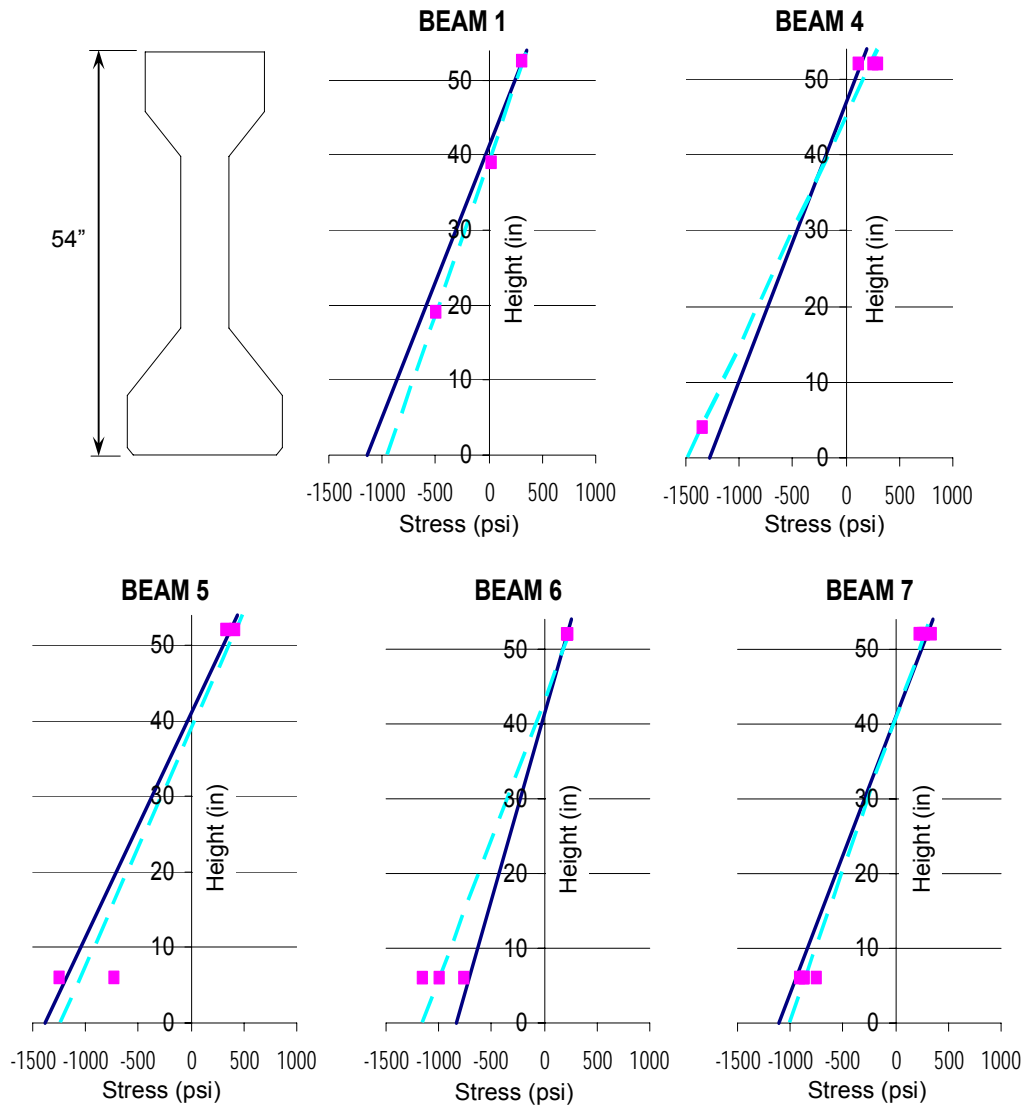


Figure 4-16 Stress profile located 3-feet from end of beam.

4'-0" from End of Beam

--- Best Fit Line
— Theoretical Line

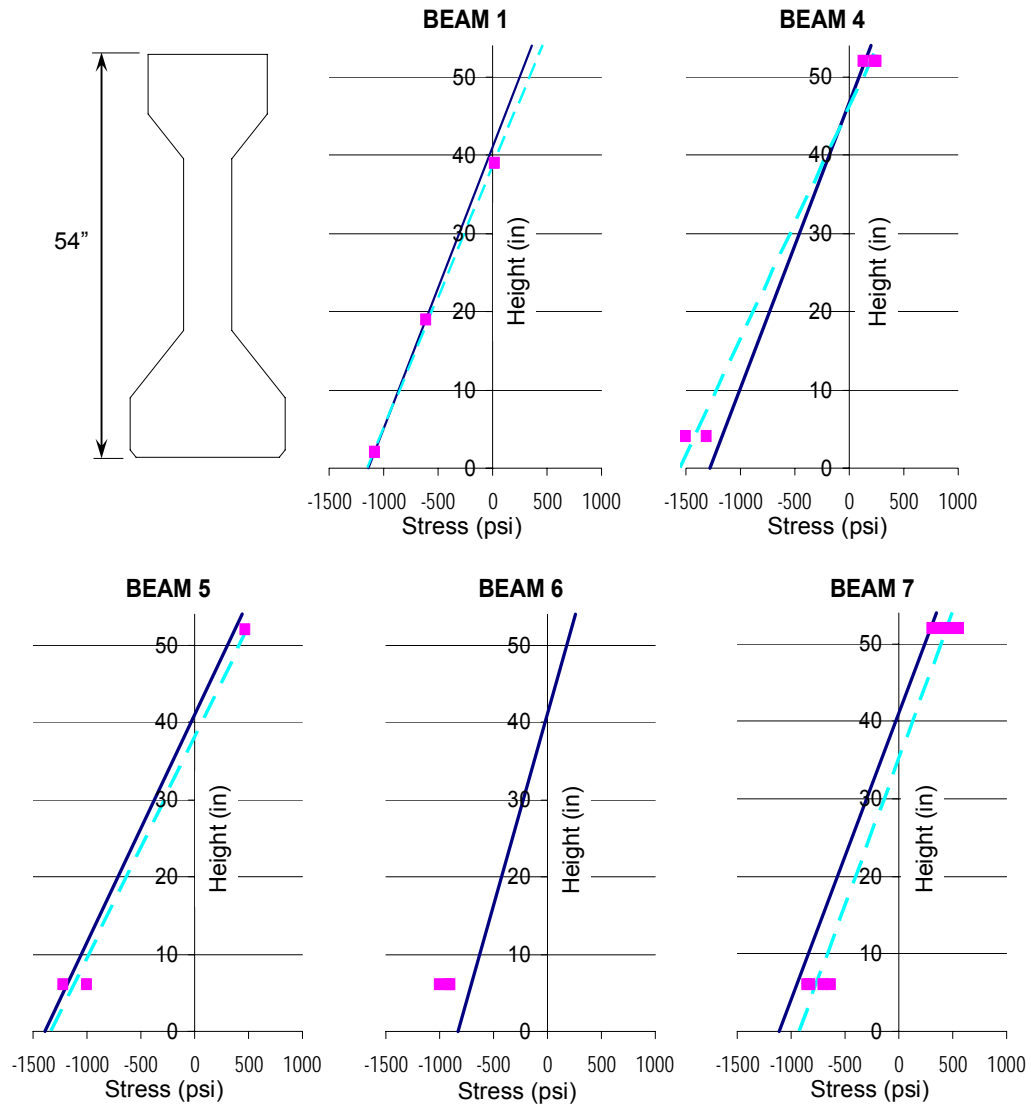


Figure 4-17 Stress profile located 4-feet from end of beam.

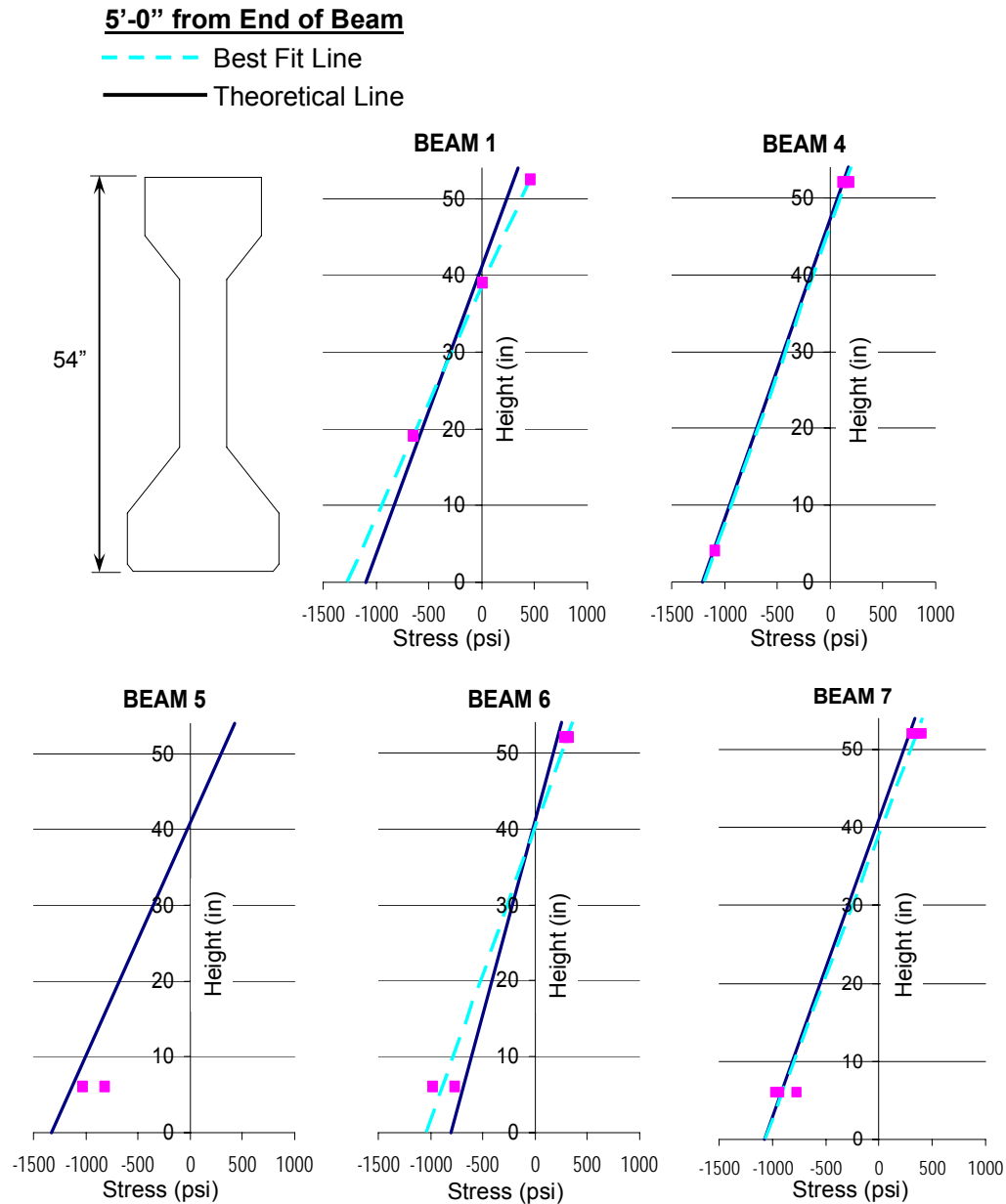


Figure 4-18 Stress profile located 5-feet from end of beam.

Strains within a beam section are measured directly with strain gauges. However, in order to compare these strains with theoretical values the modulus of elasticity must be determined. For this research project the modulus of elasticity was measured for a 6x54-inch cylinder (Figure 4-5) and assumed to be the same as the modulus of elasticity of the beam. Therefore, the accuracy of predicted stresses depends on the accuracy of the measured modulus of elasticity. In addition, the accuracy of the measured applied force will vary slightly depending on strand properties. These variables contribute to inaccuracies built into the measured stress values. Nonetheless, given the inherent inaccuracies in measuring stress, the research team was able to consistently predict beam behavior at a distance of 3-feet, 4-feet, and 5-feet. Therefore, from the

perspective of an engineer interested in predicting the behavior of a short Type IV beam at release, indications are that stresses predicted at the location of prestress transfer are reliable and accurate.

4.7.3 Cracking in End Regions of Short Type IV Beams

The research team was able to fairly accurately predict the magnitude of stress applied to the extreme concrete fiber. However, prediction of the corresponding tensile capacity of concrete was more difficult. Cracking at release was observed when the applied stress was as low as $4.5\sqrt{f'_{ci}}$. Currently, AASHTO limits the maximum tensile stress at release to $3\sqrt{f'_{ci}}$. Therefore, in accordance with AASHTO, if cracking is to be prevented at release it is recommended that the maximum tensile stress be limited to $3\sqrt{f'_{ci}}$.

Currently, the section with the highest risk of cracking at release is the short-span Type IV girder. According to TxDOT, other beam shapes such as the Type C or AASHTO Type VI have not exhibited a similar problem with cracking. As it turns out, instances of other beam shapes designed with a short length and high strand eccentricity are rare (Cotham et al. 2005). The only sections experiencing a cracking problem are the short Type IVs. Consequently, this is the only section that is subjected to such large tensile stresses. For a short Type IV girder, two basic ways to reduce the tensile stress at release from $7.5\sqrt{f'_{ci}}$ to $3\sqrt{f'_{ci}}$ are as follows.

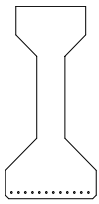
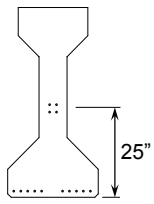
- 1.) Reduce the eccentricity of the prestress force.
- 2.) Reduce the magnitude of the prestress force.

If cracking at release is permitted, then the tensile stress at release may be as high as $7.5\sqrt{f'_{ci}}$ and sufficient mild steel should be provided longitudinally across cracks in order to control their widths (Section 4.5).

4.7.3.1 Solution 1: Reduce the eccentricity of the prestress force

The eccentricity of the total prestress force can be reduced simply by providing raised or draped strands (Solution 1). Providing draped strands is most likely not practical depending on the length of the girder. Table 4-7 illustrates the advantages of adding a few raised strands to a highly eccentrically loaded section.

Table 4-7 Result of Reducing Strand Eccentricity

		
Total Number of Strands	12	14
Maximum Tensile Stress at Release	475 psi	240 psi
Bottom Flange Cracking Moment	1385 kip-ft	1340 kip-ft
Ultimate Moment Capacity	1900 kip-ft	1890 kip-ft

The two sections were analyzed using a sectional analysis computer program (Collins and Mitchell 1990). The moment-curvature plot is presented in Figure 4-19. As expected, there is very little reduction in the maximum moment capacity of the two sections. More importantly, the difference between the critical cracking moments of the two sections is so small that these differences can be considered negligible. Finally, the maximum tensile stress is reduced by almost 50-percent. This is a very beneficial reduction considering that the cracking capacity of the section remains practically unchanged.

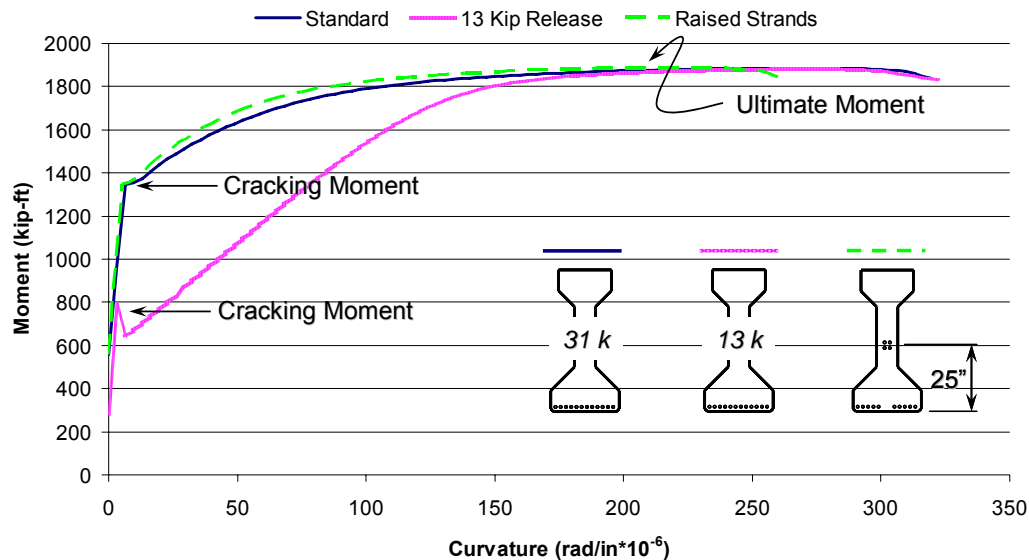
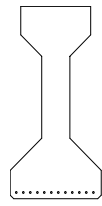
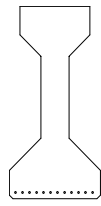


Figure 4-19 Moment curvature relationship for different strand arrangements and prestress forces.

4.7.3.2 Solution 2: Reduce the magnitude of the prestress force

Another viable option available for reducing the tensile stress at release is to reduce the magnitude of prestress force (Solution 2); the implications of this solution are illustrated in Figure 4-19 and Table 4-8.

Table 4-8 Result of Reducing Magnitude of Prestress Force

		
Total Number of Strands	12	12
Force per Strand	31 kip	13 kip
Maximum Tensile Stress at Release	475 psi	190 psi
Bottom Flange Cracking Moment	1385 kip-ft	770 kip-ft
Ultimate Moment Capacity	1900 kip-ft	1900 kip-ft

The two sections were analyzed using a sectional analysis computer program (Collins and Mitchell 1990). The moment-curvature plot is presented in Figure 4-19. As expected the ultimate moment capacity did not change. However, the ultimate moment is less crucial a factor of design than the cracking moment. The cracking moment is reduced by almost 50-percent (from 1385 kip-ft to 770 kip-ft). Such a large reduction in cracking capacity may not be as significant as it seems. The design of a Type IV girder spanning a short distance will often be controlled by the shear capacity of the section. For example: assume that a Type IV with 13-kips/strand is utilized with 1.2 girders per lane (10-foot center to center girder spacing). Per the HS-20 load table in Appendix A of the AASHTO Bridge Design Specifications (AASHTO 2002), a span with a length of 65-ft will result in a moment per girder of about 770-ft kips. This does not account for overloading of the span, but it does illustrate that for a span less than 65-feet, the cracking moment of the section is not as significant. Recall, Type IV girders that have cracked at release in the field are typically less than 65-feet in length. Therefore, the required cracking moment would most likely be low enough that the prestress force could be reduced as recommended. A summary of the two solutions are summarized in Figure 4-19.

The moment-curvature plots for the two solutions illustrates that Solution 1 is the most efficient. Solution 1 only requires two additional strands and the behavior is essentially identical to the original. Yet, the maximum tensile stress is reduced by half. Solution 2 has its merits as the currently used standard strand configuration has not changed. Both Solutions 1 and 2 would result in changes to TxDOT's design specifications and QA/QC procedure. The best solution may be the one that is easiest to implement within current TxDOT design parameters. According to Jeff Cotham (2006), TxDOT Project Director, Solution 2 may be more difficult to implement within TxDOT's system compared with Solution 1.

4.8 CURING TEMPERATURE PROFILE

Monitoring temperatures of a section during curing is of interest due to the role that temperature plays on concrete strength. Precast prestressed beam manufacturers control the match-curing temperature based on discrete locations in the beams. They are required to match-cure based on temperatures from a "cool" location. Where the cool location is located varies between manufacturers based on their curing methods and types of stressing beds. Manufacturers

that tarp their beams usually have lower temperatures at the bottom of the bottom flange. Otherwise, the cool location is located either in the web or at the top of the top flange. It is of interest to examine the importance the “cool location” assumption plays on the “actual” strength of concrete at release. Typical temperature data for a beam specimen cast as part of this research program is presented in Figures 4-19 and 4-21. The data presented in Figure 4-19 is for Beam 6, cast during the month of November. Thermocouples shown are located 5-feet from the end of the beam. The data presented in Figure 4-21 is for Beam 4, cast during the month of July. Temperature data for collected from all beam specimens can be found in Appendix H.

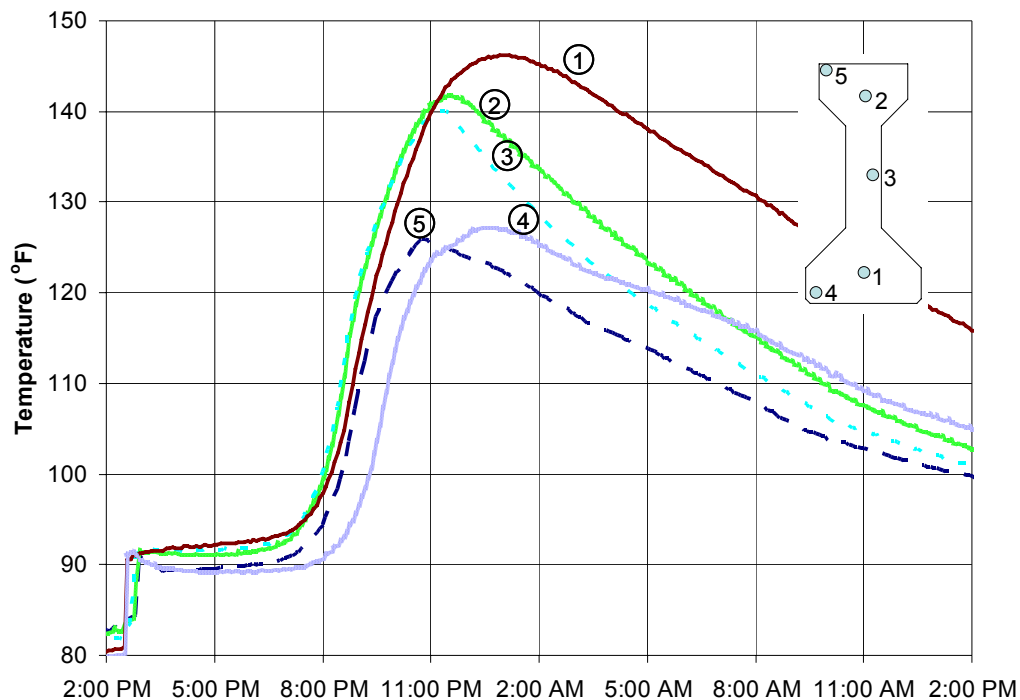


Figure 4-20 Time vs. temperature at various section locations (Beam 6).

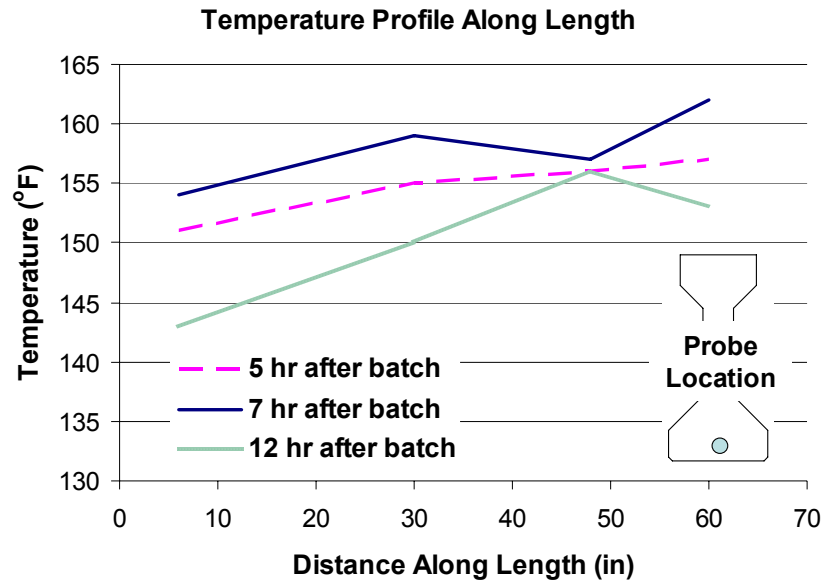


Figure 4-21 Time vs. temperature along length of beam (Beam 4).

As shown in Figure 4-19, the coolest temperature of a beam cast in the laboratory is at location 5. The temperature at location 4 is almost the same. Figure 4-20 illustrates that temperature differences greater than 10-°F can be found between the end of a beam and a location 5-feet from the end. Recall that beams cast in the laboratory are covered with burlap and plastic. Beams tarped in the field are covered with much thicker plastic and heavy fabric. The lack of heavy tarping for beams cast in the laboratory may contribute to the fact that the top of the top flange is the coolest location. Regardless of the tarping method used, it is important to track the behavior of the concrete in the top flange because that is the location where cracking has occurred. The information collected from all beams was used in determining a hot and cool location to study for Beam 7. Details on the curing temperatures of Beams 5 through 7 are included in Appendix G. The difference between the hottest and coolest location measured within Beam 6 was approximately 20-°F.

In conjunction with the fabrication of Beam 7, 48 cylinders were match-cured to a hot and cool location; 24 cylinders cured under the ambient conditions of the laboratory; and concrete strength gain was measured for these three locations (Figure 4-22). Compression and split-cylinder tension tests were conducted on cylinders from all three locations. Cylinders were tested approximately every 2-hours for the first 24 hours; and then tested about once a day until a time of 3-days. Figure 4-22 presents the time vs. temperature data for the hot, cold and ambient temperatures of the curing cylinders. The corresponding gains in compressive and tensile strength are presented in Figure 4-23.

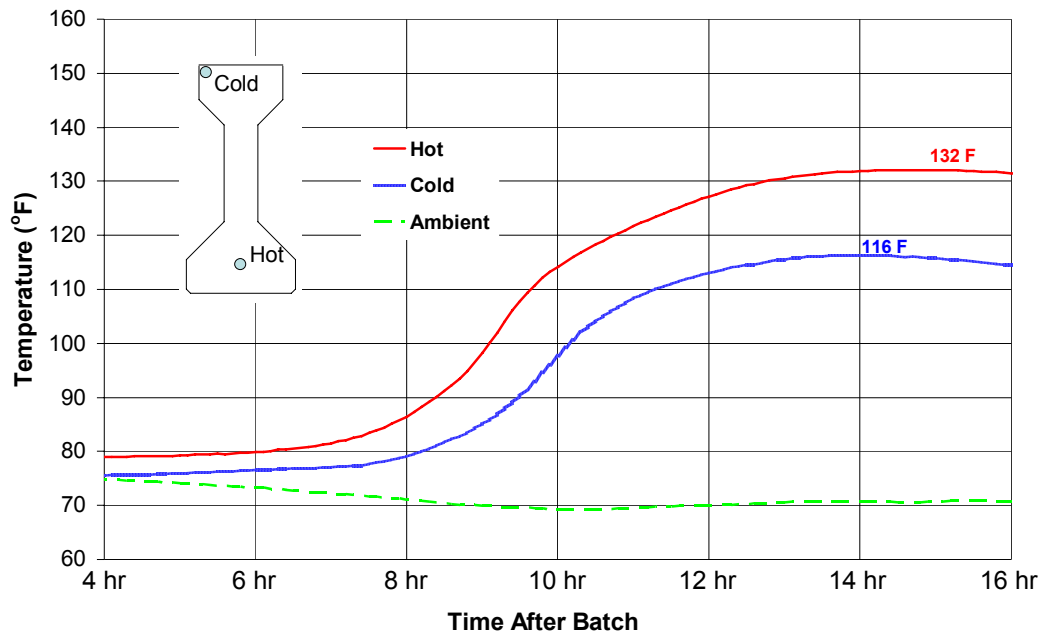


Figure 4-22 Time vs. temperature data for match-cured cylinders.

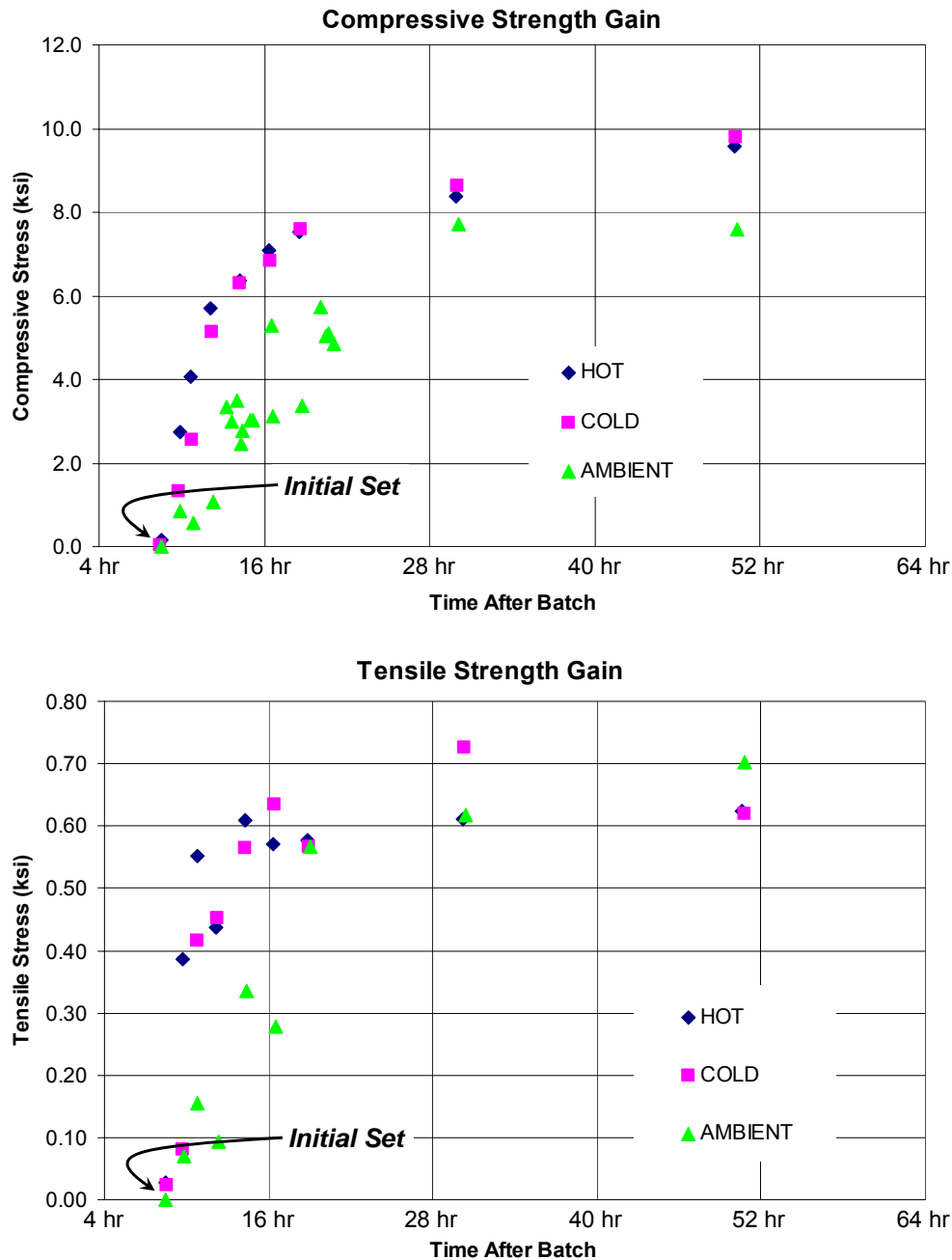


Figure 4-23 Compressive and tensile strength gains for different curing temperatures.

The maximum temperature difference between the hot and cold locations is 16-°F. For this particular mix and laboratory temperature, the concrete did not initially set until approximately 8-hours after batching. The ambient cylinders gained strength at a significantly lower rate. 4-hours after initial set, the compressive and tensile strength of the hot and cold match-cured cylinders converge to approximately similar values. This 4-hour time period also corresponds to the time when concrete is gaining strength at its most rapid rate. It is assumed that

the largest differences in tensile or compressive strengths will be realized during this stage when hydration of cement is the most active. Afterwards, a temperature difference of 16-°F has a small impact on the compressive or tensile strength gain of concrete. Beam 7 was cast during the relatively cool month of March.

For this particular specimen, when the compressive strength of the hot location reached 4000-psi, the corresponding compressive strength of the cold location was only 2500-psi. Similarly, the tensile strengths differed by about 130-psi. Therefore, based on the findings of this match-curing study, it would seem that the best time to release strands would be after the internal temperature of a beam has reached its peak value. That way, there will not be such large variations in compressive or tensile strengths due to differences in curing temperatures. Prior to that time, significant differences in strength may be expected between internal locations.

CHAPTER 5

Conclusions and Recommendations

5.1 SUMMARY OF SHORT TYPE IV BEAM CRACKING PROBLEM

This research project is a portion of a broader overlying research program investigating allowable design stresses; specifically as they pertain to the fabrication of precast prestressed concrete. For this portion of the project, the allowable design stress that was investigated was the extreme fiber tensile stress that develops and is most critical at the time of release. This research project was sponsored by TxDOT partly due to the field observations of flexural cracking of AASHTO Type IV beams at the time of prestress transfer. Girders that exhibited cracking were relatively short in length (20 to 60-ft) with highly eccentric strand configurations resulting in tensile stresses in the range of $6\sqrt{f'_c}$ to $7.5\sqrt{f'_c}$.

The goal of this research project was to identify the source of the cracking problem in short Type IV beams and suggest practical solutions to eliminate or reduce crack widths. From the onset of the research project it was theorized that cracking at release was due to one of two things: lack of knowledge on the early-age material properties of concrete; or lack of knowledge on the structural mechanics of prestress transfer.

Seven full-scale AASHTO Type IV beam specimens were fabricated and tested at the Ferguson Laboratory at the University of Texas at Austin. Strains were measured in the end regions of each beam; resulting in 14 separate tests. The purpose of experimentally measuring the strains was so assumptions on the mechanics of prestress transfer could be validated.

In addition to the full-scale beam tests, an extensive amount of material data was collected through testing and literature review. The purpose was to determine the early-age mechanical properties of concrete and describe its behavior based on a comparison within the body of knowledge. Properties measured included the compressive strength, split cylinder tensile strength, flexural tensile strength (modulus of rupture), and the modulus of elasticity. Over 60 cylinders were collected on separate occasions from four precast prestressed beam manufacturers and tested between 6 to 24-hours after batching. Also, in combination with the fabrication of each Type IV beam, anywhere from 25 to 72 cylinders were prepared and tested; resulting in 19 modulus of elasticity, 148 compression, 76 split cylinder, and 15 modulus of rupture tests. Cylinders were electronically match-cured, cured next to a curing beam, and cured at the ambient laboratory temperature.

Based on the wealth of data collected from the full-scale beam specimens and material tests, the following recommendations/conclusions are made.

5.2 SHORT TYPE IV BEAM CRACKING PROBLEM: SOURCE

The early-age material properties of concrete, differences in strength between control specimens and in-situ concrete, and the “plane sections remain plane” method of predicting beam behavior were evaluated as part of this research project. The purpose was to determine the source of the cracking problem. These three aspects of the project are discussed as follows.

Early-Age Material Properties

- 1.) The empirical relationship relating the compressive strength of a 4-inch cylinder to its split cylinder tensile strength ($f_t = 6\sqrt{f'_c}$) was valid for concrete made with Type III cement, air-dried, 14-hours after batching. Less than 14-hours, the relationship was often unconservative and unreliable.
- 2.) The curing temperature of a cylinder caused a significant difference in strength gain during the stage when the heat of hydration was increasing most rapidly. After the curing temperature had peaked, there was very little difference in the compressive or tensile strength between cylinders that had experienced maximum temperature differences up to 20-°F.
- 3.) For concrete compressive strengths between 4000 and 8000-psi, the lower bound to the tensile strength relationship for 6x6x21-inch beams is conservatively equal to $5\sqrt{f'_c}$. This value is based on a composite plot of all the data (1330 tests) collected from previous researchers; and data (15 tests) contributed from the current study.
- 4.) The empirical relationship relating the compressive strength of a match-cured 4-inch cylinder to the flexural strength of a next-to-beam cured 6x6x21-inch beam ($f_t = 7.5\sqrt{f'_c}$) was valid for concrete made with Type III cement, as soon as 10-hours after batching.
- 5.) The empirical relationship relating the compressive strength of a match-cured 4-inch cylinder to the modulus of elasticity of an ambient air-cured 6-inch cylinder ($E_c = 57000\sqrt{f'_c}$) was valid for concrete made with Type III cement, as soon as 13-hours after batching.

Strength of Control Specimens vs. In-Situ Strength

The tensile strength of the extreme fiber of a short AASHTO Type IV bridge beam was not accurately represented by the tensile strength of a next-to-beam cured 6x6x21-inch beam or match-cured 4-inch cylinder. Contributing factors to the difference between the tensile strength of concrete in the top flange of a Type IV beam and representative specimens may include the following:

- The difference in strain gradient between the two specimens. A 6x6-inch beam specimen has a much steeper gradient than an AASHTO Type IV girder (Figure 4-12). The tensile capacity of concrete decreases as the volume of concrete in extreme tension increases. The tensile capacity of a Type IV beam is most likely between $4\sqrt{f'_c}$ and $7.5\sqrt{f'_c}$.
- Compared to a 6x6-inch beam, 54-inch deep Type IV girders have increased segregation and bleeding of water to the top surface. Extreme fiber concrete that has been subjected to bleeding and segregation will have a relatively weaker strength compared to concrete of better quality.
- A relatively large mass Type IV girder exhibits more differential drying than a 6x6-inch beam. Differential drying induces tensile stresses in the concrete surface due to

the restraining forces provided by shrinkage. These shrinkage stresses add to the tensile stresses at release; reducing the load necessary to cause cracking.

Mechanics of Prestress Transfer

- 1.) Using the principles of classic beam theory (i.e. “ $P/A \pm Mc/I$ ”) to calculate stresses within the end regions of short Type IV beams with high strand eccentricity provided reasonably accurate results from 3 to 5-feet from the end. Stresses calculated at a distance less than 2-feet were not as consistent with experimentally measured values.
- 2.) Using AASHTO LRFD §5.11.4.2 to calculate the development length associated with the transfer of prestressing force provided reasonably accurate results.

5.3 SHORT TYPE IV BEAM CRACKING PROBLEM: SOLUTIONS

Crack Control

TxDOT’s current reinforcement detail provided sufficient reinforcement to limit crack widths. For beams that cracked and were reinforced per TxDOT’s current detail, crack widths were limited to 0.004-inches at the time of release.

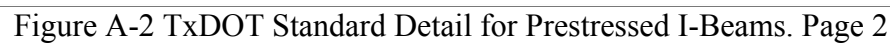
Crack Prevention

Limiting the applied concrete tensile stress at release to less than $4\sqrt{f'_c}$ was sufficient to prevent flexural tensile cracks from forming at the time of release. The current TxDOT detail for a short AASHTO Type IV girder has 12 strands, located 2-inches from the bottom surface, and stressed to 31-kips. Assuming a release strength of 4000-psi, the following changes to the current TxDOT detail will reduce the top fiber tensile stress to $4\sqrt{f'_c}$ or less.

- Raise two strands and provide 2 additional strands a distance approximately 25-inches above the beams bottom surface. This modification will reduce the top fiber tensile stress to approximately $3.8\sqrt{f'_c}$ (Section 4.6.3.1).
- Keep the current strand configuration the way it is and reduce the force per strand from 31-kips to 13-kips. This modification will reduce the top fiber tensile stress to approximately $3\sqrt{f'_c}$ (Section 4.6.3.2).

APPENDIX A

Texas Department of Transportation Standard Detail, AASHTO Type IV Bridge Girder



APPENDIX B

Prestressing Strand Calibration Curves

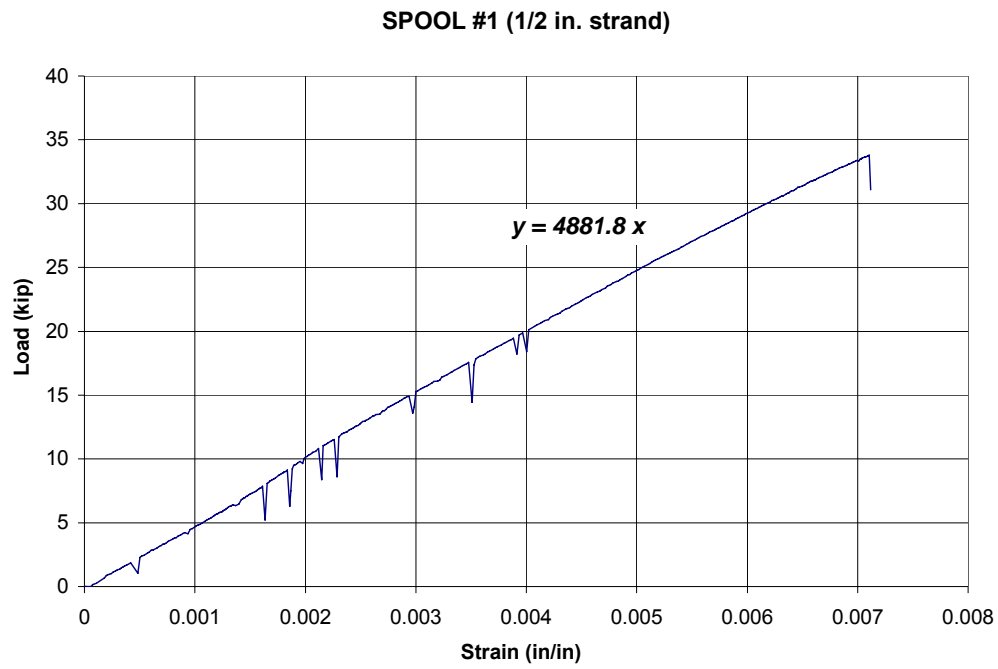


Figure B-1 Strand Test, Spool #1

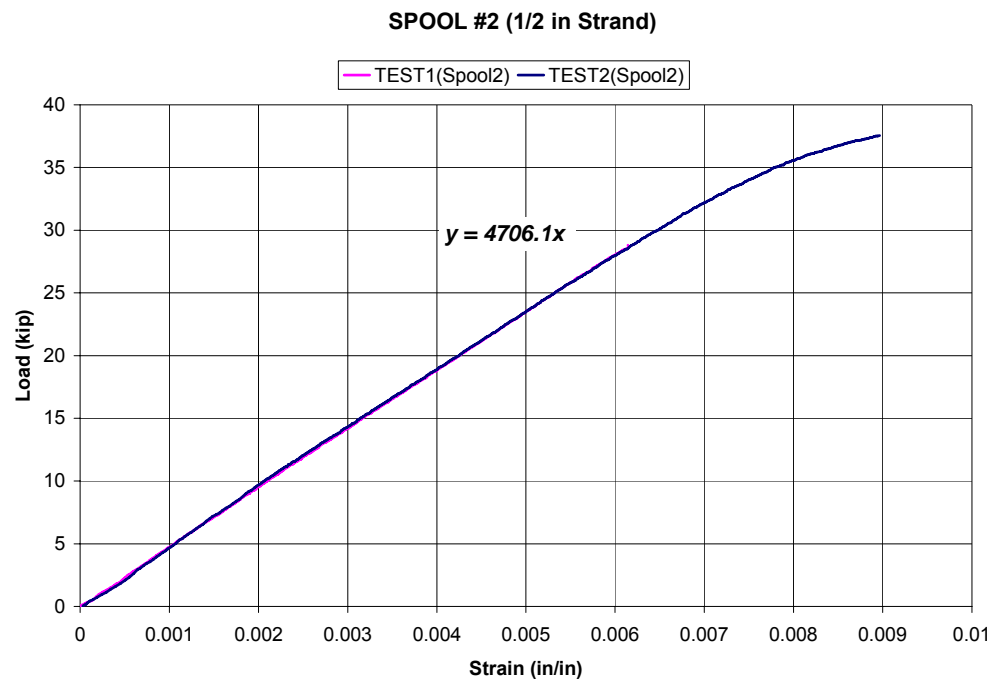


Figure B-2 Strand Test, Spool #2

APPENDIX C

Calculation of Strand Forces

Table C-1 Determination of Prestressing Force per Strand

	Strand No.	Gauge No.	Strain (in/in)	Ave. Preload (kip)	F_o (kip)
BEAM 1	2	110	0.004584	4.0	26.4
	4	115	0.004977	4.0	28.3
	4	119	0.004268	4.0	24.8
	4	209	0.004620	4.0	26.6
	6	201	0.005550	4.0	31.1
	6	214	0.004766	4.0	27.3
	7	604	0.003830	4.0	22.7
	9	106	0.004090	4.0	24.0
	9	602	0.003490	4.0	21.0
	9	601	0.003832	4.0	22.7
	11	105	0.005251	4.0	29.6
	11	600	0.004795	4.0	27.4
	Average =				26.0
BEAM 2	1	305	0.006020	3.0	31.3
	2	306	0.006080	3.0	31.6
	3	307	0.005946	3.0	31.0
	5	309	0.006012	3.0	31.3
	6	310	0.005604	3.0	29.4
	7	311	0.005232	3.0	27.6
	8	312	0.004983	3.0	26.5
	9	313	0.006054	3.0	31.5
	10	314	0.006002	3.0	31.2
	11	315	0.005921	3.0	30.9
	12	316	0.005864	3.0	30.6
	Average =				30.3
BEAM 3	2	306	0.006068	3.0	31.6
	4	308	0.005783	3.0	30.2
	5	309	0.006005	3.0	31.3
	6	310	0.006105	3.0	31.7
	7	311	0.006286	3.0	32.6
	8	312	0.006175	3.0	32.1
	9	313	0.006164	3.0	32.0
	10	314	0.005995	3.0	31.2
	11	315	0.005144	3.0	27.2
	12	316	0.006051	3.0	31.5
	Average =				31.1

Table C-2 Determination of Prestressing Force per Strand

	<i>Strand No.</i>	<i>Gauge No.</i>	<i>Strain</i> (in/in)	<i>Ave. Preload</i> (kip)	<i>F_o</i> (kip)
BEAM 4	1	305	0.005977	2.5	30.6
	2	306	0.006564	2.5	33.4
	3	307	0.006254	2.5	31.9
	5	309	0.006026	2.5	30.9
	6	310	0.006227	2.5	31.8
	9	313	0.006051	2.5	31.0
	13	400	0.005328	2.5	27.6
	14	404	0.005851	2.5	30.0
Average =					30.9
BEAM 5	1	305	0.006337	1.5	31.3
	2	306	0.006449	1.5	31.8
	3	307	0.006258	1.5	31.0
	4	308	0.006474	1.5	32.0
	5	309	0.005980	1.5	29.6
	6	310	0.006395	1.5	31.6
	7	311	0.006436	1.5	31.8
	8	312	0.006629	1.5	32.7
	9	313	0.006448	1.5	31.8
	10	314	0.006144	1.5	30.4
	11	315	0.006441	1.5	31.8
	12	316	0.006405	1.5	31.6
Average =					31.5
BEAM 6	1	305	0.003320	2.0	17.6
	2	306	0.003224	2.0	17.2
	3	307	0.003629	2.0	19.1
	4	308	0.003509	2.0	18.5
	5	309	0.003910	2.0	20.4
	6	310	0.003938	2.0	20.5
	7	311	0.003869	2.0	20.2
	8	312	0.003910	2.0	20.4
	9	313	0.003751	2.0	19.7
	10	314	0.003560	2.0	18.8
	11	315	0.003143	2.0	16.8
	12	316	0.003277	2.0	17.4
Average =					18.9

Table C-3 Determination of Prestressing Force per Strand

	Strand No.	Gauge No.	Strain (in/in)	Ave. Preload (kip)	F_o (kip)
BEAM 7	1	305	0.0052439	3.5	28.2
	2	306	0.0038973	3.5	21.8
	3	307	0.0043504	3.5	24.0
	4	308	0.0046463	3.5	25.4
	5	309	0.0047563	3.5	25.9
	6	310	0.0047713	3.5	26.0
	7	311	0.0048022	3.5	26.1
	8	312	0.0046549	3.5	25.4
	9	313	0.0046549	3.5	25.4
	10	314	0.0045387	3.5	24.9
	11	315	0.0043159	3.5	23.8
	12	316	0.0049718	3.5	26.9
Average =					25.3

APPENDIX D

Experimentally Measured Material Properties of Concrete

Table D-1 Compressive Strength of Concrete

	<i>Time Tested</i>	<i>Cure Type</i>	<i>Test Type</i>	<i>Load (kip)</i>	<i>f'_c (ksi)</i>
PLANT A	1/28/2004 19:55	Amb	C39	3.5	279
Batch:	1/28/2004 20:01	Amb	C39	4.8	382
1/28/2004 14:00	1/28/2004 20:07	Amb	C39	4.2	334
	1/28/2004 21:55	Amb	C39	13.2	1,050
	1/28/2004 22:03	Amb	C39	17.4	1,385
	1/28/2004 22:08	Amb	C39	16.3	1,297
	1/29/2004 0:00	Amb	C39	35.7	2,841
	1/29/2004 0:07	Amb	C39	35.8	2,849
	1/29/2004 0:11	Amb	C39	35.9	2,857
	1/29/2004 2:00	Amb	C39	57.5	4,576
	1/29/2004 2:05	Amb	C39	59.2	4,711
	1/29/2004 2:15	Amb	C39	60.3	4,799
	1/29/2004 3:56	Amb	C39	66.6	5,300
	1/29/2004 4:09	Amb	C39	66.8	5,316
	1/29/2004 4:15	Amb	C39	66.2	5,268
	1/29/2004 5:55	Amb	C39	73.9	5,881
	1/29/2004 6:05	Amb	C39	78.5	6,247
	1/29/2004 6:13	Amb	C39	78.0	6,207
	1/29/2004 7:55	Amb	C39	86.1	6,852
	1/29/2004 8:03	Amb	C39	88.7	7,059
	1/29/2004 8:07	Amb	C39	84.6	6,732
	1/29/2004 10:10	Amb	C39	94.5	7,520
	1/29/2004 10:15	Amb	C39	87.9	6,995
	1/29/2004 10:20	Amb	C39	91.0	7,242
	1/29/2004 12:25	Amb	C39	93.6	7,449
	1/29/2004 12:32	Amb	C39	91.1	7,250
	1/29/2004 12:40	Amb	C39	94.4	7,512
	1/29/2004 14:25	Amb	C39	96.6	7,687
	1/29/2004 14:30	Amb	C39	96.5	7,679
	1/29/2004 14:33	Amb	C39	94.9	7,552
PLANT B	3/25/2004 19:55	Amb	C39	5.6	446
Batch:	3/25/2004 20:00	Amb	C39	6.1	485
3/25/2004 13:30	3/25/2004 20:05	Amb	C39	7.5	597
	3/25/2004 21:55	Amb	C39	19.4	1,544
	3/25/2004 21:56	Amb	C39	12.0	955
	3/25/2004 22:00	Amb	C39	19.1	1,520
	3/25/2004 23:55	Amb	C39	42.7	3,398
	3/26/2004 0:00	Amb	C39	39.2	3,119

"Amb" = ambient air-cured

Table D-2 Compressive Strength of Concrete

	<i>Time Tested</i>	<i>Cure Type</i>	<i>Test Type</i>	<i>Load (kip)</i>	<i>f'_c (ksi)</i>
PLANT B cont...	3/26/2004 0:05	Amb	C39	40.5	3,223
	3/26/2004 2:00	Amb	C39	46.6	3,708
	3/26/2004 2:05	Amb	C39	49.3	3,923
	3/26/2004 2:10	Amb	C39	46.3	3,684
	3/26/2004 4:30	Amb	C39	55.9	4,448
	3/26/2004 4:35	Amb	C39	52.8	4,202
	3/26/2004 4:40	Amb	C39	54.8	4,361
	3/26/2004 6:08	Amb	C39	56.7	4,512
	3/26/2004 6:12	Amb	C39	58.5	4,655
	3/26/2004 6:15	Amb	C39	59.3	4,719
	3/26/2004 8:10	Amb	C39	66.5	5,292
	3/26/2004 8:16	Amb	C39	65.9	5,244
	3/26/2004 8:30	Amb	C39	67.5	5,371
	3/26/2004 9:50	Amb	C39	64.7	5,149
	3/26/2004 9:55	Amb	C39	64.4	5,125
	3/26/2004 9:58	Amb	C39	70.5	5,610
	3/26/2004 11:55	Amb	C39	65.2	5,188
	3/26/2004 12:00	Amb	C39	65.2	5,188
	3/26/2004 12:02	Amb	C39	66.6	5,300
	3/26/2004 13:45	Amb	C39	70.9	5,642
	3/26/2004 13:45	Amb	C39	75.1	5,976
	3/26/2004 13:45	Amb	C39	75.4	6,000
PLANT C Batch: 4/22/2004 11:00	4/22/2004 19:30	Amb	C39	29.3	2,332
	4/22/2004 19:50	Amb	C39	33.6	2,674
	4/22/2004 19:55	Amb	C39	33.1	2,634
	4/22/2004 21:36	Amb	C39	37.3	2,968
	4/22/2004 21:43	Amb	C39	42.2	3,358
	4/22/2004 21:50	Amb	C39	47.5	3,780
	4/22/2004 23:30	Amb	C39	53.3	4,241
	4/22/2004 23:35	Amb	C39	58.6	4,663
	4/22/2004 23:38	Amb	C39	53.6	4,265
	4/23/2004 1:24	Amb	C39	57.8	4,600
	4/23/2004 1:31	Amb	C39	56.7	4,512
	4/23/2004 1:36	Amb	C39	55.7	4,432
	4/23/2004 4:05	Amb	C39	60.7	4,830
	4/23/2004 4:15	Amb	C39	62.0	4,934
	4/23/2004 4:20	Amb	C39	63.9	5,085
	4/23/2004 5:45	Amb	C39	66.2	5,268

"Amb" = ambient air-cured

Table D-3 Compressive Strength of Concrete

	<i>Time Tested</i>	<i>Cure Type</i>	<i>Test Type</i>	<i>Load (kip)</i>	<i>f'_c (ksi)</i>
PLANT C cont...	4/23/2004 5:50	Amb	C39	66.9	5,324
	4/23/2004 6:00	Amb	C39	66.5	5,292
	4/23/2004 7:05	Amb	C39	67.2	5,348
	4/23/2004 7:10	Amb	C39	70.0	5,570
	4/23/2004 7:15	Amb	C39	66.4	5,284
	4/23/2004 10:25	Amb	C39	66.1	5,260
	4/23/2004 10:30	Amb	C39	70.7	5,626
	4/23/2004 10:35	Amb	C39	69.0	5,491
	4/23/2004 11:20	Amb	C39	69.5	5,531
	4/23/2004 11:25	Amb	C39	70.4	5,602
	4/23/2004 11:35	Amb	C39	67.9	5,403
	4/23/2004 13:10	Amb	C39	72.9	5,801
	4/23/2004 13:15	Amb	C39	73.8	5,873
	4/23/2004 13:19	Amb	C39	73.8	5,873
PLANT D Batch: 2/26/2004 12:00	2/26/2004 18:50	Amb	C40	0.7	56
	2/26/2004 19:00	Amb	C41	0.6	48
	2/26/2004 19:05	Amb	C42	0.6	48
	2/26/2004 20:50	Amb	C43	4.6	366
	2/26/2004 20:55	Amb	C44	4.2	334
	2/26/2004 21:00	Amb	C45	5.1	406
	2/26/2004 22:55	Amb	C46	10.8	859
	2/26/2004 23:00	Amb	C47	12.2	971
	2/26/2004 23:03	Amb	C48	11.9	947
	2/27/2004 0:45	Amb	C49	20.0	1,592
	2/27/2004 0:50	Amb	C50	19.0	1,512
	2/27/2004 0:53	Amb	C51	21.4	1,703
	2/27/2004 2:50	Amb	C52	30.8	2,451
	2/27/2004 2:55	Amb	C53	29.3	2,332
	2/27/2004 3:00	Amb	C54	30.4	2,419
	2/27/2004 4:55	Amb	C55	42.7	3,398
	2/27/2004 5:00	Amb	C56	42.5	3,382
	2/27/2004 5:05	Amb	C57	44.8	3,565
	2/27/2004 6:25	Amb	C58	50.5	4,019
	2/27/2004 6:32	Amb	C59	52.3	4,162
	2/27/2004 6:38	Amb	C60	51.6	4,106
	2/27/2004 9:00	Amb	C61	58.9	4,687
	2/27/2004 9:05	Amb	C62	64.1	5,101
	2/27/2004 9:08	Amb	C63	57.4	4,568

Table D-4 Compressive Strength of Concrete

	<i>Time Tested</i>	<i>Cure Type</i>	<i>Test Type</i>	<i>Load (kip)</i>	<i>f'_c (ksi)</i>
<i>PLANT D</i>	2/27/2004 10:50	Amb	C64	62.9	5,005
<i>cont...</i>	2/27/2004 10:56	Amb	C65	61.6	4,902
	2/27/2004 13:00	Amb	C66	70.2	5,586
	2/27/2004 13:05	Amb	C67	65.9	5,244
	2/27/2004 13:10	Amb	C68	66.1	5,260

"Amb" = ambient air-cured

Table D-5 Compressive Strength of Concrete

	<i>Time Tested</i>	<i>Cure Type</i>	<i>Test Type</i>	<i>Load</i> (kip)	<i>f'_c</i> (psi)
BEAM 1	12/20/2004 10:45	Amb	C39	127.8	10,170
Batch:	12/20/2004 10:45	Amb	C39	126.4	10,059
11/11/2004 13:30	12/20/2004 10:45	Amb	C39	127.6	10,154
	12/20/2004 10:45	MC	C39	103.0	8,197
	12/20/2004 10:45	MC	C39	100.0	7,958
	12/20/2004 10:45	MC	C39	103.0	8,197
BEAM 2	4/25/2005 22:40	Amb	C39	0.8	64
Batch:	4/25/2005 22:52	Amb	C39	1.5	119
4/25/2005 14:30	4/25/2005 23:15	Amb	C39	5.0	398
	4/26/2005 0:34	Amb	C39	25.0	1,989
	4/26/2005 1:08	Amb	C39	36.4	2,897
	4/26/2005 1:30	Amb	C39	42.5	3,382
	4/26/2005 1:50	Amb	C39	39.0	3,104
	4/26/2005 1:58	Amb	C39	49.0	3,899
	4/26/2005 2:02	Amb	C39	50.0	3,979
	4/25/2005 22:27	MC	C39	40.0	3,183
	4/25/2005 22:36	MC	C39	68.0	5,411
	4/25/2005 22:44	MC	C39	37.0	2,944
	4/25/2005 23:50	MC	C39	52.5	4,178
	4/25/2005 23:55	MC	C39	58.0	4,616
	4/26/2005 0:00	MC	C39	58.1	4,626
	4/26/2005 3:00	MC	C39	74.0	5,889
BEAM 3	6/27/2005 19:40	Amb	C39	20.0	1,592
Batch:	6/27/2005 21:00	Amb	C39	38.5	3,064
6/27/2005 14:30	6/27/2005 22:00	Amb	C39	51.5	4,098
	6/27/2005 22:45	Amb	C39	52.5	4,178
	6/27/2005 23:00	Amb	C39	54.5	4,337
	6/27/2005 23:15	Amb	C39	67.5	5,372
	6/27/2005 18:45	NB	C39	7.0	557
	6/27/2005 19:40	NB	C39	35.5	2,825
	6/27/2005 20:45	NB	C39	55.0	4,377
	6/27/2005 21:30	NB	C39	57.0	4,536
	6/27/2005 21:30	NB	C39	61.5	4,894
	6/27/2005 22:40	NB	C39	64.0	5,093
	6/27/2005 18:30	MC	C39	16.0	1,273
	6/27/2005 19:30	MC	C39	38.5	3,064

"Amb" = ambient air-cured

"NB" = match-cured next-to-beam

"MC" = match-cured using electronic controller

Table D-6 Compressive Strength of Concrete

	<i>Time Tested</i>	<i>Cure Type</i>	<i>Test Type</i>	<i>Load (kip)</i>	<i>f'_c (psi)</i>
BEAM 3 cont...	6/27/2005 20:13	MC	C39	49.0	3,899
	6/27/2005 20:30	MC	C39	54.0	4,297
	6/27/2005 21:00	MC	C39	57.5	4,576
	6/27/2005 21:15	MC	C39	52.5	4,178
	6/27/2005 21:20	MC	C39	61.0	4,854
	6/27/2005 21:50	MC	C39	62.5	4,974
BEAM 4 Batch: 7/25/2005 15:00	7/25/2005 21:05	Amb	C39	32.0	2,547
	7/25/2005 22:00	Amb	C39	46.5	3,700
	7/25/2005 23:20	Amb	C39	57.5	4,576
	7/25/2005 23:35	Amb	C39	58.5	4,655
	7/25/2005 23:40	Amb	C39	54.5	4,337
	7/26/2005 0:45	Amb	C39	63.5	5,053
	7/26/2005 6:00	Amb	C39	81.7	6,502
	7/25/2005 21:00	NB	C39	55.0	4,377
	7/25/2005 23:25	NB	C39	73.5	5,849
	7/26/2005 0:40	NB	C39	83.0	6,605
	7/26/2005 2:20	NB	C39	89.0	7,083
	7/26/2005 4:55	NB	C39	97.0	7,719
	7/26/2005 8:30	NB	C39	104.0	8,276
	7/25/2005 19:15	NB	C39	22.5	1,791
	7/26/2005 7:05	NB	C39	79.0	6,287
	7/26/2005 7:11	NB	C39	81.0	6,446
	7/26/2005 7:15	NB	C39	83.0	6,605
	7/25/2005 19:10	MC	C39	5.5	438
	7/25/2005 20:53	MC	C39	56.0	4,456
	7/25/2005 23:20	MC	C39	76.5	6,088
	7/26/2005 0:37	MC	C39	84.0	6,685
	7/26/2005 2:15	MC	C39	94.0	7,481
	7/26/2005 4:50	MC	C39	100.2	7,974
	7/26/2005 8:20	MC	C39	104.0	8,276
BEAM 5 Batch: 8/26/2005 12:30	8/26/2005 20:50	Amb	C39	20.5	1,631
	8/26/2005 21:25	Amb	C39	41.5	3,303
	8/26/2005 22:00	Amb	C39	60.5	4,815
	8/26/2005 22:05	Amb	C39	54.5	4,337
	8/26/2005 22:10	Amb	C39	62.5	4,974
	8/26/2005 23:05	Amb	C39	69.1	5,499
	8/29/2005 11:50	Amb	C39	122.4	9,741
	8/26/2005 18:51	NB	C39	3.5	279
	8/26/2005 20:40	NB	C39	59.5	4,735

"Amb" = ambient air-cured

"NB" = match-cured next-to-beam

"MC" = match-cured using electronic controller

Table D-7 Compressive Strength of Concrete

	<i>Time Tested</i>	<i>Cure Type</i>	<i>Test Type</i>	<i>Load (kip)</i>	<i>f'_c (psi)</i>
BEAM 5 cont...	8/26/2005 20:45	NB	C39	61.5	4,894
	8/26/2005 22:50	NB	C39	80.6	6,414
	8/26/2005 23:00	NB	C39	80.0	6,366
	8/26/2005 23:40	NB	C39	83.2	6,621
	8/26/2005 23:55	NB	C39	85.0	6,764
	8/27/2005 16:45	NB	C39	106.6	8,483
	8/27/2005 16:55	NB	C39	107.3	8,539
	8/28/2005 12:45	NB	C39	115.0	9,152
	8/28/2005 12:55	NB	C39	112.3	8,937
	8/29/2005 10:45	NB	C39	119.3	9,494
	8/29/2005 10:55	NB	C39	115.2	9,168
	8/26/2005 18:50	MC	C39	25.0	1,989
	8/26/2005 20:35	MC	C39	64.5	5,133
	8/26/2005 22:35	MC	C39	81.5	6,486
	8/26/2005 23:50	MC	C39	84.0	6,685
	8/27/2005 16:38	MC	C39	112.6	8,961
	8/28/2005 12:40	MC	C39	116.2	9,247
	8/29/2005 11:05	MC	C39	122.0	9,709
	8/29/2005 11:15	MC	C39	123.2	9,804
BEAM 6 Batch: 11/7/2005 14:00	11/7/2005 22:30	Amb	C39	8.5	676
	11/8/2005 0:32	Amb	C39	42.5	3,382
	11/8/2005 1:14	Amb	C39	53.0	4,218
	11/8/2005 1:23	Amb	C39	57.0	4,536
	11/8/2005 1:27	Amb	C39	54.5	4,337
	11/7/2005 21:05	NB	C39	6.0	477
	11/7/2005 22:04	NB	C39	36.0	2,865
	11/7/2005 23:25	NB	C39	59.5	4,735
	11/7/2005 23:30	NB	C39	56.5	4,496
	11/8/2005 0:21	NB	C39	78.5	6,247
	11/8/2005 0:28	NB	C39	69.0	5,491
	11/7/2005 20:00	MC	C39	2.5	199
	11/7/2005 21:00	MC	C39	22.0	1,751
	11/7/2005 22:01	MC	C39	49.0	3,899
	11/7/2005 23:15	MC	C39	66.5	5,292
	11/7/2005 23:20	MC	C39	64.5	5,133
	11/8/2005 0:07	MC	C39	60.0	4,775
	11/8/2005 0:12	MC	C39	73.5	5,849
BEAM 7 Batch: 2/27/2006 14:00	2/27/2006 22:30	Amb	C39	0.0	0
	2/27/2006 23:50	Amb	C39	10.5	836

"Amb" = ambient air-cured

"NB" = match-cured next-to-beam

"MC" = match-cured using electronic controller

Table D-8 Compressive Strength of Concrete

	<i>Time Tested</i>	<i>Cure Type</i>	<i>Test Type</i>	<i>Load (kip)</i>	<i>f'_c (psi)</i>
BEAM 7	2/28/2006 0:50	Amb	C39	7.0	557
cont...	2/28/2006 2:15	Amb	C39	13.5	1,074
	2/28/2006 3:15	Amb	C39	42.0	3,342
	2/28/2006 3:35	Amb	C39	37.5	2,984
	2/28/2006 4:00	Amb	C39	44.0	3,502
	2/28/2006 4:20	Amb	C39	31.0	2,467
	2/28/2006 4:25	Amb	C39	35.0	2,785
	2/28/2006 5:00	Amb	C39	38.0	3,024
	2/28/2006 5:10	Amb	C39	38.0	3,024
	2/28/2006 6:30	Amb	C39	66.5	5,292
	2/28/2006 6:35	Amb	C39	39.0	3,104
	2/28/2006 8:45	Amb	C39	42.5	3,382
	2/28/2006 10:05	Amb	C39	72.0	5,730
	2/28/2006 10:30	Amb	C39	63.5	5,053
	2/28/2006 10:40	Amb	C39	64.0	5,093
	2/28/2006 11:00	Amb	C39	61.0	4,854
	2/28/2006 20:06	Amb	C39	97.0	7,719
	3/1/2006 16:20	Amb	C39	95.5	7,600
	3/3/2006 15:00	Amb	C39	134.8	10,727
	2/27/2006 22:25	Cold	C39	0.5	40
	2/27/2006 23:45	Cold	C39	16.5	1,313
	2/28/2006 0:45	Cold	C39	32.0	2,547
	2/28/2006 2:10	Cold	C39	64.5	5,133
	2/28/2006 4:15	Cold	C39	79.0	6,287
	2/28/2006 6:25	Cold	C39	86.0	6,844
	2/28/2006 8:40	Cold	C39	95.5	7,600
	2/28/2006 20:00	Cold	C39	108.5	8,634
	3/1/2006 16:15	Cold	C39	123.0	9,788
	3/3/2006 14:50	Cold	C39	134.5	10,703
	2/27/2006 22:30	Hot	C39	2.0	159
	2/27/2006 23:55	Hot	C39	34.5	2,746
	2/28/2006 0:40	Hot	C39	51.0	4,059
	2/28/2006 2:05	Hot	C39	71.5	5,690
	2/28/2006 4:10	Hot	C39	80.0	6,366
	2/28/2006 6:20	Hot	C39	89.0	7,083
	2/28/2006 8:30	Hot	C39	94.5	7,520
	2/28/2006 19:55	Hot	C39	105.2	8,372
	3/1/2006 16:10	Hot	C39	120.2	9,565
	3/3/2006 14:45	Hot	C39	132.0	10,505

"Amb" = ambient air-cured

"Cold" = electronically match-cured to a cold spot in beam

"Hot" = electronically match-cured to hot spot in beam

Table D-9 Tensile Strength of Concrete

	<i>Time Tested</i>	<i>Cure Type</i>	<i>Test Type</i>	<i>Load</i>	<i>f_t</i>
PLANT A	1/28/2004 19:55	Amb	C496	1	19.9
Batch:	1/28/2004 20:01	Amb	C496	2.54	50.5
1/28/2004 14:00	1/28/2004 20:07	Amb	C496	2.83	56.3
	1/28/2004 21:55	Amb	C496	5.75	114.4
	1/28/2004 22:03	Amb	C496	4.98	99.1
	1/28/2004 22:08	Amb	C496	8.01	159.4
	1/29/2004 0:00	Amb	C496	12.87	256.0
	1/29/2004 0:07	Amb	C496	12.24	243.5
	1/29/2004 0:11	Amb	C496	12.25	243.7
	1/29/2004 2:00	Amb	C496	20.68	411.4
	1/29/2004 2:05	Amb	C496	20.5	407.8
	1/29/2004 2:15	Amb	C496	21.76	432.9
	1/29/2004 3:56	Amb	C496	18.71	372.2
	1/29/2004 4:09	Amb	C496	27.31	543.3
	1/29/2004 4:15	Amb	C496	18.56	369.2
	1/29/2004 5:55	Amb	C496	24.99	497.2
	1/29/2004 6:05	Amb	C496	24.48	487.0
	1/29/2004 6:13	Amb	C496	22.68	451.2
	1/29/2004 7:55	Amb	C496	25.32	503.7
	1/29/2004 8:03	Amb	C496	33.38	664.1
	1/29/2004 8:07	Amb	C496	26.67	530.6
	1/29/2004 10:10	Amb	C496	27.98	556.6
	1/29/2004 10:15	Amb	C496	23.64	470.3
	1/29/2004 10:20	Amb	C496	26.2	521.2
	1/29/2004 12:25	Amb	C496	29.59	588.7
	1/29/2004 12:32	Amb	C496	33.1	658.5
	1/29/2004 12:40	Amb	C496	28.48	566.6
	1/29/2004 14:25	Amb	C496	27.22	541.5
	1/29/2004 14:30	Amb	C496	32.04	637.4
	1/29/2004 14:33	Amb	C496	31.68	630.3
PLANT B	3/25/2004 19:55	Amb	C496	4.65	92.5
Batch:	3/25/2004 20:00	Amb	C496	3.19	63.5
3/25/2004 13:30	3/25/2004 20:05	Amb	C496	5.01	99.7
	3/25/2004 21:55	Amb	C496	11.51	229.0
	3/25/2004 21:56	Amb	C496	10.03	199.5
	3/25/2004 22:00	Amb	C496	11.21	223.0
	3/25/2004 23:55	Amb	C496	17.26	343.4
	3/26/2004 0:00	Amb	C496	15.44	307.2
	3/26/2004 0:05	Amb	C496	13.83	275.1

"Amb" = ambient air-cured

Table D-10 Tensile Strength of Concrete

	<i>Time Tested</i>	<i>Cure Type</i>	<i>Test Type</i>	<i>Load (kip)</i>	<i>f_t (ksi)</i>
PLANT B cont...	3/26/2004 2:00	Amb	C496	21.56	428.9
	3/26/2004 2:05	Amb	C496	16.56	329.5
	3/26/2004 2:10	Amb	C496	17.5	348.2
	3/26/2004 4:30	Amb	C496	19.75	392.9
	3/26/2004 4:35	Amb	C496	22.54	448.4
	3/26/2004 4:40	Amb	C496	20.12	400.3
	3/26/2004 6:08	Amb	C496	22.83	454.2
	3/26/2004 6:12	Amb	C496	21.64	430.5
	3/26/2004 6:15	Amb	C496	19.19	381.8
	3/26/2004 8:10	Amb	C496	23.25	462.5
	3/26/2004 8:16	Amb	C496	23.82	473.9
	3/26/2004 8:30	Amb	C496	21.74	432.5
	3/26/2004 9:50	Amb	C496	23.63	470.1
	3/26/2004 9:55	Amb	C496	24.18	481.0
	3/26/2004 9:58	Amb	C496	23.46	466.7
	3/26/2004 11:55	Amb	C496	25.13	499.9
	3/26/2004 12:00	Amb	C496	25.51	507.5
	3/26/2004 12:02	Amb	C496	23.22	461.9
	3/26/2004 13:45	Amb	C496	24.44	486.2
	3/26/2004 13:45	Amb	C496	23.54	468.3
	3/26/2004 13:45	Amb	C496	26.37	524.6
PLANT C Batch: 4/22/2004 11:00	4/22/2004 19:30	Amb	C496	13.28	264.2
	4/22/2004 19:50	Amb	C496	14.73	293.0
	4/22/2004 19:55	Amb	C496	12.7	252.7
	4/22/2004 21:36	Amb	C496	21.91	435.9
	4/22/2004 21:43	Amb	C496	15.56	309.6
	4/22/2004 21:50	Amb	C496	19.83	394.5
	4/22/2004 23:30	Amb	C496	25.01	497.6
	4/22/2004 23:35	Amb	C496	16.5	328.3
	4/22/2004 23:38	Amb	C496	19.84	394.7
	4/23/2004 1:24	Amb	C496	21.28	423.4
	4/23/2004 1:31	Amb	C496	12.3	244.7
	4/23/2004 1:36	Amb	C496	28.1	559.0
	4/23/2004 4:05	Amb	C496	23.63	470.1
	4/23/2004 4:15	Amb	C496	30.48	606.4
	4/23/2004 4:20	Amb	C496	26.64	530.0
	4/23/2004 5:45	Amb	C496	25.85	514.3
	4/23/2004 5:50	Amb	C496	27.09	538.9

"Amb" = ambient air-cured

Table D-11 Tensile Strength of Concrete

	<i>Time Tested</i>	<i>Cure Type</i>	<i>Test Type</i>	<i>Load (kip)</i>	<i>f_t (ksi)</i>
PLANT C cont...	4/23/2004 6:00	Amb	C496	28.1	559.0
	4/23/2004 7:05	Amb	C496	30.01	597.0
	4/23/2004 7:10	Amb	C496	30.28	602.4
	4/23/2004 7:15	Amb	C496	31.8	632.6
	4/23/2004 10:25	Amb	C496	32.18	640.2
	4/23/2004 10:30	Amb	C496	30.8	612.7
	4/23/2004 10:35	Amb	C496	27.83	553.7
	4/23/2004 11:20	Amb	C496	28.15	560.0
	4/23/2004 11:25	Amb	C496	27.61	549.3
	4/23/2004 11:35	Amb	C496	28.33	563.6
	4/23/2004 13:10	Amb	C496	33.47	665.9
	4/23/2004 13:15	Amb	C496	23.51	467.7
	4/23/2004 13:19	Amb	C496	28.03	557.6
PLANT D Batch: 2/26/2004 12:00	2/26/2004 18:50	Amb	C496	1.18	23.5
	2/26/2004 19:00	Amb	C496	1.19	23.7
	2/26/2004 19:05	Amb	C496	1.11	22.1
	2/26/2004 20:50	Amb	C496	1.84	36.6
	2/26/2004 20:55	Amb	C496	2.77	55.1
	2/26/2004 21:00	Amb	C496	1.76	35.0
	2/26/2004 22:55	Amb	C496	6.25	124.3
	2/26/2004 23:00	Amb	C496	4.58	91.1
	2/26/2004 23:03	Amb	C496	6.09	121.2
	2/27/2004 0:45	Amb	C496	8.67	172.5
	2/27/2004 0:50	Amb	C496	7.21	143.4
	2/27/2004 0:53	Amb	C496	10.08	200.5
	2/27/2004 2:50	Amb	C496	17.06	339.4
	2/27/2004 2:55	Amb	C496	12.06	239.9
	2/27/2004 3:00	Amb	C496	13.09	260.4
	2/27/2004 4:55	Amb	C496	19.29	383.8
	2/27/2004 5:00	Amb	C496	23.61	469.7
	2/27/2004 5:05	Amb	C496	22.52	448.0
	2/27/2004 6:25	Amb	C496	24.74	492.2
	2/27/2004 6:32	Amb	C496	21.16	421.0
	2/27/2004 6:38	Amb	C496	24.05	478.5
	2/27/2004 9:00	Amb	C496	24.15	480.4
	2/27/2004 9:05	Amb	C496	24.78	493.0
	2/27/2004 9:08	Amb	C496	21.77	433.1
	2/27/2004 10:50	Amb	C496	26.44	526.0

"Amb" = ambient air-cured

Table D-12 Tensile Strength of Concrete

	<i>Time Tested</i>	<i>Cure Type</i>	<i>Test Type</i>	<i>Load (kip)</i>	<i>f_t (ksi)</i>
PLANT D cont...	2/27/2004 10:56	Amb	C496	23.71	471.7
	2/27/2004 13:00	Amb	C496	26.59	529.0
	2/27/2004 13:05	Amb	C496	25.69	511.1
	2/27/2004 13:10	Amb	C496	22.28	443.2

"Amb" = ambient air-cured

Table D-13 Tensile Strength of Concrete

	<i>Time Tested</i>	<i>Cure Type</i>	<i>Test Type</i>	<i>Load (kip)</i>	<i>f_t (psi)</i>
BEAM 1	12/20/2004 10:45	Amb	C496	34.0	675
Batch:	12/20/2004 10:45	Amb	C496	33.7	671
11/11/2004 13:30	12/20/2004 10:45	Amb	C496	39.2	779
	12/20/2004 10:45	MC	C496	37.4	744
	12/20/2004 10:45	MC	C496	35.5	706
	12/20/2004 10:45	MC	C496	31.8	632
BEAM 2	4/26/2005 3:00	Amb	C496	21.4	426
Batch:	4/25/2005 23:03	MC	C496	17.6	350
4/25/2005 14:30	4/26/2005 0:20	MC	C496	24.1	479
	4/26/2005 0:25	MC	C496	26.0	516
BEAM 3	6/27/2005 20:05	NB	C496	16.5	329
Batch:	6/27/2005 20:35	NB	C496	20.2	401
6/27/2005 14:30	6/27/2005 22:10	NB	C496	26.0	517
	6/27/2005 23:25	NB	C496	25.4	504
	6/27/2005 19:55	MC	C496	14.8	295
	6/27/2005 20:40	MC	C496	19.8	394
	6/27/2005 20:58	MC	C496	20.2	401
	6/27/2005 21:03	MC	C496	19.6	389
	6/27/2005 22:05	MC	C496	22.6	449
	6/27/2005 22:15	NB	C78	6.5	541
	6/27/2005 22:25	NB	C78	6.3	522
	6/27/2005 22:30	NB	C78	6.5	540
BEAM 4	7/26/2005 8:05	NB	C496	31.8	633
Batch:	7/26/2005 8:30	NB	C496	32.4	645
7/25/2005 15:00	7/26/2005 8:35	NB	C496	25.0	498
	7/26/2005 8:40	NB	C496	28.8	574
	7/26/2005 5:25	MC	C496	30.9	615
	7/26/2005 5:30	MC	C496	32.7	651
	7/26/2005 8:10	MC	C496	30.57	608
	7/26/2005 8:20	MC	C496	33.05	658
	7/26/2005 5:40	NB	C78	8.32	693
	7/26/2005 8:45	NB	C78	8.341667	695
	7/26/2005 8:50	NB	C78	8.200833	683
BEAM 5	8/26/2005 23:45	NB	C496	23.94	476
Batch:	8/26/2005 23:50	NB	C496	27.65	550
8/26/2005 12:30	8/29/2005 11:10	NB	C496	32.59	648
	8/29/2005 11:16	NB	C496	26.85	534

"Amb" = ambient air-cured

"NB" = match-cured next-to-beam

"MC" = match-cured using electronic controller

Table D-14 Tensile Strength of Concrete

	<i>Time Tested</i>	<i>Cure Type</i>	<i>Test Type</i>	<i>Load (kip)</i>	<i>f_t (psi)</i>
BEAM 5 cont...	8/26/2005 23:55	MC	C496	25.93	516
	8/29/2005 11:00	MC	C496	26.54	528
	8/29/2005 11:05	MC	C496	34.48	686
	8/27/2005 0:05	NB	C78	8.61	718
	8/29/2005 10:40	NB	C78	10.37	864
	8/29/2005 10:50	NB	C78	11.28	940
BEAM 6 Batch: 11/7/2005 14:00	11/7/2005 22:25	NB	C496	17.47	348
	11/7/2005 22:25	NB	C496	21.34	425
	11/7/2005 23:45	NB	C496	29.73	592
	11/7/2005 22:20	MC	C496	24.74	492
	11/7/2005 23:26	MC	C496	29.65	590
	11/7/2005 23:40	MC	C496	25.41	506
	11/8/2005 0:05	NB	C78	6.06	505
	11/8/2005 0:10	NB	C78	6.85	571
	11/8/2005 0:20	NB	C78	6.87	573
BEAM 7 Batch: 2/27/2006 14:00	2/27/2006 22:30	NB	C496	0	0.0
	2/27/2006 23:50	NB	C496	3.51	70
	2/28/2006 0:50	NB	C496	7.82	156
	2/28/2006 2:20	NB	C496	4.73	94
	2/28/2006 4:25	NB	C496	16.89	336
	2/28/2006 6:30	NB	C496	13.93	277
	2/28/2006 9:00	NB	C496	28.53	568
	2/28/2006 20:25	NB	C496	30.99	617
	3/1/2006 16:50	NB	C496	35.3	702
	3/3/2006 14:40	NB	C496	29.59	589
	2/27/2006 22:35	Cold	C496	1.18	24
	2/27/2006 23:45	Cold	C496	4.1	82
	2/28/2006 0:50	Cold	C496	20.89	416
	2/28/2006 2:15	Cold	C496	22.7	452
	2/28/2006 4:20	Cold	C496	28.38	565
	2/28/2006 6:25	Cold	C496	31.86	634
	2/28/2006 8:55	Cold	C496	28.46	566
	2/28/2006 20:20	Cold	C496	36.52	727
	3/1/2006 16:45	Cold	C496	31.11	619
	3/3/2006 14:35	Cold	C496	33	657
	2/27/2006 22:30	Hot	C496	1.34	27
	2/27/2006 23:45	Hot	C496	19.4	386
	2/28/2006 0:45	Hot	C496	27.74	552
	2/28/2006 2:10	Hot	C496	21.94	437

"Amb" = ambient air-cured

"NB" = match-cured next-to-beam

"MC" = match-cured using electronic controller

Table D-15 Tensile Strength of Concrete

	<i>Time Tested</i>	<i>Cure Type</i>	<i>Test Type</i>	<i>Load (kip)</i>	<i>f_t (psi)</i>
BEAM 7	2/28/2006 4:15	Hot	C496	30.61	609
cont...	2/28/2006 6:20	Hot	C496	28.74	572
	2/28/2006 8:50	Hot	C496	28.98	577
	2/28/2006 20:15	Hot	C496	30.73	611
	3/1/2006 16:35	Hot	C496	31.4	625
	3/3/2006 14:30	Hot	C496	31.74	631
	3/3/2006 15:15	NB	C78	11.714	976
	3/3/2006 15:15	NB	C78	11.5	958
	3/3/2006 15:20	NB	C78	12.323	1027

"Amb" = ambient air-cured

"Cold" = electronically match-cured to a cold spot in beam

"Hot" = electronically match-cured to hot spot in beam

Table D-16 Modulus of Elasticity of Concrete

	<i>Test</i>	<i>Time Tested</i>	<i>Stress (ksi)</i>	<i>Top Strain (in/in)</i>	<i>Bot Strain (in/in)</i>	<i>E_{top} (ksi)</i>	<i>E_{bot} (ksi)</i>
BEAM 1	Test 1	12/20/2004 11:45	3.96	0.000709	0.000691	5,584	5,736
	Test 2	12/20/2004 12:00	3.96	0.000675	0.000650	5,868	6,094
	Test 3	12/20/2004 12:15	3.96	0.000744	0.000706	5,326	5,609
					Average =	5,593	5,813
BEAM 2	Test 1	4/26/2005 2:10	1.59	0.000350	0.000425	4,547	3,745
	Test 2	4/26/2005 2:30	1.59	0.000341	0.000363	4,672	4,390
	Test 3	4/26/2005 2:45	1.59	0.000322	0.000316	4,945	5,043
					Average =	4,721	4,393
BEAM 3	Test 1	6/27/2005 23:20	1.53	0.000331	0.000266	4,612	5,752
	Test 2	6/27/2005 23:30	1.53	0.000313	0.000288	4,889	5,314
	Test 3	6/27/2005 23:45	1.53	0.000306	0.000313	4,989	4,889
					Average =	4,830	5,319
BEAM 4	Test 1	7/26/2005 6:00	2.55	0.000525	0.000422	4,850	6,036
	Test 2	7/26/2005 6:20	2.55	0.000516	0.000488	4,939	5,224
	Test 3	7/26/2005 6:35	2.55	0.000475	0.000488	5,361	5,224
						5,050	5,494
BEAM 5	Test 1	8/29/2005 14:00	3.82	0.000642	0.000566	5,948	6,753
	Test 2	8/29/2005 14:20	3.82	0.000630	0.000623	6,066	6,127
					Average =	6,007	6,440
BEAM 6	Test 1-1	11/8/2005 2:00	1.98	0.000306	0.000263	6,467	7,545
	Test 1-2	11/8/2005 2:00	1.98	0.000344	0.000275	5,762	7,202
	Test 2-1	11/8/2005 2:20	1.95	0.000344	0.000372	5,659	5,231
	Test 2-2	11/8/2005 2:20	1.95	0.000325	0.000381	5,985	5,102
	Test 3-1	11/8/2005 2:40	1.95	0.000347	0.000347	5,608	5,608
	Test 3-2	11/8/2005 2:40	1.95	0.000291	0.000344	6,693	5,659
					Average =	6,029	6,058
BEAM 7	Test 1-1	3/3/2006 16:00	4.10	0.000684	0.000609	5,995	6,733
	Test 1-2	3/3/2006 16:00	4.10	0.000678	0.000600	6,050	6,838
	Test 2-1	3/3/2006 16:15	4.10	0.000694	0.000713	5,914	5,758
	Test 2-2	3/3/2006 16:15	4.17	0.000706	0.000669	5,909	6,241
					Average =	5,967	6,392

APPENDIX E

Calculated Concrete Stresses in Beam Specimen

Table E-1 Top and Bottom Fiber Stress Calculations, Beam 1

Material Properties		Section Properties (include block-out)	
$f'_{ci} = 8.1 \text{ ksi}$	$y'_s = 50 \text{ in}$	$L_o = 20 \text{ ft}$	$I_g = 235067 \text{ in}^4$
$f_y = 60 \text{ ksi}$	$A_{ps} = 0.153 \text{ in}^2$	$H = 52.5 \text{ in}$	$F_o = 312 \text{ kip}$
$E_s = 29000 \text{ ksi}$	$y_p = 2 \text{ in}$	$y_b = 23.62$	$d_b = 0.5 \text{ in}$
$A'_s = 2.38 \text{ in}^2$	$E_{ci} = 5703 \text{ ksi}$	$A_g = 758.4 \text{ in}^2$	
Transfer Length (AASHTO LRFD §5.11.4.2)			
$f_{se} = \frac{(F_o - \Delta F_{pES})}{12 \cdot A_{ps}}$			$f_{se} = 164.5 \text{ ksi}$
$l_d = \frac{f_{se}}{3} \cdot d_b$			$l_d = 27 \text{ in}$
Transformed Section Properties			
$n = \frac{E_s}{E_c}$			$n = 5.1$
$y_{btr} = \frac{A_g \cdot y_b + (n-1) \cdot (A'_s \cdot y'_s + 12 A_{ps} \cdot y_p)}{A_g + (n-1) \cdot (A'_s + 12 A_{ps})}$			$y_{btr} = 23.74 \text{ in}$
$A_{tr} = A_g + (n-1) \cdot (A'_s + 12 A_{ps})$			$A_{tr} = 776 \text{ in}^2$
$I_{tr} = I_g + A_g (y_b - y_{btr})^2 + (n-1) [A'_s (y'_s - y_{btr})^2 + 12 A_{ps} (y_p - y_{btr})^2]$			$I_{tr} = 245327 \text{ in}^4$
Losses due to Elastic Shortening (AASHTO LRFD §5.9.5.2.3)			
$f_{cir} = \frac{F_o}{A_g} + \frac{F_o (y_b - y_p)^2}{I_g}$			$f_{cir} = 1.03 \text{ ksi}$
$\Delta f_{pES} = n \cdot f_{cir}$			$\Delta f_{pES} = 5.25 \text{ ksi}$
$\Delta F_{pES} = \Delta f_{pES} \cdot A_{ps} \cdot l_2$			$\Delta F_{pES} = 9.6 \text{ kip}$
Dead Load Moment due to Beam Selfweight			
$\omega_D = 0.145 \text{ kcf} \cdot A_g$			$\omega_D = 0.764 \text{ klf}$
$M_D = \frac{\omega_D \cdot l_d \cdot L_o}{2} - \frac{\omega_D \cdot l_d^2}{2}$			$M_D = 185 \text{ k} \cdot \text{in}$
Top Fiber Stress at Transfer			
$f_{top} = \frac{-(F_o - \Delta F_{pES})}{A_{tr}} + \frac{(F_o - \Delta F_{pES})(y_{btr} - y_p)(H - y_{btr})}{I_{tr}} - \frac{M_D(H - y_{btr})}{I_{tr}}$ $f_{top} = 359 \text{ psi}$ $= 4.0 \sqrt{f'_{ci}}$			
Bottom Fiber Stress at Transfer			
$f_{top} = \frac{-(F_o - \Delta F_{pES})}{A_{tr}} - \frac{(F_o - \Delta F_{pES})(y_{btr} - y_p)(H - y_{btr})}{I_{tr}} + \frac{M_D(H - y_{btr})}{I_{tr}}$ $f_{bot} = -1139 \text{ psi}$			

Table E-2 Top and Bottom Fiber Stress Calculations, Beam 2

Material Properties		Section Properties (include block-out)	
$f'_{ci} = 4.5 \text{ ksi}$	$y'_s = 50 \text{ in}$	$L_o = 20 \text{ ft}$	$I_g = 235067 \text{ in}^4$
$f_y = 60 \text{ ksi}$	$A_{ps} = 0.153 \text{ in}^2$	$H = 52.5 \text{ in}$	$F_o = 364 \text{ kip}$
$E_s = 29000 \text{ ksi}$	$y_p = 2 \text{ in}$	$y_b = 23.62$	$d_b = 0.5 \text{ in}$
$A'_s = 2.38 \text{ in}^2$	$E_{ci} = 4557 \text{ ksi}$	$A_g = 758.4 \text{ in}^2$	
Transfer Length (AASHTO LRFD §5.11.4.2)			
$f_{se} = \frac{(F_o - \Delta F_{pES})}{12 \cdot A_{ps}}$			$f_{se} = 190.6 \text{ ksi}$
$l_d = \frac{f_{se}}{3} \cdot d_b$			$l_d = 32 \text{ in}$
Transformed Section Properties			
$n = \frac{E_s}{E_c}$			$n = 6.4$
$y_{btr} = \frac{A_g \cdot y_b + (n-1) \cdot (A'_s \cdot y'_s + 12 A_{ps} \cdot y_p)}{A_g + (n-1) \cdot (A'_s + 12 A_{ps})}$			$y_{btr} = 23.78 \text{ in}$
$A_{tr} = A_g + (n-1) \cdot (A'_s + 12 A_{ps})$			$A_{tr} = 781 \text{ in}^2$
$I_{tr} = I_g + A_g (y_b - y_{btr})^2 + (n-1) [A'_s (y'_s - y_{btr})^2 + 12 A_{ps} (y_p - y_{btr})^2]$			$I_{tr} = 248534 \text{ in}^4$
Losses due to Elastic Shortening (AASHTO LRFD §5.9.5.2.3)			
$f_{cir} = \frac{F_o}{A_g} + \frac{F_o (y_b - y_p)^2}{I_g}$			$f_{cir} = 1.20 \text{ ksi}$
$\Delta f_{pES} = n \cdot f_{cir}$			$\Delta f_{pES} = 7.66 \text{ ksi}$
$\Delta F_{pES} = \Delta f_{pES} \cdot A_{ps} \cdot 12$			$\Delta F_{pES} = 14.1 \text{ kip}$
Dead Load Moment due to Beam Selfweight			
$\omega_D = 0.145 \text{ kcf} \cdot A_g$			$\omega_D = 0.764 \text{ klf}$
$M_D = \frac{\omega_D \cdot l_d \cdot L_o}{2} - \frac{\omega_D \cdot l_d^2}{2}$			$M_D = 211 \text{ k} \cdot \text{in}$
Top Fiber Stress at Transfer			
$f_{top} = \frac{-(F_o - \Delta F_{pES})}{A_{tr}} + \frac{(F_o - \Delta F_{pES})(y_{btr} - y_p)(H - y_{btr})}{I_{tr}} - \frac{M_D(H - y_{btr})}{I_{tr}}$ $f_{top} = 408 \text{ psi}$ $= 6.1 \sqrt{f'_{ci}}$			
Bottom Fiber Stress at Transfer			
$f_{top} = \frac{-(F_o - \Delta F_{pES})}{A_{tr}} - \frac{(F_o - \Delta F_{pES})(y_{btr} - y_p)(H - y_{btr})}{I_{tr}} + \frac{M_D(H - y_{btr})}{I_{tr}}$ $f_{bot} = -1304 \text{ psi}$			

Table E-3 Top and Bottom Fiber Stress Calculations, Beam 3

Material Properties		Section Properties (include block-out)	
$f'_{ci} = 5.0 \text{ ksi}$	$y'_s = 50 \text{ in}$	$L_o = 20 \text{ ft}$	$I_g = 235067 \text{ in}^4$
$f_y = 60 \text{ ksi}$	$A_{ps} = 0.153 \text{ in}^2$	$H = 52.5 \text{ in}$	$F_o = 374 \text{ kip}$
$E_s = 29000 \text{ ksi}$	$y_p = 2 \text{ in}$	$y_b = 23.62$	$d_b = 0.5 \text{ in}$
$A'_s = 2.38 \text{ in}^2$	$E_{ci} = 4830 \text{ ksi}$	$A_g = 758.4 \text{ in}^2$	
Transfer Length (AASHTO LRFD §5.11.4.2)			
$f_{se} = \frac{(F_o - \Delta F_{pES})}{12 \cdot A_{ps}}$			$f_{se} = 196.1 \text{ ksi}$
$l_d = \frac{f_{se}}{3} \cdot d_b$			$l_d = 33 \text{ in}$
Transformed Section Properties			
$n = \frac{E_s}{E_c}$			$n = 6.0$
$y_{btr} = \frac{A_g \cdot y_b + (n-1) \cdot (A'_s \cdot y'_s + 12 A_{ps} \cdot y_p)}{A_g + (n-1) \cdot (A'_s + 12 A_{ps})}$			$y_{btr} = 23.77 \text{ in}$
$A_{tr} = A_g + (n-1) \cdot (A'_s + 12 A_{ps})$			$A_{tr} = 780 \text{ in}^2$
$I_{tr} = I_g + A_g (y_b - y_{btr})^2 + (n-1) [A'_s (y'_s - y_{btr})^2 + 12 A_{ps} (y_p - y_{btr})^2]$			$I_{tr} = 247633 \text{ in}^4$
Losses due to Elastic Shortening (AASHTO LRFD §5.9.5.2.3)			
$f_{cir} = \frac{F_o}{A_g} + \frac{F_o (y_b - y_p)^2}{I_g}$			$f_{cir} = 1.24 \text{ ksi}$
$\Delta f_{pES} = n \cdot f_{cir}$			$\Delta f_{pES} = 7.43 \text{ ksi}$
$\Delta F_{pES} = \Delta f_{pES} \cdot A_{ps} \cdot 12$			$\Delta F_{pES} = 13.6 \text{ kip}$
Dead Load Moment due to Beam Selfweight			
$\omega_D = 0.145 \text{ kcf} \cdot A_g$			$\omega_D = 0.764 \text{ klf}$
$M_D = \frac{\omega_D \cdot l_d \cdot L_o}{2} - \frac{\omega_D \cdot l_d^2}{2}$			$M_D = 216 \text{ k} \cdot \text{in}$
Top Fiber Stress at Transfer			
$f_{top} = \frac{-(F_o - \Delta F_{pES})}{A_{tr}} + \frac{(F_o - \Delta F_{pES})(y_{btr} - y_p)(H - y_{btr})}{I_{tr}} - \frac{M_D(H - y_{btr})}{I_{tr}}$ $f_{top} = 423 \text{ psi}$ $= 6.0 \sqrt{f'_{ci}}$			
Bottom Fiber Stress at Transfer			
$f_{top} = \frac{-(F_o - \Delta F_{pES})}{A_{tr}} - \frac{(F_o - \Delta F_{pES})(y_{btr} - y_p)(H - y_{btr})}{I_{tr}} + \frac{M_D(H - y_{btr})}{I_{tr}}$ $bot = -1347 \text{ psi}$			

Table E-4 Top and Bottom Fiber Stress Calculations, Beam 4

Material Properties		Section Properties (include block-out)	
$f'_{ci} = 8.2 \text{ ksi}$	$y'_s = 50 \text{ in}$	$L_o = 20 \text{ ft}$	$I_g = 235067 \text{ in}^4$
$f_y = 60 \text{ ksi}$	$A_{ps} = 0.153 \text{ in}^2$	$H = 52.5 \text{ in}$	$F_{o1} = 309.5 \text{ kip}$
$E_s = 29000 \text{ ksi}$	$y_{p1} = 2 \text{ in}$	$y_b = 23.62$	$F_{o1} = 61.9 \text{ kip}$
$A'_s = 2.38 \text{ in}^2$	$y_{p2} = 24 \text{ in}$	$A_g = 758.4 \text{ in}^2$	$F_{o3} = 61.9 \text{ kip}$
$E_{ci} = 5272 \text{ ksi}$	$y_{p3} = 26 \text{ in}$	$d_b = 0.5 \text{ in}$	
Transfer Length (AASHTO LRFD §5.11.4.2)			
$f_{se} = \frac{\left(\sum F_o - \Delta F_{pES}\right)}{14 \cdot A_{ps}}$			$f_{se} = 197.6 \text{ ksi}$
$l_d = \frac{f_{se}}{3} \cdot d_b$			$l_d = 33 \text{ in}$
Transformed Section Properties			
$n = \frac{E_s}{E_c}$			$n = 5.5$
$y_{btr} = \frac{A_g \cdot y_b + (n-1) \cdot (A'_s \cdot y'_s + 10 A_{ps} \cdot y_{p1} + 2 A_{ps} \cdot y_{p2} + 2 A_{ps} \cdot y_{p3})}{A_g + (n-1) \cdot (A'_s + 14 A_{ps})}$			$y_{btr} = 23.80 \text{ in}$
$A_{tr} = A_g + (n-1) \cdot (A'_s + 14 A_{ps})$			$A_{tr} = 779 \text{ in}^2$
$I_{tr} = I_g + A_g (y_b - y_{btr})^2 + (n-1) \left[A'_s (y'_s - y_{btr})^2 + 10 A_{ps} (y_{p1} - y_{btr})^2 \right. \\ \left. + (n-1) \left[A'_s (y'_s - y_{btr})^2 + 2 A_{ps} (y_{p2} - y_{btr})^2 \right] \right. \\ \left. + (n-1) \left[A'_s (y'_s - y_{btr})^2 + 2 A_{ps} (y_{p3} - y_{btr})^2 \right] \right]$			$I_{tr} = 245724 \text{ in}^4$
Losses due to Elastic Shortening (AASHTO LRFD §5.9.5.2.3)			
$f_{cir} = \frac{\sum F_o}{A_g} + \frac{\sum F_o (y_b - 8.5 \text{ in})^2}{I_g}$			$f_{cir} = 0.99 \text{ ksi}$
$\Delta f_{pES} = n \cdot f_{cir}$			$\Delta f_{pES} = 5.46 \text{ ksi}$
$\Delta F_{pES} = \Delta f_{pES} \cdot A_{ps}$			$\Delta F_{pES} = 0.8 \text{ kip / strd}$
Dead Load Moment due to Beam Selfweight			
$\omega_D = 0.145 \text{ kcf} \cdot A_g$			$\omega_D = 0.764 \text{ klf}$
$M_D = \frac{\omega_D \cdot l_d \cdot L_o}{2} - \frac{\omega_D \cdot l_d^2}{2}$			$M_D = 217 \text{ k} \cdot \text{in}$
Top Fiber Stress at Transfer			
$f_{top} = \frac{-\left(\sum F_o - 14 \Delta F_{pES}\right)}{A_{tr}} \pm \frac{(F_{o1} - 10 \Delta F_{pES})(y_{btr} - y_{p1})(H - y_{btr})}{I_{tr}}$ $\pm \frac{(F_{o2} - 2 \Delta F_{pES})(y_{btr} - y_{p2})(H - y_{btr})}{I_{tr}} \pm \frac{(F_{o3} - 2 \Delta F_{pES})(y_{btr} - y_{p3})(H - y_{btr})}{I_{tr}}$ $\pm \frac{M_D (H - y_{btr})}{I_{tr}}$ $f_{top} = 197 \text{ psi} = 2.2 \sqrt{f'_{ci}}$ $f_{bot} = -1283 \text{ psi}$			

Table E-5 Top and Bottom Fiber Stress Calculations, Beam 5

Material Properties		Section Properties (include block-out)	
$f'_{ci} = 9.5 \text{ ksi}$	$y'_s = 50 \text{ in}$	$L_o = 20 \text{ ft}$	$I_g = 235067 \text{ in}^4$
$f_y = 60 \text{ ksi}$	$A_{ps} = 0.153 \text{ in}^2$	$H = 52.5 \text{ in}$	$F_o = 377.5 \text{ kip}$
$E_s = 29000 \text{ ksi}$	$y_p = 2 \text{ in}$	$y_b = 23.62$	$d_b = 0.5 \text{ in}$
$A'_s = 2.38 \text{ in}^2$	$E_{ci} = 6224 \text{ ksi}$	$A_g = 758.4 \text{ in}^2$	
Transfer Length (AASHTO LRFD §5.11.4.2)			
$f_{se} = \frac{(F_o - \Delta F_{pES})}{12 \cdot A_{ps}}$			$f_{se} = 200.2 \text{ ksi}$
$l_d = \frac{f_{se}}{3} \cdot d_b$			$l_d = 33 \text{ in}$
Transformed Section Properties			
$n = \frac{E_s}{E_c}$			$n = 4.7$
$y_{btr} = \frac{A_g \cdot y_b + (n-1) \cdot (A'_s \cdot y'_s + 12 A_{ps} \cdot y_p)}{A_g + (n-1) \cdot (A'_s + 12 A_{ps})}$			$y_{btr} = 23.73 \text{ in}$
$A_{tr} = A_g + (n-1) \cdot (A'_s + 12 A_{ps})$			$A_{tr} = 774 \text{ in}^2$
$I_{tr} = I_g + A_g (y_b - y_{btr})^2 + (n-1) [A'_s (y'_s - y_{btr})^2 + 12 A_{ps} (y_p - y_{btr})^2]$			$I_{tr} = 244259 \text{ in}^4$
Losses due to Elastic Shortening (AASHTO LRFD §5.9.5.2.3)			
$f_{cir} = \frac{F_o}{A_g} + \frac{F_o (y_b - y_p)^2}{I_g}$			$f_{cir} = 1.25 \text{ ksi}$
$\Delta f_{pES} = n \cdot f_{cir}$			$\Delta f_{pES} = 5.82 \text{ ksi}$
$\Delta F_{pES} = \Delta f_{pES} \cdot A_{ps} \cdot 12$			$\Delta F_{pES} = 10.7 \text{ kip}$
Dead Load Moment due to Beam Selfweight			
$\omega_D = 0.145 \text{ kcf} \cdot A_g$			$\omega_D = 0.764 \text{ klf}$
$M_D = \frac{\omega_D \cdot l_d \cdot L_o}{2} - \frac{\omega_D \cdot l_d^2}{2}$			$M_D = 219 \text{ k} \cdot \text{in}$
Top Fiber Stress at Transfer			
$f_{top} = \frac{-(F_o - \Delta F_{pES})}{A_{tr}} + \frac{(F_o - \Delta F_{pES})(y_{btr} - y_p)(H - y_{btr})}{I_{tr}} - \frac{M_D(H - y_{btr})}{I_{tr}}$ $f_{top} = 439 \text{ psi}$ $= 4.5 \sqrt{f'_{ci}}$			
Bottom Fiber Stress at Transfer			
$f_{top} = \frac{-(F_o - \Delta F_{pES})}{A_{tr}} - \frac{(F_o - \Delta F_{pES})(y_{btr} - y_p)(H - y_{btr})}{I_{tr}} + \frac{M_D(H - y_{btr})}{I_{tr}}$ $f_{bot} = -1387 \text{ psi}$			

Table E-6 Top and Bottom Fiber Stress Calculations, Beam 6

Material Properties		Section Properties (include block-out)	
$f'_{ci} = 5.4 \text{ ksi}$	$y'_s = 50 \text{ in}$	$L_o = 20 \text{ ft}$	$I_g = 235067 \text{ in}^4$
$f_y = 60 \text{ ksi}$	$A_{ps} = 0.153 \text{ in}^2$	$H = 52.5 \text{ in}$	$F_o = 226.6 \text{ kip}$
$E_s = 29000 \text{ ksi}$	$y_p = 2 \text{ in}$	$y_b = 23.62$	$d_b = 0.5 \text{ in}$
$A'_s = 2.38 \text{ in}^2$	$E_{ci} = 6043 \text{ ksi}$	$A_g = 758.4 \text{ in}^2$	
Transfer Length (AASHTO LRFD §5.11.4.2)			
$f_{se} = \frac{(F_o - \Delta F_{pES})}{12 \cdot A_{ps}}$			$f_{se} = 119.6 \text{ ksi}$
$l_d = \frac{f_{se}}{3} \cdot d_b$			$l_d = 20 \text{ in}$
Transformed Section Properties			
$n = \frac{E_s}{E_c}$			$n = 4.8$
$y_{btr} = \frac{A_g \cdot y_b + (n-1) \cdot (A'_s \cdot y'_s + 12 A_{ps} \cdot y_p)}{A_g + (n-1) \cdot (A'_s + 12 A_{ps})}$			$y_{btr} = 23.73 \text{ in}$
$A_{tr} = A_g + (n-1) \cdot (A'_s + 12 A_{ps})$			$A_{tr} = 774 \text{ in}^2$
$I_{tr} = I_g + A_g (y_b - y_{btr})^2 + (n-1) [A'_s (y'_s - y_{btr})^2 + 12 A_{ps} (y_p - y_{btr})^2]$			$I_{tr} = 244609 \text{ in}^4$
Losses due to Elastic Shortening (AASHTO LRFD §5.9.5.2.3)			
$f_{cir} = \frac{F_o}{A_g} + \frac{F_o (y_b - y_p)^2}{I_g}$			$f_{cir} = 0.75 \text{ ksi}$
$\Delta f_{pES} = n \cdot f_{cir}$			$\Delta f_{pES} = 3.60 \text{ ksi}$
$\Delta F_{pES} = \Delta f_{pES} \cdot A_{ps} \cdot 12$			$\Delta F_{pES} = 6.6 \text{ kip}$
Dead Load Moment due to Beam Selfweight			
$\omega_D = 0.145 \text{ kcf} \cdot A_g$			$\omega_D = 0.764 \text{ klf}$
$M_D = \frac{\omega_D \cdot l_d \cdot L_o}{2} - \frac{\omega_D \cdot l_d^2}{2}$			$M_D = 140 \text{ k} \cdot \text{in}$
Top Fiber Stress at Transfer			
$f_{top} = \frac{-(F_o - \Delta F_{pES})}{A_{tr}} + \frac{(F_o - \Delta F_{pES})(y_{btr} - y_p)(H - y_{btr})}{I_{tr}} - \frac{M_D(H - y_{btr})}{I_{tr}}$ $f_{top} = 262 \text{ psi}$ $= 3.6 \sqrt{f'_{ci}}$			
Bottom Fiber Stress at Transfer			
$f_{top} = \frac{-(F_o - \Delta F_{pES})}{A_{tr}} - \frac{(F_o - \Delta F_{pES})(y_{btr} - y_p)(H - y_{btr})}{I_{tr}} + \frac{M_D(H - y_{btr})}{I_{tr}}$ $f_{bot} = -830 \text{ psi}$			

Table E-7 Top and Bottom Fiber Stress Calculations, Beam 7

Material Properties		Section Properties (include block-out)	
$f'_{ci} = 10.7 \text{ ksi}$	$y'_s = 50 \text{ in}$	$L_o = 20 \text{ ft}$	$I_g = 235067 \text{ in}^4$
$f_y = 60 \text{ ksi}$	$A_{ps} = 0.153 \text{ in}^2$	$H = 52.5 \text{ in}$	$F_o = 303.3 \text{ kip}$
$E_s = 29000 \text{ ksi}$	$y_p = 2 \text{ in}$	$y_b = 23.62$	$d_b = 0.5 \text{ in}$
$A'_s = 2.38 \text{ in}^2$	$E_{ci} = 5967 \text{ ksi}$	$A_g = 758.4 \text{ in}^2$	
Transfer Length (AASHTO LRFD §5.11.4.2)			
$f_{se} = \frac{(F_o - \Delta F_{pES})}{12 \cdot A_{ps}}$			$f_{se} = 160.3 \text{ ksi}$
$l_d = \frac{f_{se}}{3} \cdot d_b$			$l_d = 27 \text{ in}$
Transformed Section Properties			
$n = \frac{E_s}{E_c}$			$n = 4.9$
$y_{btr} = \frac{A_g \cdot y_b + (n-1) \cdot (A'_s \cdot y'_s + 12 A_{ps} \cdot y_p)}{A_g + (n-1) \cdot (A'_s + 12 A_{ps})}$			$y_{btr} = 23.74 \text{ in}$
$A_{tr} = A_g + (n-1) \cdot (A'_s + 12 A_{ps})$			$A_{tr} = 775 \text{ in}^2$
$I_{tr} = I_g + A_g (y_b - y_{btr})^2 + (n-1) [A'_s (y'_s - y_{btr})^2 + 12 A_{ps} (y_p - y_{btr})^2]$			$I_{tr} = 244763 \text{ in}^4$
Losses due to Elastic Shortening (AASHTO LRFD §5.9.5.2.3)			
$f_{cir} = \frac{F_o}{A_g} + \frac{F_o (y_b - y_p)^2}{I_g}$			$f_{cir} = 1.00 \text{ ksi}$
$\Delta f_{pES} = n \cdot f_{cir}$			$\Delta f_{pES} = 4.87 \text{ ksi}$
$\Delta F_{pES} = \Delta f_{pES} \cdot A_{ps} \cdot 12$			$\Delta F_{pES} = 9.0 \text{ kip}$
Dead Load Moment due to Beam Selfweight			
$\omega_D = 0.145 \text{ kcf} \cdot A_g$			$\omega_D = 0.764 \text{ klf}$
$M_D = \frac{\omega_D \cdot l_d \cdot L_o}{2} - \frac{\omega_D \cdot l_d^2}{2}$			$M_D = 181 \text{ k} \cdot \text{in}$
Top Fiber Stress at Transfer			
$f_{top} = \frac{-(F_o - \Delta F_{pES})}{A_{tr}} + \frac{(F_o - \Delta F_{pES})(y_{btr} - y_p)(H - y_{btr})}{I_{tr}} - \frac{M_D(H - y_{btr})}{I_{tr}}$ $f_{top} = 351 \text{ psi}$ $= 3.4 \sqrt{f'_{ci}}$			
Bottom Fiber Stress at Transfer			
$f_{top} = \frac{-(F_o - \Delta F_{pES})}{A_{tr}} - \frac{(F_o - \Delta F_{pES})(y_{btr} - y_p)(H - y_{btr})}{I_{tr}} + \frac{M_D(H - y_{btr})}{I_{tr}}$ $f_{bot} = -1111 \text{ psi}$			

APPENDIX F

Predicted vs. Measured Stress Profiles

5 feet from end of Beam

	MathCAD	All Data	All Data	MathCAD	MathCAD	Experimentally Measured Strain Values								Strain Values Converted to Stress Values							
	Transfer Length	Top MOE	Bot MOE	Theoretical Stresses f _{bot} f _{top}	NET	NWT	SET	SWT	NEB	NWB	SEB	SWB	NET	NWT	SET	SWT	NEB	NWB	SEB	SWB	
BEAM1	27	5593	5813	-1100 349	0.000083	0.000003			-0.000110				464	17	0	0	-639	0	0	0	
BEAM2				Cracked!																	
BEAM3				Cracked!																	
BEAM4	33	5050	5494	-1212 170	0.000029	0.000024	0.000037			-0.000197			147	119	188	0	0	-1.083	0	0	
BEAM5	33	6007	6440	-1329 426					-0.000159	-0.000126			0	0	0	0	-1.024	-811	0	0	
BEAM6	20	6029	6058	-801 254		0.000052	0.000054	0.000048			-0.000160	-0.000126	0	311	324	287	0	0	-972	-762	
BEAM7	27	5967	6392	-1074 341	0.000061	0.000051	0.000068	0.000054	-0.000121	-0.000152	-0.000245	-0.000146	362	305	405	324	-770	-970		-934	
Location, y _b (in.) =				0	54								52.5	39			19	2	Beam 1		
													52				6		All Others		
																	4		Beam 4		

Best Fit Line

BEAM1	
x	y
464	52.5
17	39
-639	19

Slope = 0.0303631
y - int = 38.436827

x ₀	y ₀
-1286	0
513	54

BEAM4	
x	y
147	52
119	52
188	52
-1,083	4

Slope = 0.0387921
y - int = 46.101081

x ₀	y ₀
-1188	0
204	54

BEAM5	
x	y
-1,024	6
-811	6

Slope =
y - int =

x ₀	y ₀

BEAM6	
x	y
311	52
324	52
287	52
-972	6
-762	6

Slope = 0.038633
y - int = 39.879754

x ₀	y ₀
-1032	0
365	54

BEAM7	
x	y
362	52
305	52
405	52
324	52
-770	6
-970	6
-934	6

Slope = 0.0366877
y - int = 38.977748

x ₀	y ₀
-1062	0
409	54

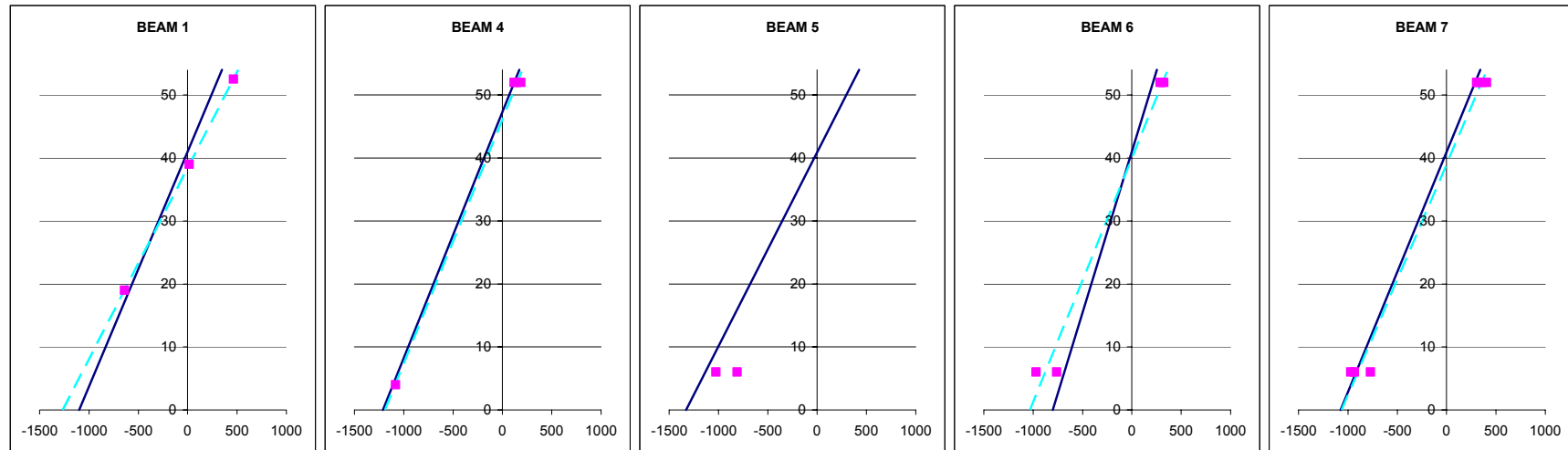


Figure F-1 Predicted Stress Profiles 5-feet from End of AASHTO Type IV Beams.

4 feet from end of Beam

	MathCAD	All Data	All Data	MathCAD	MathCAD	Experimentally Measured Strain Values								Strain Values Converted to Stress Values							
	Transfer Length	Top MOE	Bot MOE	Theoretical Stresses fbot	ftop	NET	NWT	SET	SWT	NEB	NWB	SEB	SWB	NET	NWT	SET	SWT	NEB	NWB	SEB	SWB
BEAM1	27	5593	5813	-1139	359		0.000004			-0.000105	-0.000186			0	22	0	0	-610	-1,081	0	0
BEAM2				Cracked!																	
BEAM3				Cracked!																	
BEAM4	33	5050	5494	-1280	197	0.000026	0.000045	0.000049			-0.000238	-0.000272		133	227	246	0	0	-1,310	-1,495	0
BEAM5	33	6007	6440	-1387	439	0.000079				-0.000156	-0.000190			475	0	0	0	-1,005	-1,224	0	0
BEAM6	20	6029	6058	-830	262						-0.000165	-0.000149	-0.000151	0	0	0	0	0	-1,001	-903	-912
BEAM7	27	5967	6392	-1111	351	0.000081	0.000094	0.000052	0.000066	-0.000098	-0.000109	-0.000133	-0.000129	481	562	311	392	-626	-696	-849	-824
Location, y _b (in.) =																					
				0	54									52.5	39			19	2	Beam 1	
														52				6		All Others	
																		4		Beam 4	

Best Fit Line

x	y
22	39
-610	19
-1,081	2

Slope =	0.0334202
y - int =	38.595098

xo	yo
-1155	0
461	54

x	y
133	52
227	52
246	52
-1,310	4
-1,495	4

Slope =	0.0296732
y - int =	45.852413

xo	yo
-1545	0
275	54

x	y
475	52
-1,005	6
-1,224	6

Slope =	0.0285483
y - int =	38.021569

xo	yo
-1332	0
560	54

x	y
-1,001	5
-903	5
-912	5

Slope =
y - int =

xo	yo

BEAM7	
x	y
481	5
562	5
311	5
392	5
-626	
-696	
-849	
-824	

Slope =	0.037882
y - int =	34.92015

xo	yo
-922	0
504	54

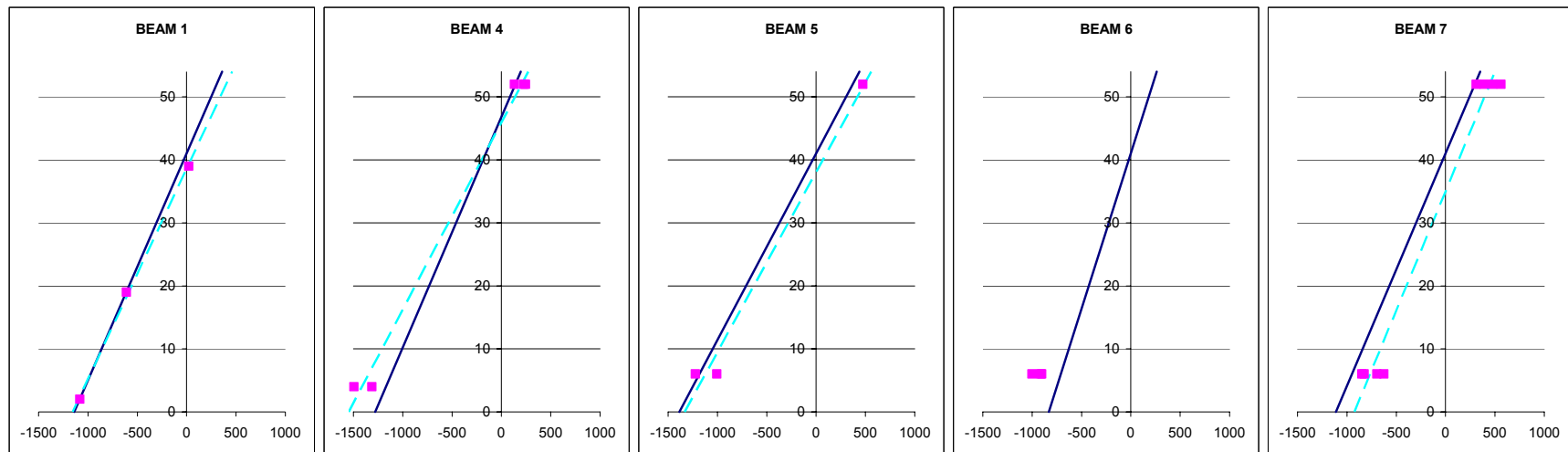


Figure F-2 Predicted Stress Profile 4-feet from End of AASHTO Type IV Beams.

3 feet from end of Beam

	MathCAD	All Data	All Data	MathCAD	MathCAD	Experimentally Measured Strain Values								Strain Values Converted to Stress Values							
	Transfer Length	Top MOE	Bot MOE	Theoretical Stresses f _{bot}	f _{top}	NET	NWT	SET	SWT	NEB	NWB	SEB	SWB	NET	NWT	SET	SWT	NEB	NWB	SEB	SWB
BEAM1	27	5593	5813	-1139	359	0.000055	0.000004			-0.000085				308	22	0	0	-494	0	0	0
BEAM2																					
BEAM3																					
BEAM4	33	5050	5494	-1280	197	0.000059	0.000052	0.000025			-0.000244			300	264	125	0	0	-1,339	0	0
BEAM5	33	6007	6440	-1387	439	0.000070	0.000055			-0.000113	-0.000194			420	330	0	0	-728	-1,249	0	0
BEAM6	20	6029	6058	-830	262	0.000037	0.000035	0.000038		-0.000126		-0.000190	-0.000164	0	224	212	230	-763	0	-1,152	-991
BEAM7	27	5967	6392	-1111	351	0.000058	0.000044	0.000037	0.000046	-0.000142	-0.000135	-0.000118	-0.000135	348	261	224	276	-906	-862	-752	-862
Location, y _b (in.) =		0	54											52.5	39			19	2	Beam 1	
												52					6		All Others		
																	4		Beam 4		

Beam 1
All Others
Beam 4

Best Fit Line

BEAM1	
x	y
308	52.5
22	39
-494	19
Slope = 0.0414162 y - int = 39.099048	
x ₀	y ₀
-944	0
360	54

BEAM4	
x	y
300	52
264	52
125	52
-1,339	4
Slope = 0.0303178 y - int = 44.934116	
x ₀	y ₀
-1482	0
299	54

BEAM5	
x	y
420	52
330	52
-728	6
-1,249	6
Slope = 0.0313629 y - int = 38.614332	
x ₀	y ₀
-1231	0
491	54

BEAM6	
x	y
224	52
212	52
230	52
-763	6
-1,152	6
-991	6
Slope = 0.0372863 y - int = 42.92053	
x ₀	y ₀
-1151	0
297	54

BEAM7	
x	y
348	52
261	52
224	52
276	52
-906	6
-862	6
-752	6
-862	6
Slope = 0.0406407 y - int = 40.54821	
x ₀	y ₀
-998	0
331	54

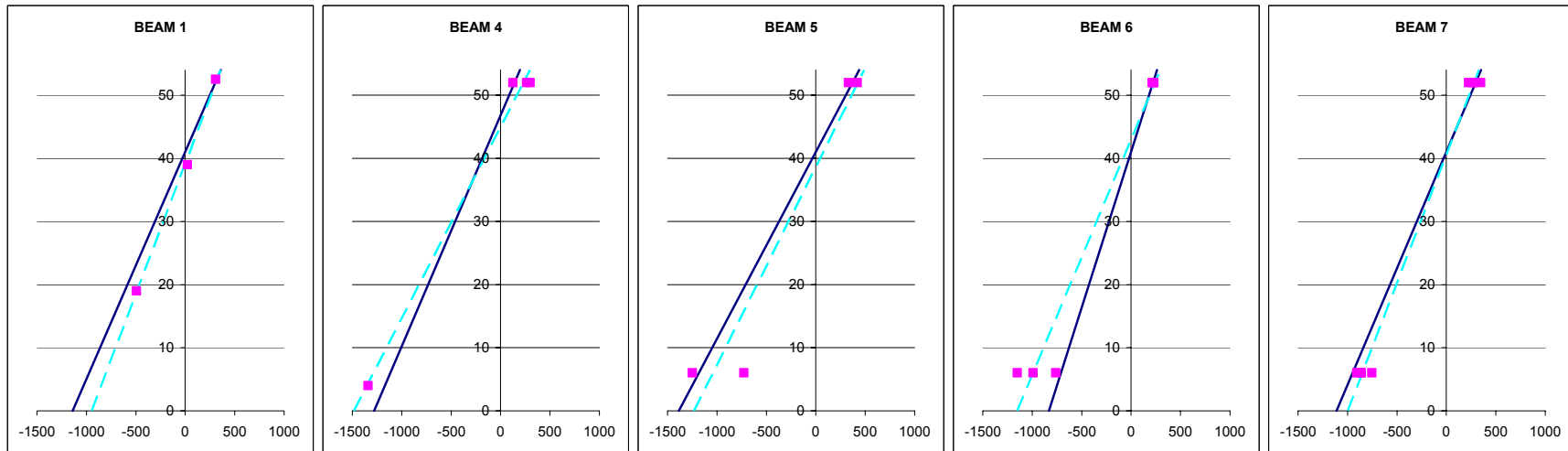


Figure F-3 Predicted Stress Profile 3-feet from End of AASHTO Type IV Beams.

2 feet from end of Beam

	MathCAD	All Data	All Data	MathCAD	MathCAD	Experimentally Measured Strain Values								Strain Values Converted to Stress Values							
	Transfer Length	Top MOE	Bot MOE	Theoretical Stresses f _{bot}	f _{top}	NET	NWT	SET	SWT	NEB	NWB	SEB	SWB	NET	NWT	SET	SWT	NEB	NWB	SEB	SWB
BEAM1	27	5593	5813			0.000025	0.000003			-0.000042				140	17	0	0	-244	0	0	0
BEAM2																					
BEAM3																					
BEAM4	33	5050	5494	-931	143	0.000021	0.000020	0.000030		-0.000241	-0.000224	-0.000269		108	99	151	0	0	-1,323	-1,231	-1,480
BEAM5	33	6007	6440	-1009	319	0.000036	0.000041			-0.000168	-0.000153			216	246	0	0	-1,082	-985	0	0
BEAM6	20	6029	6058	-830	262	0.000026	0.000025	0.000011	0.000012	-0.000137	-0.000150	-0.000151	-0.000136	157	150	67	71	-828	-910	-916	-827
BEAM7	27	5967	6392	-988	312		0.000025	0.000009	0.000028			-0.000137	-0.000135	0	149	54	165	0	0	-877	-862

Location, y_b (in.) =

0

54

52.5

39

19

2

Beam 1

All Others

Beam 4

Best Fit Line

<div>BEAM1</div> <table><tr><th>x</th><th>y</th></tr><tr><td>140</td><td>52.5</td></tr><tr><td>17</td><td>39</td></tr><tr><td>-244</td><td>19</td></tr></table> <div>Slope = 0.0855935 y - int = 39.331009</div> <table><tr><th>x0</th><th>y0</th></tr><tr><td>-460</td><td>0</td></tr><tr><td>171</td><td>54</td></tr></table>	x	y	140	52.5	17	39	-244	19	x0	y0	-460	0	171	54	<div>BEAM4</div> <table><tr><th>x</th><th>y</th></tr><tr><td>108</td><td>52</td></tr><tr><td>99</td><td>52</td></tr><tr><td>151</td><td>52</td></tr><tr><td>-1,323</td><td>4</td></tr><tr><td>-1,231</td><td>4</td></tr><tr><td>-1,480</td><td>4</td></tr></table> <div>Slope = 0.0324446 y - int = 47.875734</div> <table><tr><th>x0</th><th>y0</th></tr><tr><td>-1476</td><td>0</td></tr><tr><td>189</td><td>54</td></tr></table>	x	y	108	52	99	52	151	52	-1,323	4	-1,231	4	-1,480	4	x0	y0	-1476	0	189	54	<div>BEAM5</div> <table><tr><th>x</th><th>y</th></tr><tr><td>216</td><td>52</td></tr><tr><td>246</td><td>52</td></tr><tr><td>-1,082</td><td>6</td></tr><tr><td>-985</td><td>6</td></tr></table> <div>Slope = 0.0362509 y - int = 43.542955</div> <table><tr><th>x0</th><th>y0</th></tr><tr><td>-1201</td><td>0</td></tr><tr><td>288</td><td>54</td></tr></table>	x	y	216	52	246	52	-1,082	6	-985	6	x0	y0	-1201	0	288	54	<div>BEAM6</div> <table><tr><th>x</th><th>y</th></tr><tr><td>157</td><td>52</td></tr><tr><td>150</td><td>52</td></tr><tr><td>67</td><td>52</td></tr><tr><td>71</td><td>52</td></tr><tr><td>-828</td><td>6</td></tr><tr><td>-910</td><td>6</td></tr><tr><td>-916</td><td>6</td></tr><tr><td>-827</td><td>6</td></tr></table> <div>Slope = 0.04652 y - int = 46.649916</div> <table><tr><th>x0</th><th>y0</th></tr><tr><td>-1003</td><td>0</td></tr><tr><td>158</td><td>54</td></tr></table>	x	y	157	52	150	52	67	52	71	52	-828	6	-910	6	-916	6	-827	6	x0	y0	-1003	0	158	54	<div>BEAM7</div> <table><tr><th>x</th><th>y</th></tr><tr><td>149</td><td>52</td></tr><tr><td>54</td><td>52</td></tr><tr><td>165</td><td>52</td></tr><tr><td>-877</td><td>6</td></tr><tr><td>-862</td><td>6</td></tr></table> <div>Slope = 0.0460794 y - int = 46.226592</div> <table><tr><th>x0</th><th>y0</th></tr><tr><td>-1003</td><td>0</td></tr><tr><td>169</td><td>54</td></tr></table>	x	y	149	52	54	52	165	52	-877	6	-862	6	x0	y0	-1003	0	169	54
x	y																																																																																															
140	52.5																																																																																															
17	39																																																																																															
-244	19																																																																																															
x0	y0																																																																																															
-460	0																																																																																															
171	54																																																																																															
x	y																																																																																															
108	52																																																																																															
99	52																																																																																															
151	52																																																																																															
-1,323	4																																																																																															
-1,231	4																																																																																															
-1,480	4																																																																																															
x0	y0																																																																																															
-1476	0																																																																																															
189	54																																																																																															
x	y																																																																																															
216	52																																																																																															
246	52																																																																																															
-1,082	6																																																																																															
-985	6																																																																																															
x0	y0																																																																																															
-1201	0																																																																																															
288	54																																																																																															
x	y																																																																																															
157	52																																																																																															
150	52																																																																																															
67	52																																																																																															
71	52																																																																																															
-828	6																																																																																															
-910	6																																																																																															
-916	6																																																																																															
-827	6																																																																																															
x0	y0																																																																																															
-1003	0																																																																																															
158	54																																																																																															
x	y																																																																																															
149	52																																																																																															
54	52																																																																																															
165	52																																																																																															
-877	6																																																																																															
-862	6																																																																																															
x0	y0																																																																																															
-1003	0																																																																																															
169	54																																																																																															

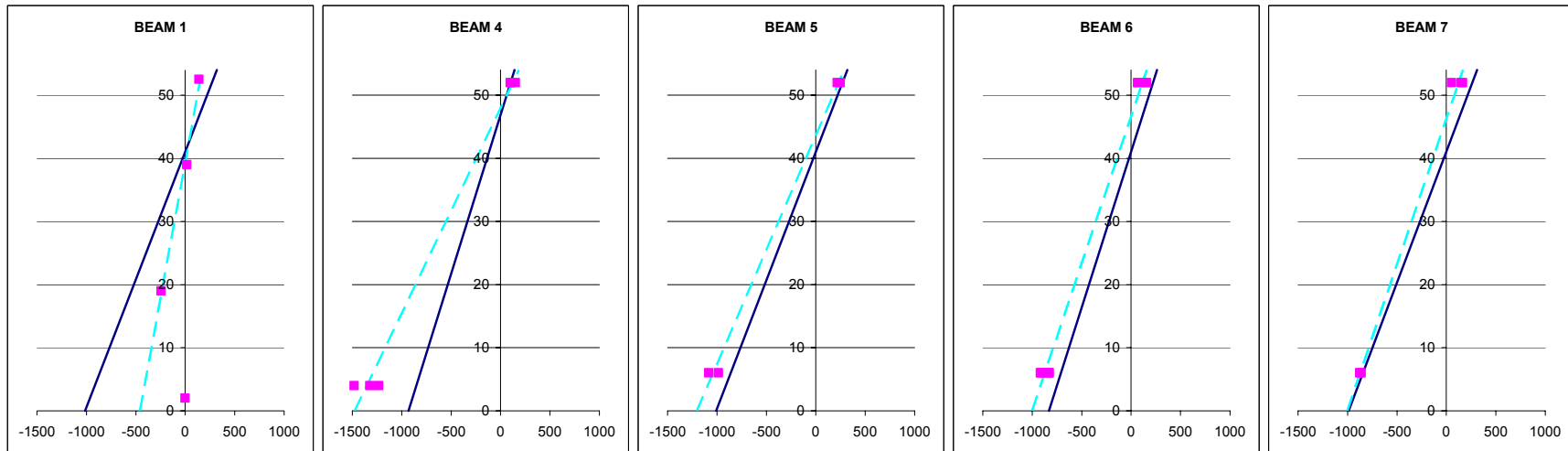


Figure F-4 Predicted Stress Profile 2-feet from End of AASHTO Type IV Beams

1 foot from end of Beam

	MathCAD	All Data	All Data	MathCAD	MathCAD	Experimentally Measured Strain Values						Strain Values Converted to Stress Values									
	Transfer Length	Top MOE	Bot MOE	Theoretical Stresses fbot	ftop	NET	NWT	SET	SWT	NEB	NWB	SEB	SWB	NET	NWT	SET	SWT	NEB	NWB	SEB	SWB
BEAM1	27	5593	5813	-506	160	0.000007	0.000001			-0.000020				39	6	0	0	-116	0	0	0
BEAM2																					
BEAM3				Cracked!	Cracked!																
BEAM4	33	5050	5494	-465	72	0.000009				-0.000208	-0.000165	-0.000180		45	0	0	0	-1,143	-908	-989	0
BEAM5	33	6007	6440	-504	160	0.000005	0.000004			-0.000114	-0.000094			30	24	0	0	-734	-605	0	0
BEAM6	20	6029	6058	-498	157	0.000009	0.000017	0.000004		-0.000124		-0.000106	-0.000162	0	53	104	22	-749	0	-640	-981
BEAM7	27	5967	6392	-494	156	0.000009	0.000007	0.000041		-0.000132		-0.000111	-0.000114	0	57	40	244	-841	0	-708	-728
Location, y _b (in.) =		0		54						52.5		39				19		2		Beam 1	
																				All Others	
																				Beam 4	

Best Fit Line

BEAM1	
x	y
39	52.5
6	39
-116	19

Slope = 0.2017691
y - int = 41.643239

x0	y0
-206	0
61	54

BEAM4	
x	y
45	52
-1,143	4
-908	4
-989	4

Slope = 0.043853
y - int = 48.830157

x0	y0
-1113	0
118	54

BEAM5	
x	y
30	52
24	52
-734	6
-605	6

Slope = 0.0649056
y - int = 49.85834

x0	y0
-768	0
64	54

BEAM6	
x	y
53	52
104	52
22	52
-749	6
-640	6
-981	6

Slope = 0.0511118
y - int = 47.666536

x0	y0
-933	0
124	54

BEAM7	
x	y
57	52
40	52
244	52
-841	6
-708	6
-728	6

Slope = 0.0511031
y - int = 45.50017

x0	y0
-890	0
166	54

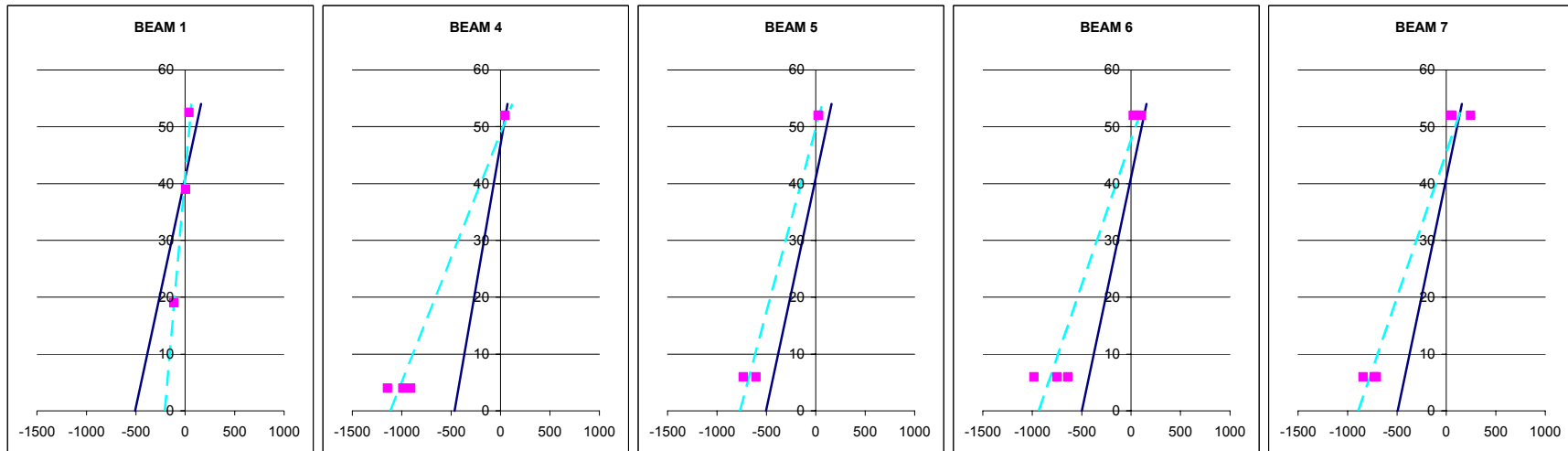


Figure F-5 Predicted Stress Profile 1-feet from End of AASHTO Type IV Beams

APPENDIX G

Curing Temperature Data

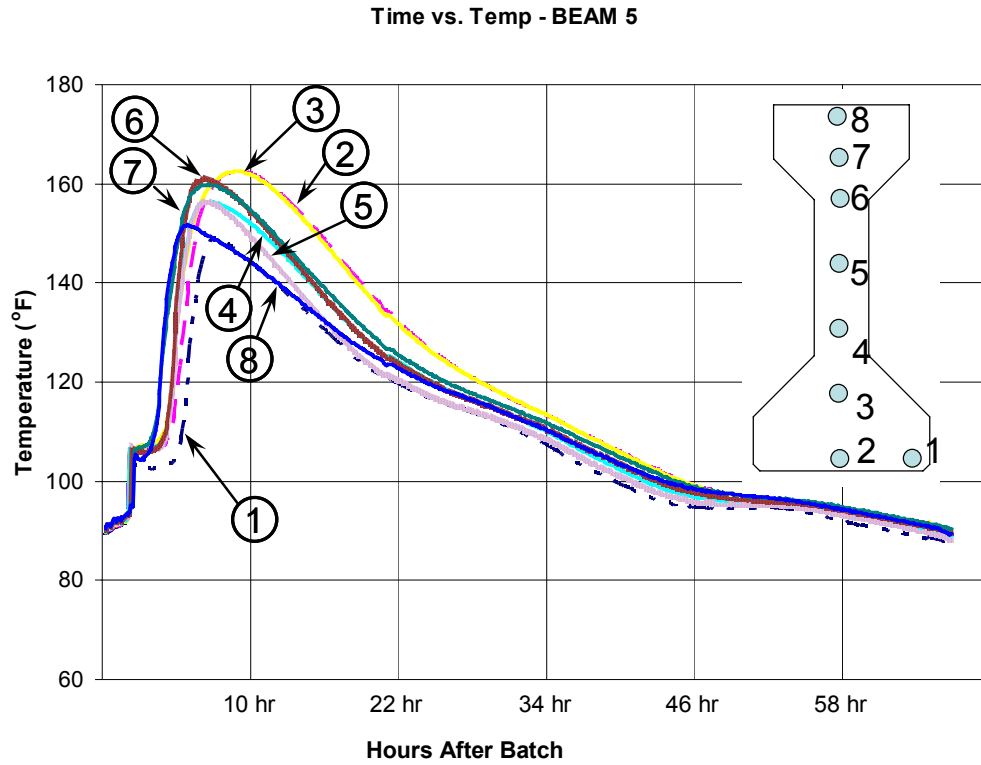


Figure G-1 Time vs. Temperature Data Collected from Beam 5

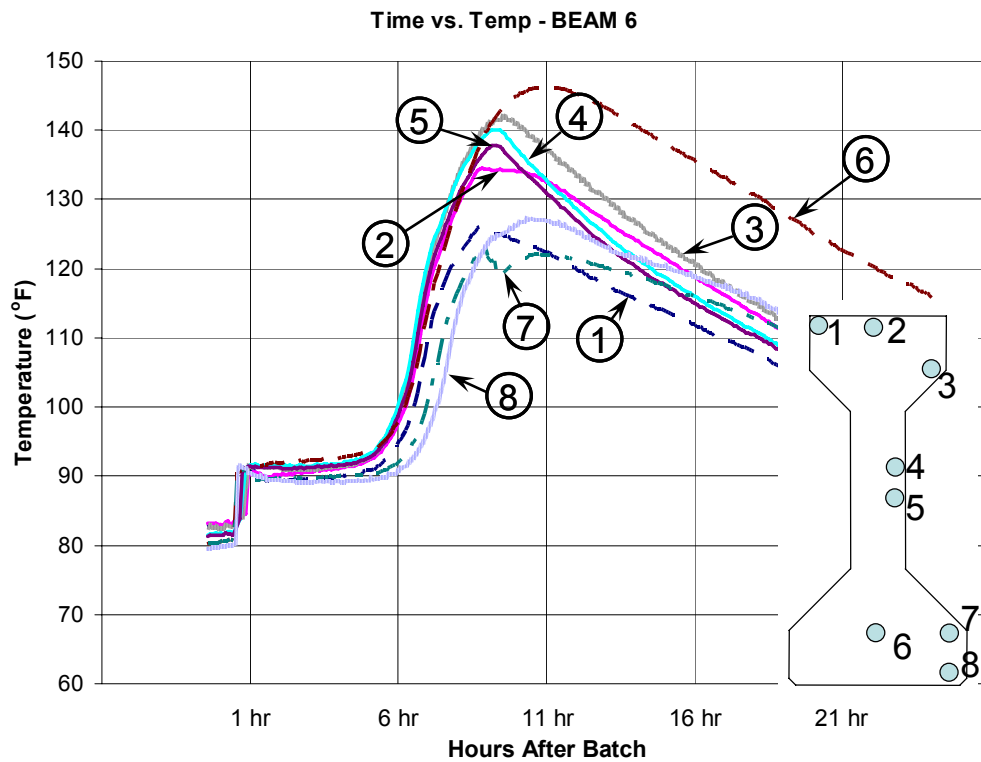


Figure G-2 Time vs. Temperature Data Collected from Beam 6

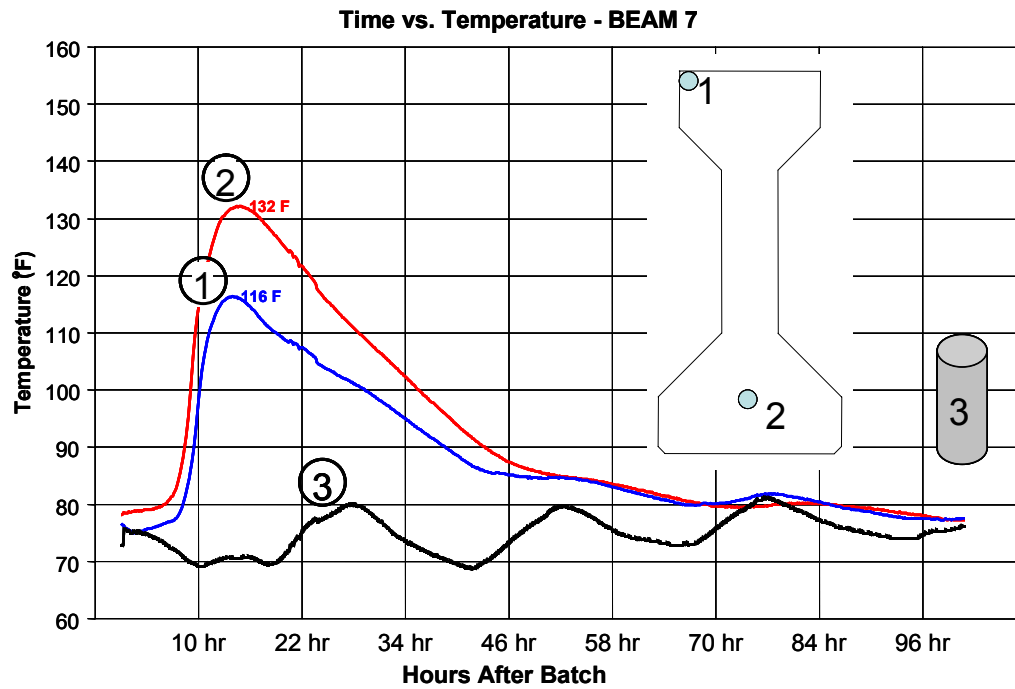


Figure G-3 Time vs. Temperature Data Collected from Beam 7

REFERENCES

1. AASHTO LRFD, *Bridge Design Specifications, Customary U.S. Units, 3rd Edition – 2004*, American Association of State Highway and Transportation Officials, Washington, D. C., 2004.
2. AASHTO, *Standard Specifications for Highway Bridges, 17th Edition – 2002*, American Association of State Highway and Transportation Officials, Washington, D. C., 2002.
3. ACI Committee 209, *Prediction of Creep, Shrinkage, and Temperature Effects in Concrete Structures (ACI 209R-92)*, American Concrete Institute, Farmington Hills, MI, 1992.
4. ACI Committee 318, *Building Code Requirements for Reinforced Concrete (ACI 318-63)*, American Concrete Institute, Detroit, MI, 1963.
5. ACI Committee 318, *Building Code Requirements for Reinforced Concrete (ACI 318-67)*, American Concrete Institute, Detroit, Michigan, 1967.
6. ACI Committee 318, *Building Code Requirements for Reinforced Concrete (ACI 318-77)*, American Concrete Institute, Detroit, Michigan, 1977.
7. ACI Committee 318, *Building Code Requirements for Reinforced Concrete (ACI 318-05)*, American Concrete Institute, Farmington Hills, MI, 2005.
8. ACI Committee 363, “State-of-the-Art Report on High-Strength Concrete,” *ACI Journal, Proceedings* V. 81, No. 4, July-Aug. 1984, pp. 364-411.
9. ACI Committee 435, “Deflections of Reinforced Concrete Flexural Members, *ACI Journal, Proceedings* V. 63, No. 6, June 1966, pp. 637-674.
10. ACI-ASCE Joint Committee 323, “Tentative Recommendations for Prestressed Concrete,” *Journal of the American Concrete Institute–Proceedings*, Vol. 54, January 1958, pp. 545-578.
11. Beer, F. P., and Johnston, E. R., *Mechanics of Materials*, McGraw-Hill Inc., New York, 1992.
12. Cannon, R. P., “Temperature-Matched Curing: Its Development, Application and Future Role in Concrete Practice and Research,” *Concrete (London)*, Part I – V. 20, No. 7, July 1986, pp. 27-30; Part 2 – V. 20, No. 10, Oct. 1986, pp. 28-32; Part 3 – V. 21, No. 2, Feb. 1987, pp. 33-34.

13. Carasquillo, R. L.; Nilson, A. H.; and Slate, F. O., "Properties of High-Strength Concrete Subjected to Short-Term Loads," *ACI Journal, Proceedings* V. 78, No. 3, May-June 1981, pp. 171-178.
14. Collins, M. P. and Mitchell, D., *Prestressed Concrete Structures*, Response Publications, Toronto and Montreal, Canada, 1997.
15. Collins, M.P. and Mitchell, D., *Response (Version 1.0) for Prestressed Concrete Structures*, Department of Civil Engineering, University of Toronto, 1990.
16. Cotham, J. C. <jcotham@dot.state.tx.us>; Tucker, J. <jtucker@dot.state.tx.us>; Holt, J. <jholt@dot.state.tx.us> "RE: Ty IV crack research (vertical cracks in web and topflange, 4' from ends)," Personal Email, Dec. 18, 2005.
17. Cotham, J.C., Personal Correspondence, Project Meeting, Sept., 2006.
18. Gonnerman, H. F., and Shuman, E. C., "Compression, Flexural, and Tension Tests of Plain Concrete," *Proceedings, ASTM*, V. 28, Part II, 1928, pp. 527-564.
19. Grieb, W. E., and Werner, G., "Comparison of Splitting Tensile Strength of Concrete with Flexural and Compressive Strengths," *Public Roads*, V. 32, No. 5, Dec. 1962.
20. Houk, "Concrete Aggregate and Concrete Properties Investigations, Dworshak Dam and Reservoir," *Design Memorandum*, No. 16, U. S. Army Engineer District, Walla Walla, 1965, pp. 203-212.
21. Hueste, M. B. D.; Chompreda, P.; Trejo, D.; Cline, D. B.; and Keating, P. B., "Mechanical Properties of High-Strength Concrete for Prestressed Members," *ACI Structural Journal*, V. 101, No. 4, July-Aug. 2004, pp. 457-474.
22. Kaplan, M. F., "Flexural and Compressive Strength Concretes as Affected by the Properties of Coarse Aggregates," *ACI Journal, Proceedings* V. 55, No. 11, May 1959, pp. 1193-1208.
23. Khan, A. A.; Cook, W. D.; and Mitchell, D., "Tensile Strength of Low, Medium, and High-Strength Concrete at Early Ages," *ACI Materials Journal*, V. 93, No. 5, Sept.-Oct. 1996, pp. 487-493.
24. Kehl, R. J., and Carrasquillo, R. L., *Investigation of the Use of Match Cure Technology in the Precast Industry*, Research Report No. 1714-2, Center for Transportation Research, The University of Texas at Austin, Aug. 1998.

25. Mirza, S. A.; Hatzinikolas, M.; and MacGregor, J. G., "Statistical Descriptions of Strength of Concrete," *Journal of the Structural Division, ASCE*, V. 105, No. ST6, June 1979.
26. Mokhtarzadeh, A. and French, C., "Mechanical Properties of High-Strength Concrete with Consideration for Precast Applications," *ACI Materials Journal*, Vol. 97, No. 2, March-April 2000, pp. 136-147.
27. Pauw, A., "Static Modulus of Elasticity of Concrete as Affected by Density," *Journal of the American Concrete Institute-Proceedings*, Vol. 32, No. 6, November-December 1960.
28. Raphael, J. M., "Tensile Strength of Concrete," *ACI Journal, Proceedings*, V. 81, No. 2, Mar.-Apr. 1984, pp. 158-165.
29. Rogers, S., "Allowable Design Release Stresses for Pretensioned Concrete Beams—Preliminary Results, MS Thesis, The University of Texas at Austin, 2002.
30. Russell, B., *Design Guidelines for Transfer, Development and Debonding of Large Diameter Seven Wire Strands in Pretensioned Concrete Girders*, Dissertation, The University of Texas at Austin, 1992.
31. Schlaich, J.; Schäfer, K.; and Jennewein, M., "Toward a Consistent Design of Structural Concrete," *Journal of the Prestressed Concrete Institute*, V. 32, No. 3, May-June 1987, pp. 74-149.
32. Shah, S. P., and Ahmad, S. H., "Structural Properties of High-Strength Concrete and Its Implications for Precast Prestressed Concrete," *Journal of the Prestressed Concrete Institute*, V. 30, No. 6, Nov.-Dec. 1985, pp. 92-119.
33. Shah, S.P. and Winter, G., "Inelastic Behavior and Fracture of Concrete," *Journal of the American Concrete Institute-Proceedings*, Vol. 63, No. 9, September 1966, pp. 925-930.
34. Walker, S., and Bloem, D. L., "Effects of Aggregate Size on Properties of Concrete," *ACI Journal, Proceedings*, V. 57, No. 3, Sept. 1960, pp. 283-298.